The design and behaviour of a novel WAAM integrated plug & play beam-column connection

FE-analysis of a novel plug & play joint

Grigor Ayvazyan

Delft University of Technology

TU Delft

The design and behaviour of a novel WAAM integrated plug & play beam-column connection

FE-analysis of a novel plug & play joint

by

Grigor Ayvazyan

to obtain the degree of
Master of Science in Civil Engineering
at the Delft University of Technology

Student number: 4256506

Thesis committee:

Prof.dr. M. Veljkovic	TU Delft	Chair
Prof.dr. P.C. Louter	TU Delft	
Dr. T. Tankova	TU Delft	Supervisor

Cover: Steel structure Jachtwerf by Evers Staalconstructies (modified)

An electronic version of this thesis is available at `http://repository.tudelft.nl/`.

TU Delft

Acknowledgements

I would like to express my deepest gratitude to my supervisor, Dr. Trayana Tankova, for her invaluable guidance and patience throughout the course of this thesis. Her support and encouragement have been essential to the development of my work.

I also wish to thank the other members of the thesis committee - Professor Milan Veljkovic and Professor Christian Louter - for their critical perspective and thoughtful feedback. Their questions and comments challenged me to improve my thinking, refine my writing, and become a better version of myself.

My heartfelt thanks go to my parents, whose immense sacrifices and courage in seeking a safe place for their children to study and build their future have paved the way for this achievement. I dedicate this thesis to them.

I thank my wife for her love, unwavering support, and patience during the many hours devoted to this work. Her encouragement helped me stay motivated and committed to complete this thesis.

Finally, I thank my children for their unconditional love, which is the most invaluable thing in my life. I hope that the accomplishment of this study serves as an example for them to strive and persevere for their personal goals and ambitions, while never losing sight of the most important things in life: God, family and love.

Grigor Ayvazyan
Delft, April 2025

Abstract

Beam-to-column joints in steel structures are critical in both the design and execution phase. Bolted beam-to-column joints are widely applied in structures, due to their cost-effectiveness, ease of installation, and well described design guidelines in Eurocode 3. However, bolted connections to hollow section columns are challenging and limited, due to the limited access to the interior of the column. Hollow sections provide several advantages with regard to aesthetics and resistance. Welded beam-to-column joints can be applied to hollow section columns but are costly, require on-site welding and limit the reuse of structural members.

This thesis presents a novel plug-and-play beam-to-column connection, which adheres to modular construction and reuse. Design requirements for the plug-and-play connection were determined based on existing plug-and-play connections to overcome existing limitations and leverage the advantages.

In order to analyse the structural behaviour of the plug-and-play joint, a validated numerical finite element model is developed, using ABAQUS software. First, the plug-and-play joint's global behaviour is analysed in terms of stiffness and moment resistance. Iteratively the conceptual design is finalised, by analysing the Von Mises stresses in the joint, and reducing material use in the connection. The structural behaviour and material use of the plug-and-play connection were compared to an equivalent single extended end-plate bolted connection, to quantify the improvements.

The plug-and-play joint is then divided into separate active joint components which act together to establish the joint's behaviour, similar to the component method in Eurocode 3, part 1-8. The identified joint components were analysed in terms of strength and stiffness. Selected data from defined nodes were extracted and processed to determine the isolated behaviour and contribution of each component.

The outputs of the analyses are: i) the plug-and-play joint is significantly stiffer and stronger than its equivalent bolted connection; ii) it uses less material than its equivalent bolted connection; iii) in the considered configuration the joint's stiffness and moment resistance are dominated by the column web panel in shear; iv) failure in the joint occurs due to the pins in tension and the column web panel in shear.

In order to adapt the plug-and-play connection to hollow section columns, wire arc additive manufacturing (WAAM) is partially employed to directly print the parts of the connection that are attached to the column. WAAM eliminates the need to access the interior of the hollow section and provides a plug-and-play solution for a beam-to-column connection for hollow section columns. The plug-and-play connection is adapted to a configuration of an open section beam and a circular hollow section (CHS) column. The connection provides an I-beam-to-CHS-column joint which is off-site manufacturable and prevents on-site welding. The adapted plug-and-play joint was compared to the single extended end-plate bolted connection used in the study to assess the structural improvements the CHS column provides. Finally, the adapted plug-and-play joint was compared to its equivalent welded joint. Analysis of the considered configuration showed stiffer and stronger joint characteristics than its equivalent welded joint or comparable bolted joint with HEA column.

The study demonstrates that the novel plug-and-play beam-to-column joint provides significant structural and practical advantages over conventional bolted and welded joints. The proposed connection enhances stiffness and strength while reducing material usage and enabling reusability. Integration of WAAM technology facilitates application to hollow section column, expanding their application in structures. These findings underscore the potential of this plug-and-play connection to enhance construction efficiency and reusability.

Contents

1

Introduction

1.1. Research context

In this era, awareness about the effects of human activity on the biosphere is growing. The urgency of transition of energy sources, reducing the emission of greenhouse gases, recycling and reuse of construction materials, and overall minimise the climate impact is becoming a collective consciousness [1]. The effects of historical and recent human activity are being observed, as all biodiversity hotspots are impacted, to different degrees, by human activities [2]. Not only animals and plants are affected but also human lives, as 11% of the global population lives in cities and settlements near the sea and are living on low-lying coasts directly exposed to interacting climatic and non-climatic coastal hazards [3].

The steel industry has a significant CO_2 emission, 5% of CO_2 emissions in the EU and 7% globally, and therefore needs to develop new technologies and adjust the design philosophy in order to be in line with climate targets and have a lower climate impact [4]. The strategy to decrease the global steel production is partly by improving steel manufacturing, design and construction, extending lifetime of structures and direct reuse of steel components without remelting [5].

A critical aspect of designing steel structures is the detailing of the beam-to-column joints, which are essential to ensure load transfer and overall structural stability. The detailing of these joints requires careful attention to meet all structural requirements while also ensuring material and time efficiency, specifically during installation. The type of joint significantly influences the effectiveness of load transfer, material efficiency, the required time and skills to install the connection and consequently the costs.

The conventional beam-to-column joints are typically classified into two categories: joints with bolted or welded connections [6]. Both types of connections demand significant labour, whether in terms of on-site welding or the installation of components through bolts. The design and installation process for these connections, particularly for on-site welding, is complex, time-consuming and labour intensive, leading to high costs [7].

To adhere to the strategy to decrease steel production the design, manufacturing and installation of joints have to be reconsidered. A different, non-standard approach for the beam-column joints are plug-and-play connections. Plug-and-play connections are designed to be manufactured off-site and for a more simple and rapid installation on-site. In addition, plug-and-play connections can enable reuse of steel structures or structural members and enhance circularity and sustainability of steel structures. This can make plug-and-play connections very suitable solutions to improve steel manufacturing, design, construction, lifetime of structures and direct reuse of steel.

Tubular columns provide several advantages relative to open section columns [8, 9] but due to the limited access to the interior, bolted connections are very limited. Welded connections are more common, but are complex and costly [7]. To utilise wider application of tubular columns, innovative technologies, such as Wire Arc Additive Manufacturing (WAAM), can be employed. WAAM is an innovative 3D steel printing technology build upon welding techniques which is becoming more relevant for the construction sector due to several promising benefits: decrease the production time and the amount of

human intervention, reduce waste of material, and manufacture arbitrary shapes [10]. In comparison to other Additive Manufacturing (AM) methods, WAAM is identified as the most suitable method for application in steel construction because of its relatively high deposition rate, energy efficiency, capture efficiency of the feedstock wire and the ability of the robot to print on large structural members such as columns [11, 12]. By employing WAAM in the application of plug-and-play connections, parts of the connection can be printed on the column surface in a structural and material efficient manner, without the need to access the interior of the column. However, WAAM also presents challenges concerning higher economical and energy costs than conventional manufacturing, high heat input, high residual stresses and distortions [11, 12]. Research considering material properties of WAAM [13, 14, 15] is developing but its application in steel beam-column joints, and in particular to plug-and-play connections, is very limited despite its potential for innovation.

1.2. Problem statement

Conventional joints with bolted connections are well established and design is standardised in Eurocode 3, Part 1-8. Bolted connections offer simple installation and disassembly for reuse or repair. Even though the installation of bolted connections is simple, bolt tightening requires time.

Furthermore, Eurocode 3, part 1-8 does not include bolted connections to hollow sections but only welded connections of hollow sections. Hollow sections have several advantages relative to open sections regarding resistance, aesthetics, fire safety designing and maintenance [8, 9]. Conventional bolting is not possible with hollow sections since there is limited access to the interior of the hollow section to tighten the bolt and the nut. There are several one-side bolts available but those are only applicable to rectangular hollow sections and not to circular hollow sections [8, 16]. Those special fasteners may have limited stiffness or resistance and often lead to increased costs [8].

Due to the limited access to the interior of hollow sections and more advanced knowledge of welded joints than bolted joints of hollow sections, welding is the preferred method in the field [9, 17]. However, welding requires highly skilled labour and extensive quality control due to its susceptibility to discontinuities and defects [17] and subsequently has additional costs.

1.3. Research question and objectives of the Thesis

This thesis will address the following research question:

What novel plug-and-play beam-column joint can be designed to address the challenges of conventional connections, and what is its structural behaviour in terms of stiffness and moment resistance?

The aim of this thesis is to design a new plug-and-play beam-column connection and evaluate its structural behaviour in terms of joint stiffness and moment resistance through numerical modelling. The plug-and-play connection has to be completely manufacturable off-site and ensure a simple and easy installation on-site.

In addition to this, the thesis will pursue several objectives:

- Optimise the plug-and-play connection design for material efficiency.
- Assess the performance of the developed plug-and-play connection to a conventional bolted connection to assess how it performs in terms of stiffness and strength, relative to an established connection.
- Determine the structural response of the individual components of the plug-and-play joint in terms of stiffness and strength.
- Explore the structural and practical opportunities and challenges of integrating WAAM in the plug-and-play connection.
- Explore the adaptability of the plug-and-play connection for use with hollow section columns.

These objectives aim to deliver a comprehensive understanding of the structural behaviour of the plug-and-play joint and evaluate its applicability and limitations.

1.4. Methodology

This section describes the applied methodology to tackle the objectives of this thesis. Figure 1.1 illustrates the applied methodology. The left column shows the strategy to answer the research question. The middle column describes the processes regarding the design of the plug-and-play connection, and the right column describes the processes with regard to the structural analysis of the joints.

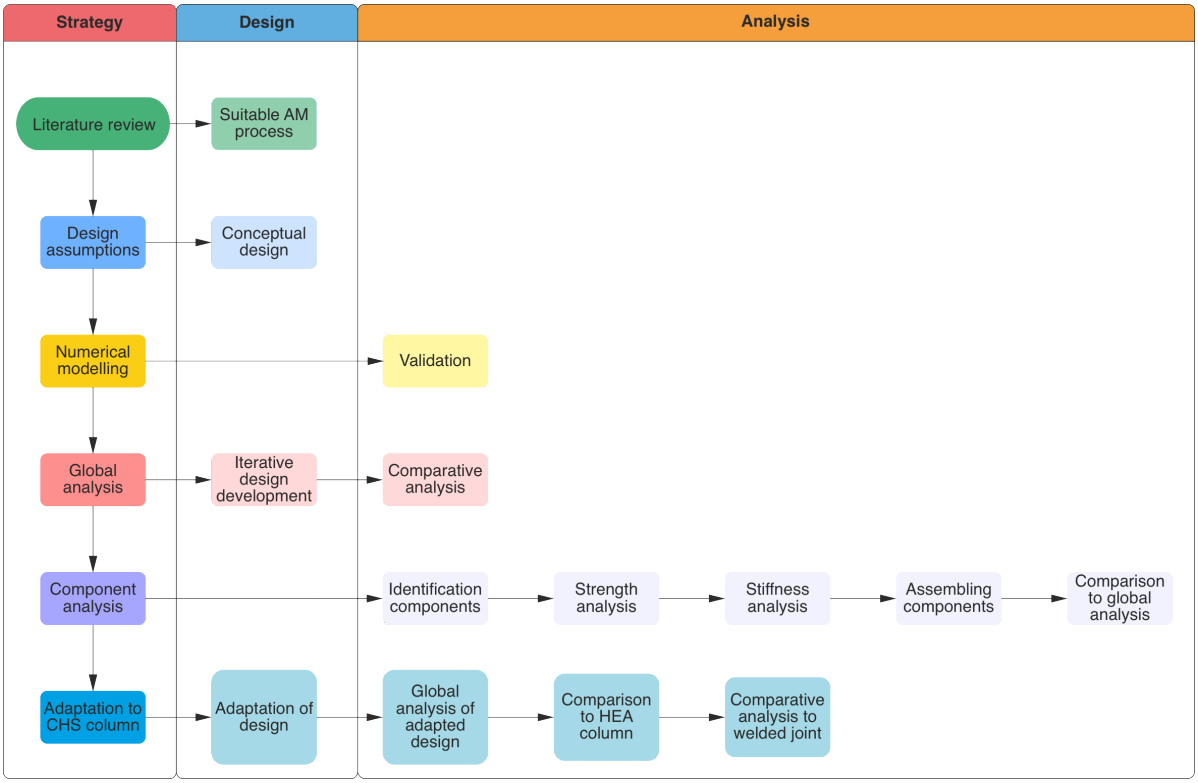

Figure 1.1: Flowchart methodology

Firstly, relevant literature regarding plug-and-play connections, additive manufacturing technologies, and application of AM technology to connections was reviewed. The literature review of the plug-and-play connections displayed the various design aspects and their practical and structural limitations and advantages. The literature review also provided insight in the various AM processes and led to the choice of the most suitable AM process for this study. The review regarding the additively manufactured connections made clear what the challenges and opportunities are for the implementation of WAAM in steel connections. The literature review led to clear requirements for the design of the plug-and-play connection to obtain a practical and structurally well performing joint. A novel plug-and-play connection, which fulfilled the determined requirements, was designed and analysed.

The structural analysis of the plug-and-play connection was conducted through numerical simulations, using the finite element software ABAQUS. The assessments are conducted with numerical simulations because experimental testing was not feasible within the scope of this study. The analysis of the structural behaviour of the plug-and-play joint was divided in two stages: global analysis and component analysis. During the global analysis, the overall behaviour of the plug-and-play joint was analysed and during the component analysis the local behaviour of joint components was analysed.

In order to evaluate the global behaviour of the plug-and-play connection it was chosen to compare its features and structural response to a pre-defined bolted connection. The numerical model of the bolted

connection was validated against an experiment and the test setup of the experiment was consequently adopted in the numerical simulations of the plug-and-play connection.

During the global analysis, the initial concept of the plug-and-play connection was iteratively developed by analysing the Von Mises stress in the connection and adapting the geometry to obtain desired practical features and minimise material usage, without compromising the determined design requirements and structural response. The structural response of the joint is analysed in terms of initial stiffness and plastic moment resistance. To derive these joint characteristics, the moment-rotation curve is formed through extracting and processing corresponding data from the numerical models. The stiffness and moment resistance were determined from the formed moment-rotation curves and compared. The iterative design development led to the final design of the plug-and-play connection.

The final plug-and-play joint is compared to the pre-defined bolted joint in terms of initial stiffness, moment resistance and material usage. An expectation regarding the manufacturing, installation and reuse of the plug-and-play joint was described but no comparative experiments were conducted because the main focus of this study was the structural behaviour of the plug-and-play joint.

During the component analysis the plug-and-play joint was divided into separate joint components which act together to establish the stiffness and moment resistance of the joint. The strength and stiffness of the identified components in the plug-and-play joint were analysed, to evaluate the failure mode of the joint, stress development and distribution in the components and the contribution of each component to the global stiffness and moment resistance of the joint. The methodology to determine the components' strength and stiffness is based on the component method described in Eurocode 3, part 1-8 and an adaptation of an extraction procedure to characterise joint components in numerical models [6, 18]. The resulting strength and stiffness of the components are assembled, and the joint's structural response is compared to the results of the global analysis.

Finally, the insights from the global and component analysis were employed in a proposed adaptation of the plug-and-play connection to a CHS column. The proposal was to illustrate the applicability of WAAM and adaptability of the plug-and-play connection to hollow sections. The numerical model of the plug-and-play connection was modified, and numerical simulations were done. The plug-and-play joint with the CHS column was globally analysed with the method described earlier, and its structural characteristics were compared to the previous configurations to assess the structural impact of the modification of the plug-and-play connection and the column.

1.5. Structure of the Thesis

The structure of this thesis is as follows:

- **Chapter 2: Literature review**
  This chapter provides an overview of relevant research and literature related to plug-and-play connections and various additive manufacturing methods, with a particular emphasis on Wire Arc Additive Manufacturing. The chapter also highlights the gaps in existing studies that this thesis aims to address.
- **Chapter 3: Plug-and-play design**
  This chapter describes the design assumptions and provides a conceptual design of the plug-and-play connection.
- **Chapter 4: Numerical model**
  This chapter describes the process of creating and validating the numerical model for the plug-and-play connection. It includes detailed explanations of the finite element modelling, material properties, boundary conditions, loading protocols, interactions and constraints. The validation against Eurocode 3 and an experimental model is also discussed here.
- **Chapter 5: Global analysis**
  This chapter focuses on the global analysis of the plug-and-play joint. It provides an iterative analysis, during which the conceptual design is developed and finalised. The material efficiency and joint classification of the final design is assessed. In this chapter, the final plug-and-play connection is compared to an equivalent single extended end-plate bolted connection.
- **Chapter 6: Component analysis**
  In this chapter the active joint components are identified and the strength and stiffness of each joint component is assessed. The components' strength and stiffness are assembled to determine the joint behaviour. The contribution of each component to the global joint behaviour is evaluated.
- **Chapter 7: Adaptation to CHS column**
  This chapter proposes an adaptation of the plug-and-play connection to apply it to CHS columns. The joints with CHS columns are compared to the joints with open sections. The plug-and-play joint with CHS column is also compared to an equivalent welded joint.
- **Chapter 8: Conclusion and recommendations**
  This chapter answers the research question. It outlines the limitations of the study, and its main contributions to the field. This chapter also addresses the gap this research fills and provides recommendations for further studies.

2

Literature review

2.1. Plug-and-play connections

A plug-and-play connection in this study refers to an off-site pre-fabricated connection with pairing parts, which joints separate structural members, with no or minimal need for additional fastening, and allows instant use of a structure. Plug-and-play connections aim for a more rapid construction, a simplified construction process, and reuse of structural members, and to eliminate erroneous erection practices by reducing human assistance during construction [17, 19]. Reducing labour and more rapid construction will lead to reducing erection costs [20].

Plug-and-play connections aim to be reusable. Reusability in structural engineering may help develop new design approaches and systems that reduce environmental impact and improve the efficiency of construction. The reuse of steel depends on widespread adoption of the approach in design and construction practices, where designers should understand how to incorporate reclaimed materials in new design applications and how to optimise their designs for deconstruction and reuse. Reusing reclaimed steel is technically feasible but is still not widely applied in practice due to practical barriers, such as availability, quality, traceability and certification of reclaimed sections, and the lack of supply chain integration [21]. In order to further improve the practicality of reuse, structures and connections need to be designed for future reuse. Therefore, disassembly and reuse depends on the followed design principles for the entire structure and not solely on the connection. However, in the design approach it is recommended to design connections relatively simple and to avoid welding [21]. The reusability of steelwork will be limited due to plastic deformation of structural elements and local plastic deformations in connecting elements [21], and should be prevented. In order for plug-and-play connections to be practically reusable it is suggested to meet these design recommendations.

Different plug-and-play connections have unique advantages and limitations. This section explores these different connections and considers their practicality, advantages, and limitations.

2.1.1. INNO3DJOINTS

The European project INNO3DJOINTS developed a plug-and-play joint with the aim to enable modularity, fast and simple construction on-site and reuse [8, 19]. The joint connects cold-formed or tubular trusses to tubular columns. The connection consists of a T-plug which is attached to the top and bottom chords of the truss by a bolted lap joint, and a socket which is welded to the column face, see Figure 2.1 [8, 19].

The installation of the joint is simple with a single downward movement of the truss and bolting of the plug to the socket [19], and does not require highly skilled labour and advanced equipment.

The advantage of this joint is that it enables the use of tubular columns which provide, as mentioned, several advantages relative to open sections [8, 9]. The socket is also applicable to CHS columns [8]. The joint enables the use of cold-formed steel trusses, which leads to weight savings compared to an equivalent hot-rolled solution [19] and is not suitable with blind bolts or other special fasteners [8].

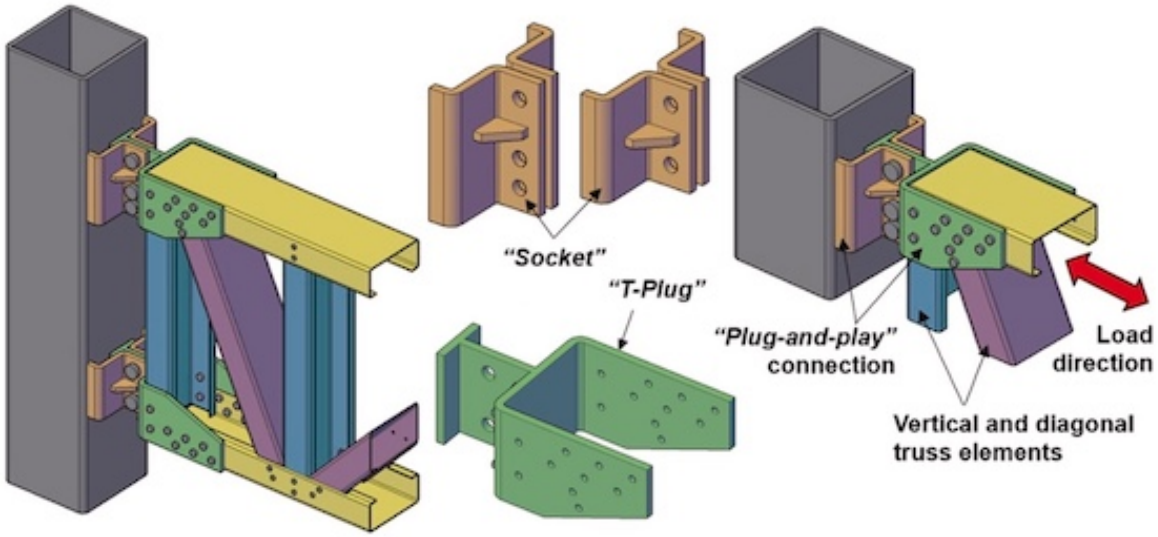

Figure 2.1: INNO3DJOINTS plug & play connection [8].

The joint behaves as semi-rigid and partial strength, allowing transfer of vertical shear and bending moment. Therefore, it is possible to design the structure as a moment-resisting frame. The socket is designed as the critical component and it governs most of the joint's global behaviour, leading to very ductile behaviour. To achieve a pinned joint only the upper chord of the truss has to be connected [8].

A full scale two storey building was erected, tested to the SLS, disassembled and reused in a different location for a different purpose, which demonstrates the reusability of this system [8, 19].

Finally, it is noted that the sockets and T-plugs can be mass-produced, making it cost-competitive [8].

2.1.2. ConXtech connections

ConXtech developed multiple plug-and-play steel beam-to-column connections, namely ConXL300, ConXL400, ConXR200 and Gravity connection. The plug-and-play connections appeal to modular construction and facilitate faster construction [22]. The ConXL series and ConXR200 connections consist of two primary components that function as a plug-and-socket assembly. The joints connect open profile beams to square hollow section (SHS) columns.

The ConXL series consist of a collar flange assembly (CFA) and the collar corner assemblies (CCA), see Figure 2.2. Off-site the CFA is robotically welded to the beam-end and the CCA are welded to the corners of the SHS column to accommodate the CFA, see Figure 2.2b [23, 24].

Installation of the joint is through a downward movement of the beam with collar flanges into the CCA of the column and fastening the CFA's, through the CCA's, to each other with bolts. The CCA has shear lugs which provide temporary vertical support. Only after emplacement of all four beam CFA's, bolts can be inserted into the holes and fastened. Although the installation process is simple and temporary vertical support is provided, the joint provides full support only after fastening all bolts on all four sides of the column, since its vertical load capacity is provided by friction due to the clamping force between the collar flanges and the column [24].

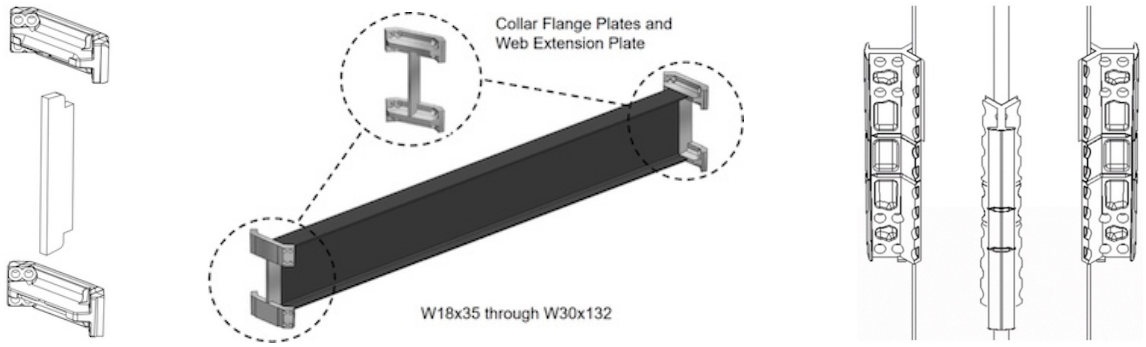

(a) CFA parts **(b)** Beam with Collar Flanges on both ends **(c)** CCA [24]

Figure 2.2: Beam to Collar Flange Assembly [24]

For the ConXR200 the outer collar plates (OC) are off-site welded to the beam-ends and inner collar plates (IC) are welded to the face of the column, see Figure 2.3a. Installation of the ConXR200 joint is through a downward movement of the beam with OC into the IC. The IC provides temporary vertical support. After all beam's are emplaced, bolts can be inserted and the OC's are fastened to each other, providing the required clamp force. An additional bolt is fastening the OC to the IC to provide for uplift shear forces in the beam [24].

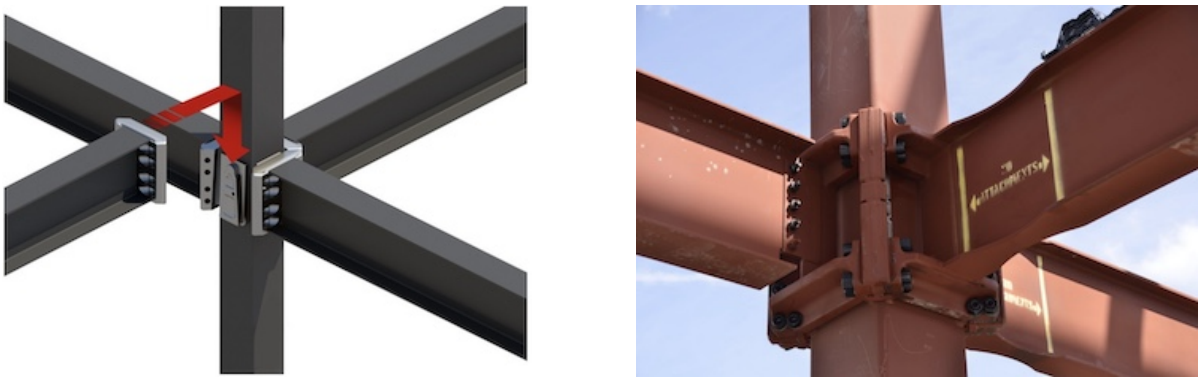

(a) Installation ConXR200 [25]. **(b)** ConXL400 connection [25].

Figure 2.3: ConXR200 and ConXL400

These joints behave rigid and form a moment resisting frame which is also qualified to resist seismic forces [22, 23, 24, 26].

The ConXL400, ConXL300 as well as the ConXR200 connections enable the use of SHS columns. However, this is very limited as they can only be used on 16", 12", 8" SHS sections respectively [24]. The connections are compatible with different beam sizes. The modularity and standardisation of the connections has advantages for construction efficiency but the compatibility of each connection to only one column configuration is very limiting. In different scenarios where smaller SHS columns are sufficient, thus less steel is required, these connections provide no adaptable option. Additionally it is noted that the connection is not suitable with CHS columns.

It is advantageous that no on-site welding is required for any of these connections and inspections are done in a controlled environment off-site instead of on-site [22]. However, as the load capacity of the joint is established by friction through the clamping force of the bolted collars, it is required that on all four faces of the column collars are placed and fastened even when less than four beams are used [24]. The robustness of the collar assembly and the requirement that on all columns a complete, four sided collar assembly is necessary, is very materially inefficient.

It is noted that ConXtech is a commercial company and has realised multiple construction projects with these connections, indicating that they are cost-competitive [22]. However, due to the specific advantages for high-seismic projects it is cost-competitive in those projects but it is expected that for non-seismic projects the cost-competitiveness will be less due to the lower requirements for the joints.

2.1.3. SidePlate connection

The SidePlate connection is a beam-column connection designed to resist seismic loading and progressive collapse [26, 27, 28]. The connection can be designed to connect open section, RHS or SHS beams to open section, RHS or SHS columns in various combinations [26]. The connection is completely pre-fabricated off-site. It consists of two side plates which are welded to the column and on the top of the side plates longitudinal angles are welded. On the top of the beam-end a cover plate is welded and on the bottom two longitudinal angles. The connection consists of simple plates and angles, see Figure 2.4 [28].

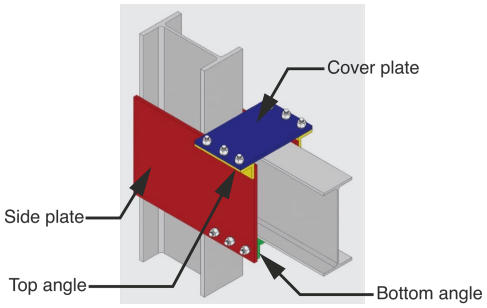

(a) SidePlate with an open section column [modified with names from [28]].

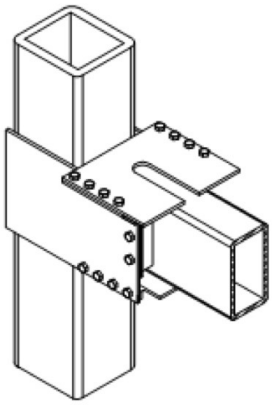

(b) SidePlate with a hollow section column [29].

Figure 2.4: SidePlate field-bolted connection

The installation of the joint is simple with a single downward movement of the beam in between the side plates. The cover plate vertically aligns the connection and provides temporary vertical support to fasten all bolts [30]. It is noted that the bolt holes need to be horizontally aligned prior to the bolting.

The SidePlate connection behaves rigid, full-strength and ductile which is qualified to resist seismic forces [26, 27].

The connection is off-site pre-fabricated by using standard plates and angles without the use of advances manufacturing technologies and does not require on-site welding. It enables the use of SHS and RHS beams and columns but is not suitable with CHS columns. No on-site welding is required but the amount of bolt fastening is significant. Typically a joint requires 12 or more bolts to be fastened [26].

Furthermore, the connection is robust and has a higher material usage than for alternative moment connections, such as stiffened end-plate bolted connections [26]. A built-up box can be assembled to create a biaxial configuration of the joint, see Figure 2.5 [26]. It is advantageous that the joint can be adapted to the required amount of beams but it is very robust and has a high material usage.

Overall, the SidePlate connection provides a connection which is applicable to a variety of column and beam sections in different directions, but it is not an easy connection.

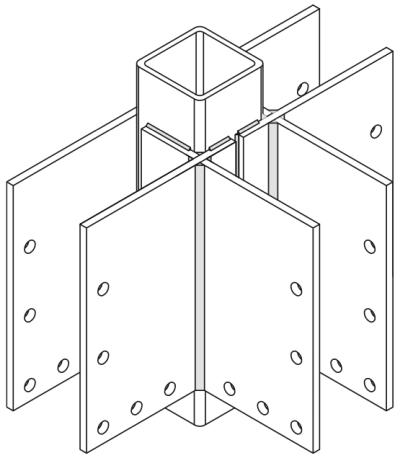

Figure 2.5: SidePlate three-sided configuration

2.2. Additive manufacturing

2.2.1. Available technologies

Additive manufacturing (AM) is an innovative manufacturing process where objects are made from a 3D model data, by successive deposition of material usually layer upon layer [13, 31]. AM refers to a broad range of production technologies which are compatible with different materials such as polymers, plastics, ceramics, concrete and metals [12]. Additive manufacturing is commonly named 3D printing and provides promising advantages over conventional manufacturing techniques, such as a higher level of automatisation, decrease production time and human intervention, greater design freedom, direct production from 3D CAD models and reduce material consumption and waste [11, 12, 13, 32, 33, 34]. The digitisation of complex industrial tasks, through new technologies such as AM, can lead to improved quality of products and overall increase in the performance, and its application in the construction industry is at its early stages and is developing [33, 34].

In case of steel beam-column connections metal additive manufacturing (MAM) technologies are of interest. MAM technologies can directly manufacture a metallic part with a complex shape without an additional manufacturing process or re-fixturing and calibration procedures because it is a complete automated process [12].

For additive manufacturing with metals several types of AM processes exist, which are mainly classified as binder jetting (BJT), directed energy deposition (DED), powder bed fusion (PBF) and sheet lamination (SHL) [11, 31]. These processes mainly differ in the additive materials (metal powder, wire or sheet) and the energy source. The different AM processes have distinct limitations and advantages compared to each other [35]. For application in steel connections the following characteristics are noticed to be priority: the deposition rate which is directly related to printing time, material and energy efficiency, and the possibility to print on large structural members. Wire Arc Additive Manufacturing (WAAM) has been identified as the most suitable AM process for applying to steel connections within this study.

2.2.2. Wire Arc Additive Manufacturing

WAAM is a wire-fed DED process which has, relative to other MAM, lower investment and material costs [10, 12, 35, 36]. WAAM allows higher deposition rates (16.7 - 66.7 g/min) than for PBF processes (1 - 10 g/min) [11, 36]. Furthermore, PBF processes are executed in a build chamber which has a limited size, making it impossible for parts to be printed on large steel columns or beams [10, 35].

Likewise a BJT process is also executed in the build chamber making it impossible to directly apply to large steel members [35]. SHL uses metal sheets which are laser cut, piled up and glued together layer by layer [37] and is very unlikely to allow for the necessary geometric forms or to be viable to apply to construction applications [36].

Within DED processes there are several classifications: Laser additive manufacturing-directed energy deposition (LAM-DED), wire arc additive manufacturing (WAAM), wire and laser additive manufacturing (WLAM) and wire and electron beam additive manufacturing (WEAM), which have different characteristics as shown in table 2.1 [11, 12].

WAAM is preferred over LAM-DED, because the deposition rate of WAAM is remarkably greater [12]. WLAM has a very poor energy efficiency relative to WAAM [11]. Finally, WEAM requires a high vacuum furnace which makes it highly impractical for application to large steel members [11, 12]. WAAM has a relatively high energy efficiency up to 90% and a high material efficiency of approximately 100%. Furthermore, it has a relative high deposition rate [10, 11, 12, 34]. WAAM is executed by a robotic arm which allows to print on large structural members and can print large parts [35, 38], see Figure 2.6b.

WAAM's material efficiency, deposition rate and its applicability to large structural members makes it the practical and optimal choice for application to steel connections within this study.

Table 2.1: Characteristics of DED processes [12]

Feedstock	Process	Typical layer thickness (μ m)	Minimum feature (width) size (μ m)	Density of heat flux (W/mm^2)	Energy efficiency (%)	Working environments	Deposition rate (g/min)	Capture efficiency of feedstock (%)
Powders	LAM-DED	200-500	380-1000	$\approx 10^6$	<40	Shielding gas	<8.3	<90
Wire	WAAM	1000-2000	1000-2000	$\approx 10^4$	<90		16.7-66.7	$\approx$ 100
	WLAM	> 1000	5-15x wire diameter	$\approx 10^6$	2-5		1.5-48.0	
	WEAM	< 3000	<1600	$\approx 10^8$	15-20	Vacuum furnace	< 330	

WAAM is a DED process that is based on welding processes. The principle of the WAAM process is illustrated in Figure 2.6. The feedstock wire is fed through the nozzle to the focused region. A molten pool is formed by melting the previous layer and the feedstock wire in and around the focused region of the formed electric arc. The movement of the nozzle and feedstock are controlled by a robotic arm. As the nozzle and feedstock move away from the molten pool, the material solidifies by cooling of the molten pool and a deposition bead is created. This procedure is repeated along the remaining toolpath to build the 3D metallic part layer by layer [12, 35].

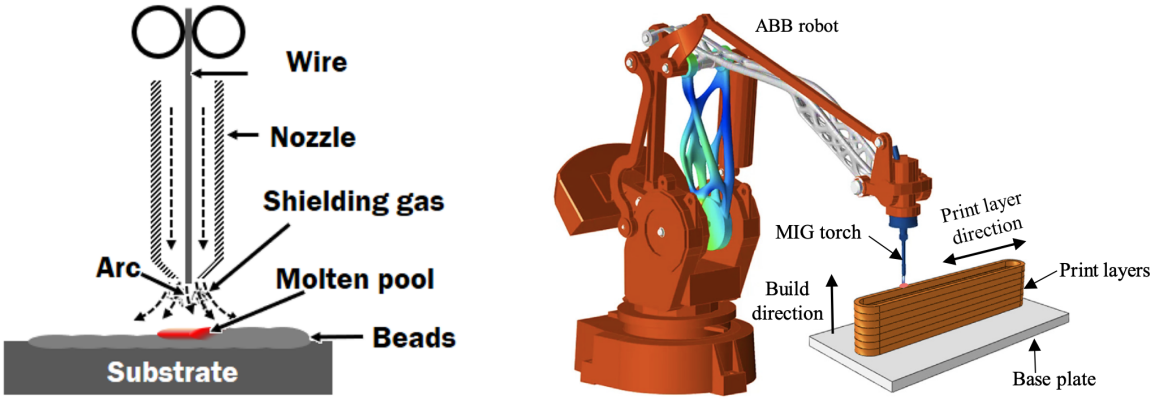

(a) WAAM detail [12]

(b) WAAM robot [11]

Figure 2.6: WAAM process

The WAAM process can be categorised into three types according to the principle of the welding process, namely gas metal arc welding (GMAW), gas tungsten arc welding (GTAW) and plasma arc welding (PAW). The advantages and disadvantages of the different categories are compared in table 2.2. GMAW is the preferred welding process as it has a relatively high deposition rate, and an easier deposition path compared to GTAW and PAW. GTAW and PAW have off-axial feeding of the wire, which requires rotation of the torch to maintain an identical feeding of the direction of the wire, resulting in a complicated path program in the WAAM process. In case of GMAW the wire is feeded through the nozzle which results in an easier deposition path relative to GTAW and PAW [12]. However, GMAW has a poor surface roughness, high residual stresses, relatively greater distortions, and high spattering. Cold metal transfer (CMT) is a modified GMAW to provide spatter-free metal transference and a stable

electric arc and is widely implemented for AM processes [11, 12, 14]. During the CMT process the wire is cyclically moved to the bead, such that molten droplets are deposited. This allows to regularly extinguish the arc at intervals, which results in a lower heat input [39]. The CMT-WAAM process is preferred in this study because of its deposition rate, easier deposition path, and stable and spatter-free welding process.

Table 2.2: Comparison of different WAAM processes [12]

Type	**Advantages**	**Disadvantages**	**Deposition rate (kg/h)**
GMAW	High efficiency and low cost Low initial set-up cost Relatively simpler process Co-axial feeding of wire Relatively easier deposition path	Unstable process in uneven deposition surfaces Low arc stability High spattering Excessive heating Excessive residual stress and deterioration Poor surface roughness Relatively greater distortion	3-4 (CMT: 2-3)
GTAW	Smooth surface finish High strength of the deposited part Reduced porosity Relatively reliable process	Off-axis feeding of wire Change of welding direction Sensitive to arc length Complicated deposition path	1-2
PAW	Narrow high temperature zone compared to GTAW Relatively reliable process Relatively high welding speed	Necessity of rotation of torch	2-4

The WAAM process manufactures a layered steel object. This layer-by-layer process could lead to anisotropic mechanical properties. Tensile coupon tests with different orientations with respect to printing direction, see Figure 2.7, were carried out for a CMT-WAAM manufactured wall [14]. The study found that the WAAM coupons showed isotropic tensile properties, with negligible influence of the tensile samples orientation on the mechanical properties of the WAAM produced wall and that the deposited material resembles steel grade S355.

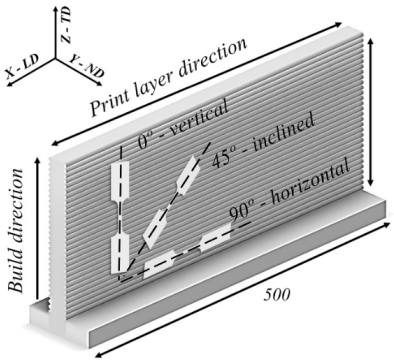

Figure 2.7: Schematic representation of the CMT-WAAM printed wall and orientations of the extracted tensile coupons [14]

2.3. AM connections

As described earlier AM processes provide several advantages such as automatisation of production process, decrease human intervention during production, allow a greater design freedom, design and directly produce from a 3D CAD model and reduce material usage and waste. It is described that WAAM is the preferred AM process within this study but given WAAM's relatively recent application in structural connections, insights from connections with other AM technologies are also evaluated to better understand the potential advantages and limitations of WAAM for connections.

2.3.1. WAAM beam-hook

An innovation of the double angle cleat connection was introduced by Lange et al. [40], as shown in Figure 2.8 and 2.9. In this design, the traditional double angle cleats are replaced by a hook directly WAAM printed onto the column flange. A corresponding component, also WAAM printed on the beam web, serves to transfer the load from the beam to the column. This establishes a pinned connection.

(a) Double angle cleat connection [40].

(b) Concept of beam-hook connection [40].

Figure 2.8: Beam-hook connection

Figure 2.9 shows that it is feasible to WAAM print directly onto the column flange. However, the installation of this beam-hook connection is through vertically lowering the beam in between the columns. The designed connection is practically impossible since the width of the beam's bottom flange will not allow to install it. No alternative installation method is described or considered possible. This highlights that during designing connections the manufacturing, construction and disassembling processes have to be considered along with the structural analysis.

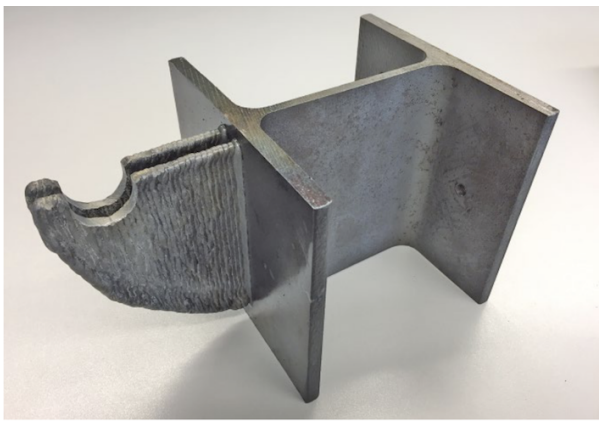

Figure 2.9: WAAM hook printed on column flange

2.3.2. Non-welded N type joint for RHS steel trusses

Figure 2.10 shows a plug-and-play connection for a tension bracing in trusses with rectangular hollow sections, which Szlendak and Szpyrka developed. This N type plug-and-play joint aims to eliminate the need to weld the bracing members with the chord [41]. The joint consists of multiple parts: two RHS chords, two anchor block bases, two anchor block cylindrical covers, a threaded tension bracing, two washers and two nuts, see Figure 2.11. The RHS chord members are 3D laser cut, to create slots in one chord member which functions as the "lock," and to cut the end of the other chord member to function as a "key" which fits into the cut "lock." Also slots for the "teeth" of the anchor blocks are laser cut into the RHS chords. The anchor block bases and cylindrical covers are manufactured with an unspecified AM technology [41]. Taking into consideration that the anchor blocks have a smooth surface finish and tight tolerances [41] the expectation is that a PBF process has been used in manufacturing, and very unlikely a DED process such as WAAM.

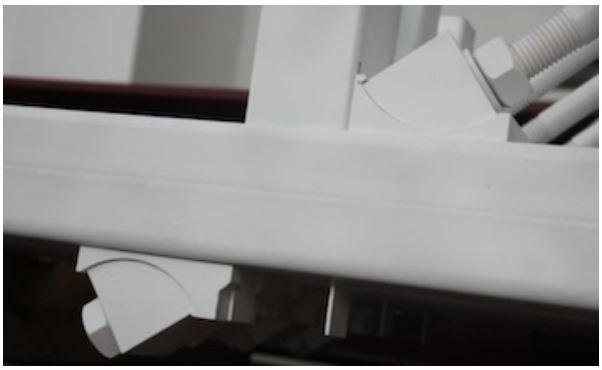

Figure 2.10: Plug & play N type RHS truss connection [41].

Installation of the connection is by inserting the vertical RHS chord, which functions as the "key," into the horizontal RHS chord's slots [41]. The following steps of the installation are not described by the authors. Here the following steps are assumed to be the logical sequence of installation. The anchor block bases are fixed into position by inserting their "teeth" into their slots in the RHS branches. The nuts, washers and cylindrical anchor covers that are located at the inner side of the truss are assembled on the bar. The bar is then inserted through the anchor block bases and RHS branches. Finally, the outer side cylindrical covers, washer and nuts are assembled, and the connection is fastened by tightening the nuts.

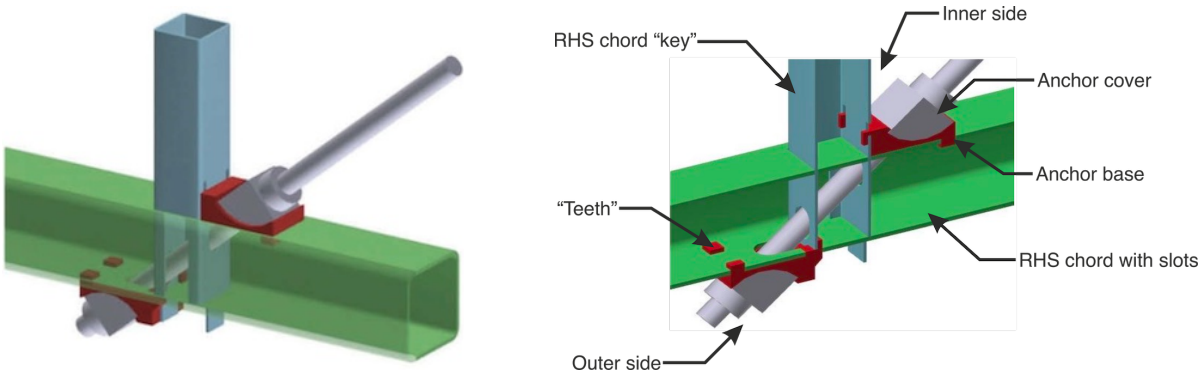

(a) Transparent view [42]

(b) Section view [modified with names from [41]]

Figure 2.11: View of components of non-welded N type RHS truss connection

Although the authors state structures with such joints are easy to assemble and disassemble [41], they

do not describe the process to assemble and disassemble and have not demonstrated its ease. A possible, logical installation sequence, as described above, indicates that the installation is complex, as it contains multiple steps with multiple parts. After inserting the first vertical RHS branch into the horizontal RHS branch, the vertical RHS branch is not fixed yet and is expected to be unstable unless the insertion of the "teeth" of the anchor block bases into the chords provide sufficient stability for the vertical branch, to continue the installation easily. Furthermore, the tension bracing is inserted through the RHS branches and is tightened on the outside of the frame, thus the needed length of the brace is much longer than the inner diagonal of the frame. To make the installation of the brace possible a turnbuckle is required, which allows the length of the brace to be adjusted, to insert the brace-ends through their corresponding holes. This means an additional step in the installation sequence and further complication of the installation procedure. Finally, the insertion of the brace is through eight holes in the anchor blocks and RHS branches which are not visible, possibly making the insertion complicated.

The manufacturing process of the joint requires several advanced technologies. The RHS chords are 3D laser cut and the anchor blocks are manufactured with an AM technology [41]. Taking the complexity of the cut slots and geometry of the anchor block, an alternative manufacturing method is unlikely. The tight tolerances of the slots and holes can be problematic [41]. It is expected that the production costs for the N type plug-and-play joint will be higher than for the typical welded joint, making the joint not cost-competitive.

2.3.3. Arup - optimised structural building element

Arup, an international engineering firm, explored the use of AM for designing over a thousand unique structural nodes for a street lighting project in the Netherlands. Due to the irregular shapes and unique attachment angles, conventional manufacturing includes high labour intensity. To address this Arup explored the opportunity to produce these nodes faster and in a smarter way using additive manufacturing, specifically Direct Metal Laser Sintering (DMLS) [43].

Through topology optimisation the achieved nodes were 75% lighter and half the original height, contributing to a 40% reduction in the structure's overall weight, see Figure 2.12. This demonstrates that AM, particularly in complex structural applications, can simplify the manufacturing process and enable lighter, optimised connections that would be challenging to produce using traditional methods. However, AM requires advanced computational skills and tools to develop the topology optimised structural nodes. At time of this project in 2014 the additively manufactured nodes cost roughly three times that of a conventionally produced node [36].

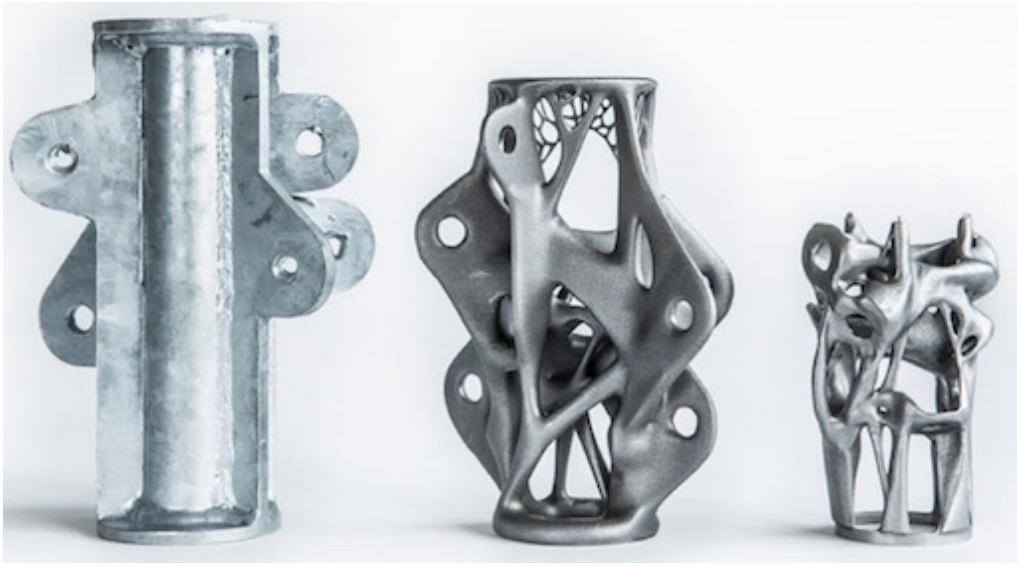

Figure 2.12: Models of the structural nodes. Traditional (left), first optimized node (middle) and final optimized node (right) [43].

While this project used DMLS rather than WAAM, the case illustrates AM's potential to enhance material efficiency and customisation but is very cost expensive. However, this example illustrates that the

possibilities AM caused an innovative design approach. The approach was to produce the nodes in a faster and smarter way due to the customised shapes and optimise material usage to minimise the total structural weight [43]. During the optimisation process the Von Mises stress was analysed to remove material when it was less loaded [43].

2.3.4. The Glass Swing

The Glass Swing, illustrated in Figure 2.13a, is a project from Delft University of Technology within a series of projects of glass vector active structures. This project integrates topology optimisation to strategically place material, resulting in a design that focusses on the structural function of the glass [44]. Due to the geometrical complexity of the nodes to connect the glass elements, as shown in Figure 2.13b, WAAM was chosen to manufacture tubular extensions on a cast steel sphere. This avoids the challenges associated with conventionally cutting and welding plates and tubes to create complex, multi-angle connections [44].

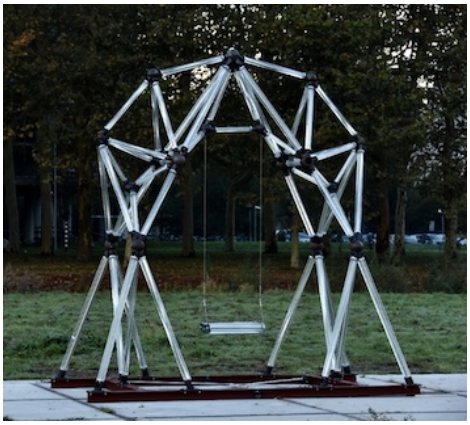

(a) Overall view [44].

(b) The upper node of the Glass Swing [44].

Figure 2.13: The Glass Swing at TU Delft

Although WAAM provided a feasible solution for fabricating these complex nodes, WAAM's inaccuracy complicated the installation. It was noted that no tolerances were included in the design strategy, a consideration that would reduce installation difficulty in future applications. Another contributing factor to the inaccuracy was insufficient cooling time during the printing process, allowing geometrical distortions [44].

For future applications, it is essential to incorporate design tolerances to improve the ease of installation. Finally, gaining further experience with WAAM will contribute to a more inclusive design approach, where machine and rotary movements, process parameters, cooling time, printing strategy, tolerances and practical installation requirements are all considered integrally within the design phase.

2.3.5. Connector for Takenaka

The Dutch company MX3D is famous for its 3D WAAM-printed steel bridge in Amsterdam [45]. In a collaboration with a Japanese engineering firm Takenaka they developed a complex connector for an organic structure, see Figure 2.14. The aim of the project was to automate the design and production of complex connectors in large structures in the building industry. This innovation can provide solutions for countries where skilled labour is less available i.e. due to ageing populations [46].

(a) Connector for Takenaka [46].

(b) Structure of Takenaka [46]

Figure 2.14: MX3D connector for Takenaka

The connector was manufactured using duplex stainless steel which provides good corrosion resistance [47]. To improve structural efficiency, the connector design incorporates internal openings that allow filling with mortar. This strategic addition of mortar significantly enhanced the buckling resistance and ultimate strength of the connector while reducing 50% of the printing material [46].

This connector exemplifies WAAM's advantage in producing customisable parts that can optimise material usage and structural performance. However, it also shows that WAAM technology and experience is not widely available. This implies that custom developed connectors are expected to be complex to develop and expensive to manufacture and transport.

2.4. Summary

The presented plug-and-play connections indicate the advantages and limitation of modular connections and the need for new plug-and-play beam-column connection. Connections such as ConXtech provide and the SidePlate connection are cost-competitive in high-seismic regions and have shown advantages during construction, but it is expected that their cost-competitiveness and application in non-seismic regions will be limited. INNO3DJOINTS's plug-and-play connection is expected to be cost-competitive and applicable in non-seismic regions but is not developed as a beam-column connection. If a single T-plug and socket would be adapted and applied to provide a beam-column connection, it is expected to establish a pinned joint and not a semi-rigid and partial strength joint. So there exists a gap in the field for a well-developed plug-and-play beam-column connection which provides a semi-rigid and partial strength joint.

The connections which incorporate AM indicate that AM has the potential to be applied in beam-column joints but have challenges and the approach has to develop. The design approach with incorporating AM requires knowledge of the AM process to integrally consider the manufacturing process, required tolerances, costs and other mentioned aspects. The application of WAAM can provide a solution to enable the use of hollow sections, as the nodes of the Glass swing showed WAAM's applicability to curved hollow surfaces. However, WAAM has practical challenges which have to be addressed in the design phase. Considering the costs and practical limitations the application of WAAM in connections is considered to be limited to a minimum.

3

Plug-and-play design

The design of the plug-and-play connection is based on the practical limitations and advantages which have been observed in the connections presented in the literature review and the absence of a plug-and-play semi-rigid and partial strength beam-column joint in the field. A semi-rigid and partial strength joint allows to design a structure as a moment-resisting frame [8] and can provide several benefits such as sufficient lateral bracing for usual wind loads in low-rise buildings to prevent the use of bracing elements and more distribution of the bending moments in the structure [48].

Within this study monotonic loading was applied. While cyclic loading is important for analysing joint behaviour in terms of fatigue, crack propagation, ductility, energy dissipation and structural integrity, it is beyond the scope of this thesis.

Considering that the plug-and-play joint was intended to be semi-rigid and partial strength, the monotonic load application and that bolted connection can be reused, a single extended end-plate bolted connection was taken as the basis for the plug-and-play design. The single extended end-plate bolted connection was designed according to Eurocode 3, Part 1-8 to be semi-rigid and partial strength. This bolted connection functioned as the established connection to which the plug-and-play connection is compared to. The plug-and-play connection design is developed from this bolted connection, as described below.

This section further describes the design assumptions for the plug-and-play connection, and presents a conceptual design of the connection which fulfils these assumptions.

3.1. Single extended end-plate bolted connection

The configuration of the single extended end-plate bolted connection is presented in Figure 3.1. The column was a HEA300 section, and the beam an IPE400 section. The 15 mm thick end-plate is 190x500 mm^2 with bolt holes Ø26 mm for eight M24 10.9 full-threaded bolts.

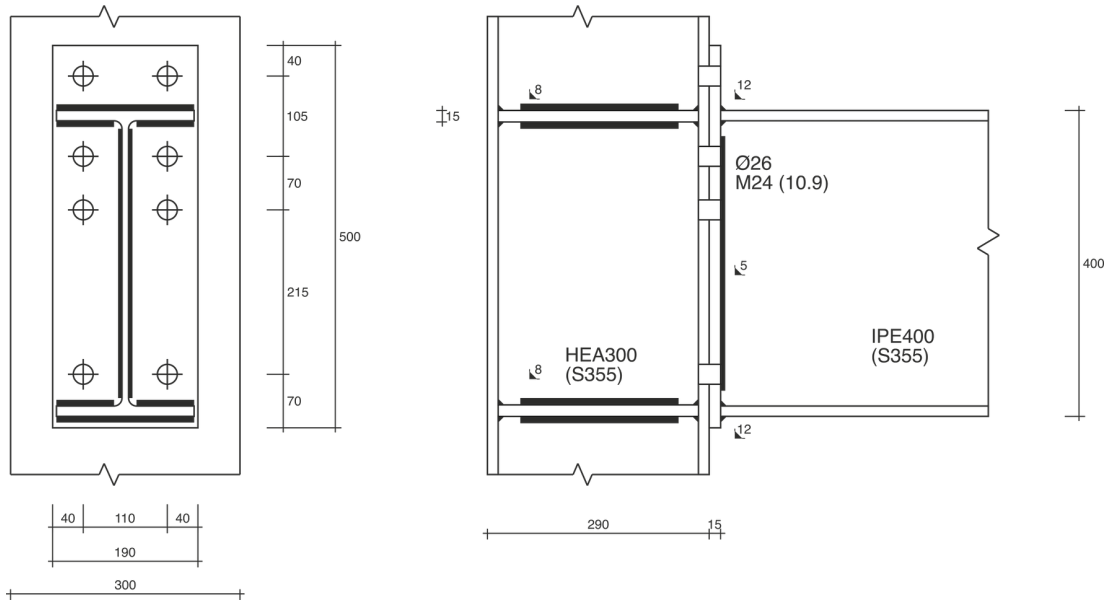

Figure 3.1: Details of the single extended end-plate bolted joint

The joint characteristics are determined with the component method, described in Eurocode 3, Part 1-8, and shown in table 3.1.

Table 3.1: Joint characteristics single extended end-plate bolted connection

	$M_{j,Rd}$ [kNm]	$S_{j,ini}$ [kNm/rad]
Component method	305.46	58911.65

3.2. Design assumptions

The following design requirements for the plug-and-play connection follow from the limitations and advantages which have been observed in the literature review.

- The joint must equal stiffness and moment resistance as the equivalent single extended end-plate bolted connection and provide a semi-rigid and partial strength joint, as the INNO3DJOINTS does. This will allow a structure to be designed as a moment-resisting frame, prevent the use of bracing elements and distribute the bending moments in the structure [8, 48].
- The design has to be simple [21] to facilitate easy and fast installation, unlike the N type connection.
- The design has to avoid on-site welding, so the connection can be reusable [21] and to avoid the need for highly skilled welders and extensive quality control of the welds [17].
- The design should be easily demountable and reusable, as the INNO3DJOINTS plug-and-play joint does, to be more sustainable.
- The design must allow complete off-site pre-fabrication to appeal to modularity, as is the case for INNO3DJOINTS, ConXtech and SidePlate connections.
- The connection has to offer immediate support after beam emplacement, and there should be no need for bolt fastening, to improve construction efficiency and safety.

- The connection has to require only one labourer on each side of the beam-end, like the SidePlate connection does [30].
- The installation should be accomplished by a single downward movement of the beam, as the INNO3DJOINTS, ConXtech, and Sideplate connections, and avoid various steps like the N type connection.
- The connection has to be capable to allow application on any side of a column, individually or simultaneously, like the INNO3DJOINTS and SidePlate connections. The ConXtech connections do not require a beam to be installed on each side but require the collar flange assembly on all sides, which has to be prevented in this plug-and-play connection's design.
- The connection has to be applicable to various column and beam configurations, unlike the ConXtech connections which are only applicable to one SHS column.
- The design should be applicable or adaptable to different column configurations, such as SHS, CHS, RHS and open sections, like the INNO3DJOINTS connection does.
- The use of additive manufacturing should be minimised as it is cost- and energy-expensive, as illustrated by ARUP's structural nodes, and has practical limitations, as the N type connection and the Glass swing's nodes showed.

3.3. Conceptual design

The plug-and-play connection consists of three parts, namely the two pins, the grip-plate and the compression foot. The grip-plate resembles the end-plate. The grip-plate is subdivided in three parts, namely the back-, middle- and front-plate. The back-plate has the same dimensions as the end-plate, namely 190x500 mm^2, but is thinner, 9 mm. The front- and middle-plate are long enough to contain the pins' height. The grip-plate contains slots where the pins fit into, to transfer the tensile stresses from the beam to the pins.

The pins resemble the upper three bolt rows of the bolted connection. They contain the same volume of steel as the upper three bolt rows, which are loaded in tension, as it is expected that the pins will be likewise loaded in tension. The pins are positioned at the same location on the width of the column flange. The top of the pins is at the same position as the upper bolt row. The pin consists of a pin shank and a pin face. The pin shank is smaller than the pin face, to function as a plug to the grip-plate.

The compression foot leans onto the column flange without mechanical fastening and transfers the compressive stresses from the beam to the column.

The conceptual design for the plug-and-play connection is illustrated in Figure 3.2.

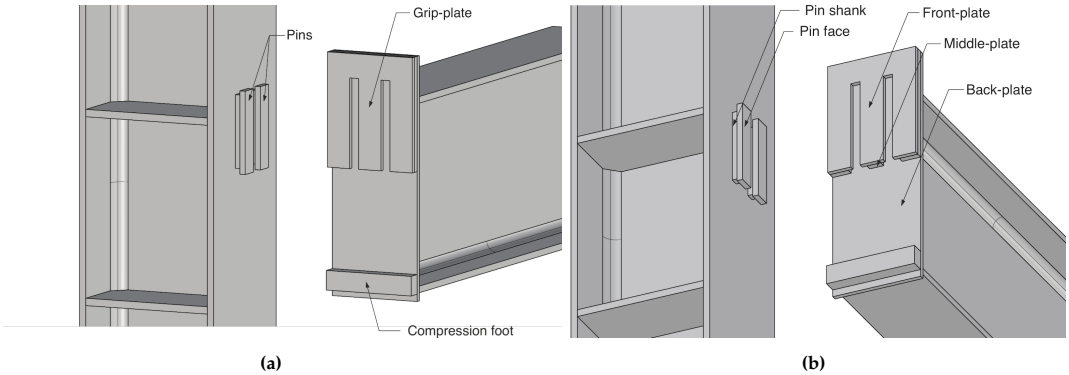

Figure 3.2: Conceptual design plug-and-play connection

The connection is established by two simple movements of the beam. First the beam is horizontally positioned to align the pins with the pin slots. Then, the beam is vertically lowered to insert the pins in the grip-plate, and the connection is established.

This conceptual design of the plug-and-play connection fulfils the determined design requirements.

- The plug-and-play connection is completely off-site manufacturable and avoids on-site welding.
- The connection is relatively simple and has affiliation with the single extended end-plate bolted connection.
- The installation is accomplished by two simple movements. The beam is horizontally position to its correct position and vertically lowered to fit the pins in the slots of the grip-plate. The horizontal positioning of the beam is inherent for every connection but due to the limited space between the front- and middle-plate and the compression foot and considering the height of the pins, it requires accurate guidance. Hence, this horizontal positioning is mentioned as an additional installation step.
- The design provides sufficient space between parts for installation. The space between the grip-plate and compression is greater than the height of the pins, to allow the beam to be horizontally positioned.
- Due to the simple installation it is expected to be rapid.
- Due to the simple installation it is expected to require only one labourer on each side of the beam.
- The design is likely to support demounting and reusing the connection. Demounting the connection is easy, by vertically lifting the beam and horizontally removing it. The reusability of the connection is depending on local plastic deformations in connecting elements [21] and needs to be determined during the component-level analysis.
- The connection provides immediate support after position the beam on its correct position and does not require any bolt fastening or other actions.
- The connection can independently be applied to any column side, as only pins are required on the respective column flange.

The requirement that the plug-and-play joint must equal stiffness and moment resistance as the equivalent single extended end-plate bolted connection was analysed during the global analysis. The plug-and-play joint's structural performance is compared to the bolted joint's performance during the global analysis. This conceptual design will be further developed during the global analysis.

This concept of the plug-and-play connection is created to compare it to common connections, with H and I profile columns and beams, but can later be extended to be applicable to hollow section columns. The details of the conceptual plug-and-play joint are presented in Figure 3.3.

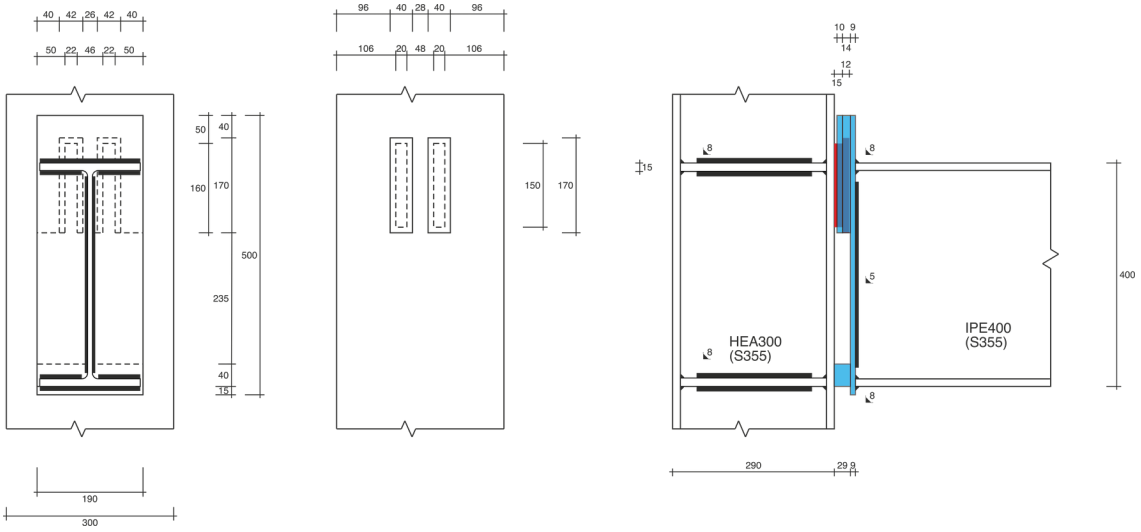

Figure 3.3: Details of conceptual plug-and-play joint

3.4. Summary

The developed plug-and-play connection avoids observed limitations in the presented connections in the literature review and utilises their advantages. The design of the connection is simple and it provides immediate support after a very simple installation process. The connection is compact and does not require on-site welding or even bolting, which is a feature not found in any of the presented connections. In the following section the numerical models of the single extended end-plate bolted connection and the conceptual plug-and-play connection are detailed.

4

Numerical model

ABAQUS finite element software was used for numerical modelling and simulation. In this section first the test setup of the single extended end-plate bolted connection numerical model is described. Then the employed element type is specified and the modelled parts and assembled model are presented. Thereafter the material properties are defined, followed by a description of the constraints and interactions between parts and surfaces, the mesh, steps and loading of the model.

This section then follows to describe the method by which the data is analysed and the joint characteristics are determined. The determined joint characteristics are then compared to the component method from Eurocode 3, part 1-8, to validate the numerical model of the single extended end-plate bolted connection.

Finally, this section describes how the single extended end-plate bolted connection numerical model is modified to the plug-and-play connection numerical model. This numerical model forms the foundation for analysing the structural behaviour of the plug-and-play connection

4.1. Test setup

The test setup for the simulations consists of a 3.0 meter high column, an 1.15 meter long beam, a 15 mm thick single extended end-plate and eight M24 bolts and nuts.

The column is a HEA300 profile supported at its top and bottom. The top of the column is supported horizontally but allows vertical displacement and rotation around the x-axis. The bottom of the column only allows rotation around the x-axis. The column is stiffened with transverse stiffeners, which are aligned with the beam flanges.

The beam is an IPE400 profile, which is connected with 45° fillets to the end-plate. The end-plate contains eight holes of 26 mm to fit the bolts. The load is applied to the open beam-end as a displacement in a constant rate, which creates a bending moment in the joint. No axial force is applied to the column. This test setup was adopted from the experiment that served as a validation for the numerical model, see Appendix A. Figure 4.1 shows the test setup, with the corresponding geometrical properties listed in Table 4.1.

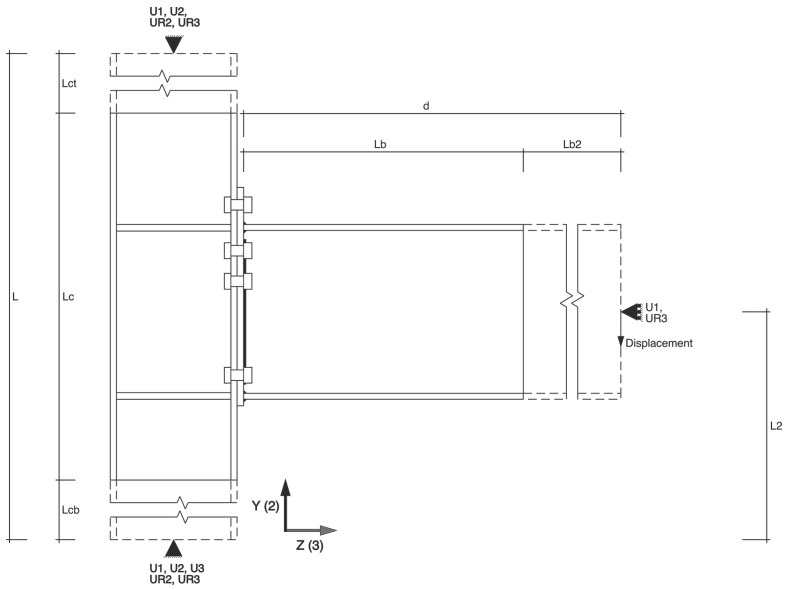

Figure 4.1: Test setup bolted connection numerical model

Table 4.1: Geometrical properties of bolted connection numerical model

L (mm)	3000
Lc (mm)	740
Lct (mm)	1375
Lcb (mm)	885
L2 (mm)	1220
Lb (mm)	468
Lb2 (mm)	680
d (mm)	1148

4.2. Modelling options

4.2.1. Element type

The numerical model employs solid elements from the ABAQUS/standard solid element library, as the analysis requires consideration of both geometrical and material nonlinearities, which involves contact interactions, plasticity and large deformations.

Specifically, the model is constructed using C3D8R finite elements, which are 8-node linear brick elements characterised by three degrees of freedom per node, making it suitable for three-dimensional analysis. Reduced integration is used to enhance computational efficiency. However reduced integration can lead to hourglassing due to the reliance on a single integration point at the centre of the element. To mitigate this issue, enhanced hourglass control is employed, to ensure numerical stability throughout the analysis. Additionally, at least three layers of elements are maintained across the thicknesses of the structural components to accurately simulate stress distribution and deformation patterns.

4.2.2. Parts

The individual parts of the joint region in the model are illustrated in Figure 4.2. The dimensions of the parts are according to the details provided in Figure 3.1.

The highest stress concentrations and deformations are expected in the joint region. To reduce computation time the column is divided in three sections: the column in the joint region, the top and bottom column parts. The column part in the joint region has a finer mesh to more accurately simulate the stress distribution and deformation in the joint. The top and bottom column parts have a coarser

mesh to reduce the computation time and not exceed the available memory capacity. The height of the column in the joint region is determined to be such that the stresses in the top and bottom column parts have dissipated or their influence is not relevant to the structural performance of the joint. It is noted that the height of the column in the joint region therefore is flexible to adjust to different configurations and load scenarios where the joints influence is larger or smaller. Similarly, for computational efficiency the beam is divided into two parts, where the column side beam-end has a finer mesh than the open beam-end.

For simplicity, the bolt and nut are modelled as a single part. The remaining parts, the end-plate and stiffeners, are modelled as individual parts with the described dimensions.

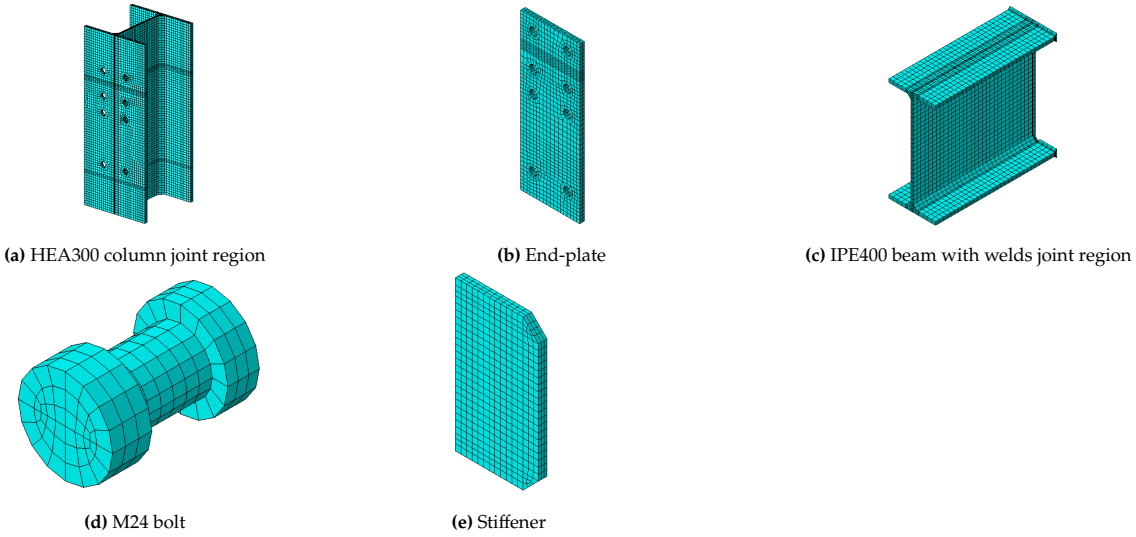

(a) HEA300 column joint region

(b) End-plate

(c) IPE400 beam with welds joint region

(d) M24 bolt

(e) Stiffener

Figure 4.2: Parts in joint region

As a simplification of the fillet root of the column and beam profiles, the fillet is modelled as a triangle with an equivalent area, see Figure 4.3 and equation 4.1. This approach intends to avoid distorted elements in the mesh [18].

$$r_t = r_c \sqrt{\frac{4-\pi}{2}} \tag{4.1}$$

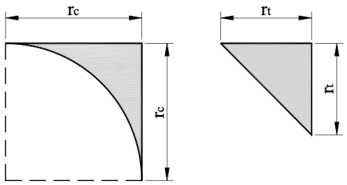

Figure 4.3: Equivalent fillet root [18]

The different parts are then positioned and connected according to the test setup, as shown in Figure 4.1, for simulation. In the assembly the orientations, interactions, constraints and boundary conditions are defined in accordance to the experiment [49], described in Appendix A, which served as the validation of the numerical model. The assembly is critical for the simulation, as the accuracy of the assembly directly influences the model's overall stability, response and performance. Figure 4.4 illustrates the joint region of the assembled model.

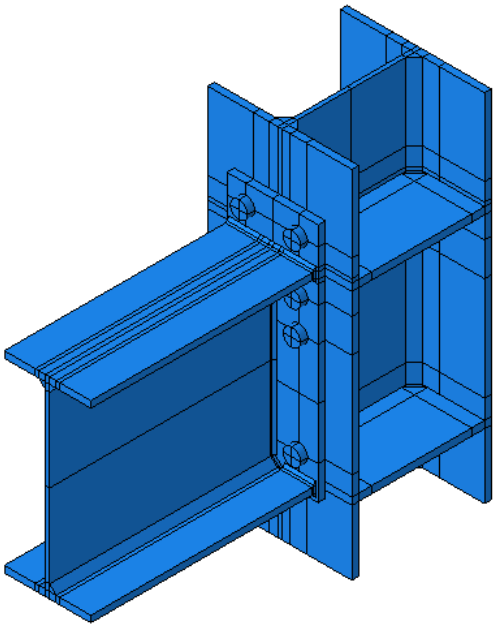

Figure 4.4: Assembled numerical model

4.2.3. Material properties

The material properties in the numerical model are derived from the average mechanical properties of tensile tested steel coupons in the experiment [49]. Steel coupons were extracted from the web and flanges of the beam and column, end-plate and stiffeners. The material properties of the bolts are also derived from the average mechanical properties of tensile tested bolts in the experiment [49]. ABAQUS requires the true stress and true plastic strain data as input for the material properties. The material properties of the tensile coupon tests are converted to the tri-linear true stress and true strain data, as shown in table 4.2 [18]. These material properties are used in the numerical model.

Table 4.2: Mean true stress and true strain mechanical properties of materials [18]

Section	Part	Yield true stress [MPa]	Ultimate true stress [MPa]	Ultimate true strain [%]	Young's modulus [MPa]
IPE400	flange	430.897	430.897	0.000	206650
			637.330	0.137	
			671.968	0.220	
	web	449.139	449.139	0.000	214270
			641.364	0.145	
			675.754	0.228	
HEA300	flange	415.600	415.600	0.000	205520
			621.738	0.154	
			664.941	0.251	
	web	450.574	450.574	0.000	208070
			636.410	0.137	
			665.630	0.212	
End-plate		393.640	393.640	0.000	208990
			596.220	0.128	
			629.064	0.212	
Stiffener		286.798	286.798	0.000	206330
			542.160	0.180	
			569.720	0.260	
Bolt 10.9		994.591	994.591	0.000	214490
			1182.87	0.005	
			1242.44	0.028	
Welds		440.908	440.908	0.000	213660
			659.8800	0.197	
			687.204	0.228	

The WAAM material properties follow from tensile tested coupons, with different orientations with respect to printing direction, from a CMT-WAAM manufactured wall [14]. The WAAM material properties are listed in Table 4.3.

Table 4.3: WAAM material properties [14]

Feedstock wire	Condition	Build direction	Yield stress [MPa]	Ultimate stress [MPa]	Ultimate strain [-]	Young's modulus [MPa]
ER70S-6	As-built	Vertical 90°	335.8	462.6	0.171	214000
		Inclined 45°	318.7	447.0	0.174	
		Horizontal 0°	303.8	428.2	0.183	
	Machined	Vertical 90°	375.7	501.5	0.192	
		Inclined 45°	383.7	511.8	0.182	
		Horizontal 0°	373.2	499.3	0.193	

4.2.4. Constraints and interactions

Interactions describe the mechanical contact between surfaces in the numerical model and constraints define the constrained degrees of freedom between regions of the model. The constraints and interactions between the various surfaces and regions of the model are detailed below.

To impose the required boundary conditions of the column, reference points are created at the centre of the top and bottom surfaces of the column. These reference points are constrained to the column surfaces using rigid body constraints. The boundary conditions are then applied directly to these reference points, ensuring that the appropriate degrees of freedom are constrained. This technique ensures consistent behaviour across all nodes within the constrained region, eliminating potential local effects and it simplifies post-processing data because the reaction force can be obtained from the reference point only instead of extracting the reaction stress from all nodes in the surface and calculating the reaction force.

A similar approach is applied to the open beam-end, where a reference point is created at the centre of the open beam-end surface. This reference point is also constrained using a rigid body constraint. The load is applied directly to this reference point and the reaction force is easily obtained from the reference point.

The fillet welds are modelled directly on the beam and constrained to the corresponding regions of the end-plate using a tie constraint. A tie constraint constrains all degrees of freedom of the secondary surface to the main surface. The fillet welds surfaces serve as the main surface and the region of the end-plate which is in contact with the fillet welds serves as the secondary surface, thus follows the motion of the fillet welds.

Furthermore, the transverse stiffeners are constrained to the corresponding column flanges and web surfaces using tie constraints. In this case, the column surfaces act as the main surfaces, while the stiffeners' serve as the secondary surfaces, ensuring that the motion of the stiffeners follows the column's.

Normal behaviour of contact interactions is modelled by the general contact algorithm, which applies hard contact formulation for the pressure-overclosure relationship. This ensures that no penetration occurs between surfaces when they come into contact and allows the transfer of compressive stresses, while permitting separation of the surfaces once contact is lost [50].

In the numerical model, the tangential behaviour of the contact interactions was defined using the penalty friction formulation. A friction coefficient of 0.3 was applied, meaning the tangential force resisting sliding was set to 30% of the normal force. This approach allowed for realistic stick-slip behaviour at the contact surfaces, ensuring accurate simulation of frictional effects while maintaining computational stability.

4.2.5. Mesh

A finer mesh is applied in the joint area to accurately simulate stress and deformation, where the highest concentrations are expected. In the regions adjacent to the joint, a coarser mesh is used to reduce computation effort without compromising accuracy.

In order to maintain accuracy in critical regions, the mesh seeding is locally controlled. A minimum of three elements is maintained through the thicknesses and a finer seeding density is applied around bolt holes to ensure a more detailed stress simulation in these regions.

The mesh size is adopted from the double extended end-plate bolted connection numerical model. Therein a mesh sensitivity analysis was conducted to determine the optimal mesh size, see Appendix A. The moment-rotation curves and initial stiffnesses of several models with different mesh sizes were compared to determine for which mesh size the results converge and computation time and required memory is limited. The global seed sizes of the generated mesh are listen in Table 4.4. In the perimeter of the bolts holes additional seeds are created, such that 20 elements are generated in the perimeter.

Table 4.4: Global seed sizes

Part	Global seed size
Column top	30
Column joint region	10
Column bottom	30
End-plate	10
Bolts	5
Beam - column side	10
Beam - open end	20

4.2.6. Steps and loading

The analysis of the model is organised into three sequential steps, which are conform to the validation experiment [49]. In the first step, the boundary conditions are established at the reference points on the top and bottom of the column, according to Figure 4.1.

In the second step, the bolts are pre-tensioned to 20% of their ultimate strength. The pre-tensioning load is applied to the shank areas of the bolts. After this pre-tensioning step, the lengths of the bolts are fixed at their current lengths and are propagated to the third step.

During the third step, a downward displacement of 100 mm is applied to the reference point at the open beam-end, resulting in a bending moment and shear force in the joint. This displacement is applied at a constant rate.

Throughout all loading steps, non-linear effects related to large deformations and displacements are considered. The maximum increment size of the loading steps is set at 0.05, ensuring that at least 20 increments are executed during the simulation. This allows to generate sufficient data points during simulation, to analyse the development of stresses and deformations.

4.3. Data analysis

As described in the methodology, the global analysis is done by determining the stiffness and moment resistance characteristics from the moment-rotation curve of the joint. The moment-rotation curve is formed through processing extracted data from the numerical model. The moment and rotation of the joint are determined at the column-side beam-end. The influence of beam deformation is avoided, as the global analysis is considered at the interface of the column-side beam-end and end-plate.

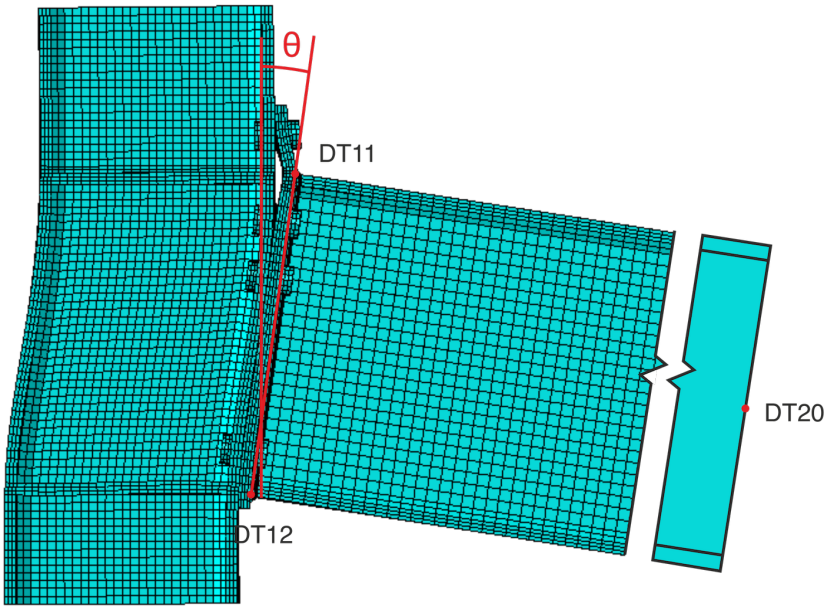

Figure 4.5: Global rotation

Nodes DT11 and DT12 are, respectively, located at the top and bottom of the beam flanges, in the middle of the column-side beam-end, see Figure 4.5. The horizontal displacements of these nodes are extracted from the model, to determine the rotation, θ in Figure 4.5. A straight line is assumed between nodes DT11 and DT12, which represents the beam-end. This line forms an angle with the vertical axis, which includes both the rotation of the beam-end and the elastic deformation of the column. The elastic deformation of the column, see equation 4.3, is extracted from the total rotation to obtain the contribution of the joint to the rotation [18]. RF_{DT20} is the reaction force at node DT20, due to the imposed vertical displacement. The global rotation of the joint for each increment is calculated using equation 4.2.

$$\theta_{global} = arctan\left(\frac{DT11_{U3} - DT12_{U3}}{\overline{DT11DT12}}\right) - \theta_{el.column} \tag{4.2}$$

$$\theta_{el.column} = \frac{\frac{RF_{DT20} \cdot d \cdot L_2^2}{L} + \frac{2 \cdot RF_{DT20} \cdot d \cdot L}{6} - RF_{DT20} \cdot d \cdot L_2}{E \cdot I_{zz,column}} \tag{4.3}$$

Node DT20, see Figure 4.5, is the reference point at the centre of the open beam-end, where the load is applied. The occurring bending moment at the column-side beam-end is determined by extracting the reaction force which occurs at node DT20 and multiplying it with the distance of the node to the column-side beam-end, see equation 4.4. The occurring bending moment for each increment is determined.

$$M_{Ed} = RF_{DT20} \cdot d \tag{4.4}$$

The moment-rotation curve of the joint is formed with the determined global rotation and bending moment for each increment during the simulation, see Figure 4.6. The moment-rotation curve is used to derive the joint's characteristics, namely the initial stiffness, elastic moment resistance and plastic moment resistance.

The initial stiffness is determined by fitting a straight line through the origin and the linear section of the moment-rotation curve. The slope of this line, relative to the horizontal axis, defines the initial stiffness $S_{j,ini}$.

The elastic moment resistance M_{el}, is indicated by a deviation of the moment-rotation curve from the initial stiffness line.

Finally, the plastic moment resistance is found at the intersection of the limit stiffness line and the initial stiffness line [51]. The limit stiffness line is a straight line that approximates the post-limit stiffness of the moment-rotation curve. Figure 4.6 illustrates the moment-rotation curve for the single extended end-plate bolted connection, along with the guiding lines and critical points used to determine the characteristics.

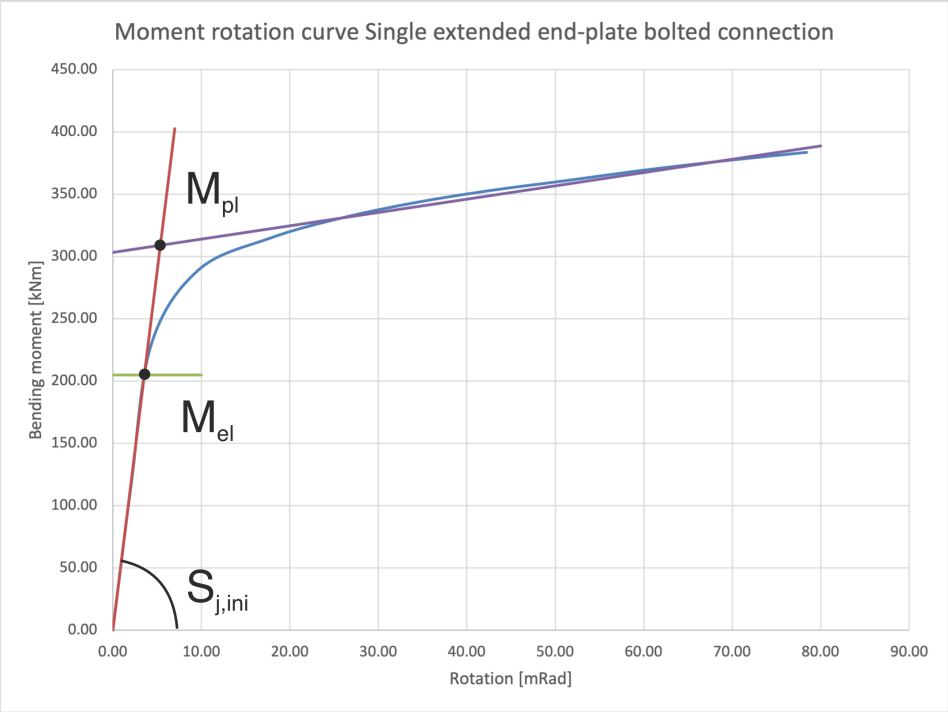

Figure 4.6: Moment-rotation curve single extended end-plate bolted connection

4.4. Validation

The numerical model is validated to determine the degree to which the numerical model accurately represents the real world's physical behaviour.

The numerical model of the single extended end-plate bolted connection is developed through modifying the configuration of a numerical model of a double extended end-plate bolted connection. This double extended end-plate bolted connection model has been validated against experimental results. The validation of the double extended end-plate bolted connection numerical model is detailed in appendix A. The test setup, material properties, boundary conditions, loading protocol, element types, interactions and constraints which were applied in the double extended end-plate bolted connection model, have been applied to the single extended end-plate bolted connection model, as is described in this chapter. Only the configuration of the numerical models is different. Given that the single extended end-plate bolted connection model is exclusively a configurational modification of the validated double extended end-plate bolted connection model, it is assumed that the single extended end-plate bolted connection numerical model is reliable to represent the real world physical behaviour.

To further substantiate this assumption, the single extended end-plate bolted connection was validated against the component method, which is outlined in Eurocode 3, part 1-8. The component method analytically determines the rotational stiffness, elastic and plastic moment resistance as the design

moment-rotation characteristics. Table 4.5 compares the joint characteristics which are determined through processing the data of the numerical model to the moment-rotation characteristics of the component method. The close alignment of the results of the numerical model and the component method reinforces that the numerical model is accurate and reliable.

Table 4.5: Comparison between numerical and component method results

	$S_{j,ini}$ [kNm/rad]	$M_{el,Rd}$ [kNm]	$M_{Pl,Rd}$ [kNm]
Component method	58912	195	305
Numerical model	57494	205	309
Error	-2.4	+4.9%	+1.2%

4.5. Plug-and-play numerical model

The validated single extended end-plate bolted connection numerical model serves as the foundation for the numerical model of the plug-and-play connection. The plug-and-play connection's model is developed from the bolted connection's model through geometrical modifications only. The following modifications are executed to the bolted connection's model to obtain the plug-and-play connection's numerical model:

- The bolts and end-plate from the bolted connection model are removed.
- The bolt holes in the column flange are eliminated from the model, since the plug-and-play connection does not utilise bolts.
- The pins are modelled and the bolt material properties are assigned to the pins.
- The grip-plate and compression foot are modelled and the end-plate material properties are assigned to them.
- The fillet welds are constrained to the corresponding regions of the grip-plate using a tie constraint.
- The pins are constrained to the corresponding column flange region using a tie constraint.
- The pins and grip-plate are meshed with a minimum of three elements through the thicknesses.
- The column is meshed, because the bolt holes were removed.
- The second step, which was the application of the pre-tensioning load to the bolts' shanks, is removed as no bolts are present in the plug-and-play connection.

The individual parts of the plug-and-play connection numerical model are illustrated in Figure 4.7. The dimensions of the parts are according to the details provided in Figure 3.3.

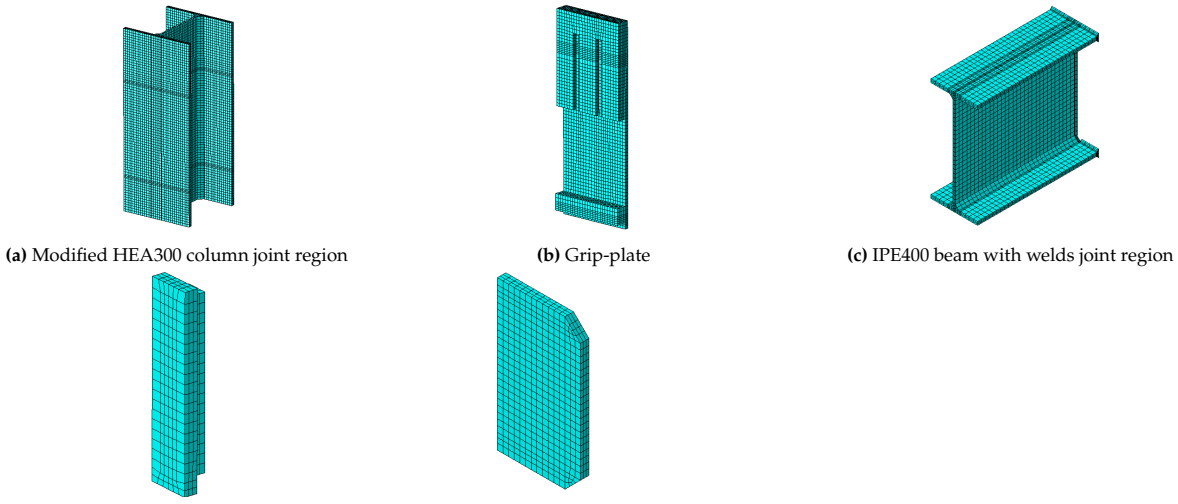

(a) Modified HEA300 column joint region

(b) Grip-plate

(c) IPE400 beam with welds joint region

(d) Pin

(e) Stiffener

Figure 4.7: Plug-and-play connection parts in joint region

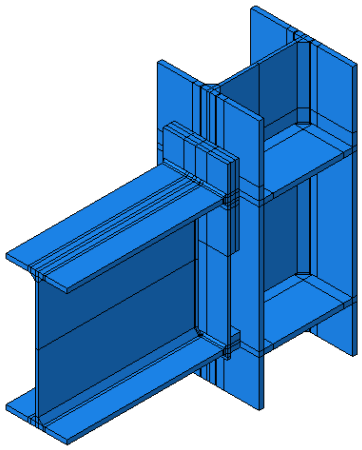

Figure 4.8: Assembled plug-and-play numerical model

All other aspects of the bolted connection model, such as element type, material properties, boundary conditions, load application and general interactions are retained identical. Figure 4.8 illustrates the joint region of the assembled model, while Figure 4.9 and table 4.6 present the test setup.

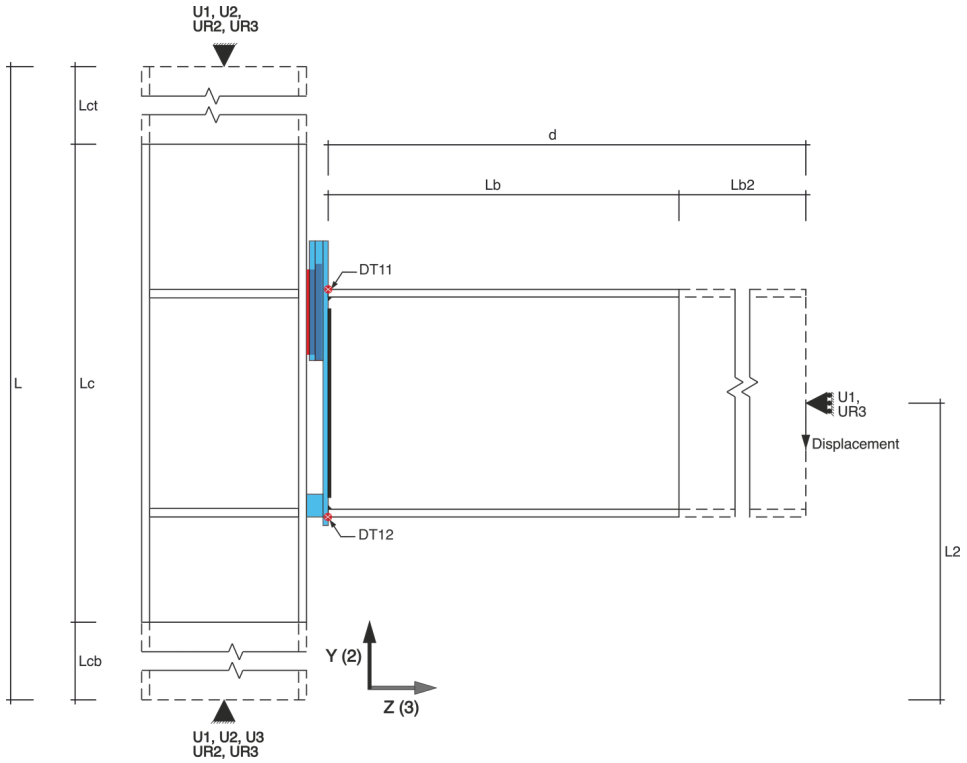

Figure 4.9: Test setup plug-and-play numerical model

Table 4.6: Geometrical properties of plug-and-play connection numerical model

L (mm)	3000
Lc (mm)	740
Lct (mm)	1375
Lcb (mm)	885
L2 (mm)	1220
Lb (mm)	468
Lb2 (mm)	660
d (mm)	1128

As described, the plug-and-play connection numerical model is solely a geometrical modification of the validated single extended end-plate bolted connection model. It is therefore assumed that the plug-and-play connection model is accurate and reliable. This assumption is justified, because the single extended end-plate bolted connection numerical model was developed through geometrical modifications of the double extended end-plate bolted connection model and remained accurate and reliable, as shown above.

5

Global analysis

This chapter describes the global analysis of the plug-and-play joint. Firstly, the conceptual design is iteratively developed to the final design. Then the final design of the plug-and-play joint is compared to its equivalent single extended end-plate bolted joint, in terms of structural response and material usage. During the global analysis the moment-rotation curves are formed for each iteration and the initial stiffnesses, elastic and plastic moment resistances are determined from the moment-rotation curves.

5.1. Iterative analysis

The development of the plug-and-play connection was achieved through a series of iterative modifications. The goal of the modifications was to minimise material usage and maintain the structural performance, without violating any of the determined design requirements. Modifications were done on the pins, grip-plate and compression foot. The iterative process is described here followed by a description of the iterations and the impact of these iterations on the joint's behaviour. The final design of the plug-and-play connection emerges through the iterative modifications. The structural performance and the material usage of the final design is compared to the conceptual design of the plug-and-play joint, to assess whether the goal of the modifications is obtained.

The iterative process starts with analysing the conceptual plug-and-play joint model. During each iteration simulation was run and the moment-rotation curve was formed through processing the data as described in section 4.3. Then the joint characteristics were determined from the moment-rotation curve. Since the conceptual plug-and-play joint was the initial iteration, its characteristics are not compared to previous results. During the following iterations, a single parameter or component's geometry was modified in the numerical model and simulation was run. The moment-rotation curve was formed through processing the data and the joint characteristics were determined. The joint characteristics were compared to the results of the previous iteration to assess the effects of the modification. This comparison completes the process of that particular iteration and can be followed by another iteration. The final numerical model, which is not followed by further modification, emerges as the final design of the plug-and-play connection. This process is schematically illustrated in Figure 5.1.

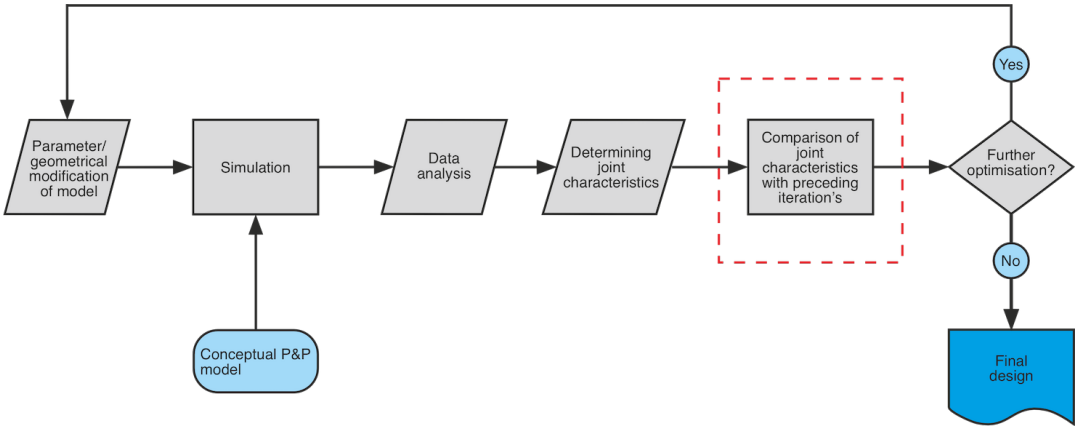

Figure 5.1: Flowchart optimisation process

The comparison of joint characteristics, marked with a red box in Figure 5.1, forms Table 5.2, shown at the end of the description of iterations.

The material efficiency is improved by removing material were it was less loaded. The Von Mises stress analysis in ABAQUS was employed to identify the low stressed material and remove it. This approach is inspired by the optimisation process of ARUP's structural nodes [43], were the Von Mises stress was analysed to remove material which was low stressed. The Von Mises stress is used as the yield criterion which indicates yielding of material and the initiation of plastic deformation [52]. The Von Mises stress was also used to identify high stressed regions in the joint. Material effectiveness is improved by repositioning low stressed material to high stressed regions. The assumption in this approach is that removing material with a low Von Mises stress will have minimal or no influence on the elastic and plastic moment resistance of the joint and that positioning material in high-stressed regions will improve them.

5.1.1. Description of iterations

The executed iterations and their rationale is described in this section. The resulting joint characteristics of each iteration are listed in Table 5.2, as described.

The conceptual design of the plug-and-play connection is shown in Figure 3.2. Initially, the bolt material properties were adopted for the pins, as the pins resemble the bolts in the single extended end-plate bolted connection. The following modifications were executed on this conceptual design:

1. **Conventional pins**
   The material properties of the pins were initially 10.9 bolt material properties. During this iteration the pins' material were changed to the material properties of the end-plate, which are the material properties of hot rolled steel. This was done to assess the possibility to conventionally manufacture and weld the pins to the column flange.

   This modification in material had minimal impact on the stiffness and moment resistance of the joint.
2. **WAAM pins**
   The pins' material was changed to WAAM material properties. In section 2.4 it is described that in order to make the plug-and-play connection adaptable to tubular columns and to minimise the use of WAAM, only the pins can be WAAM printed. The pins are the only components in the connection that are attached to the column face. In case of tubular sections, with limited access to the interior, the advantage of manufacturing the pins with WAAM is that no access to the interior is required. Taking into account that the pin shank is expected to be adapted in order to prevent chord plastification, the pins are expected to have a more complex shape. With WAAM it is expected to be easier to manufacture these complex shapes on the straight or curved column face of the tubular section.

The modification to WAAM manufactured pins in the current configuration allows to assess the impact of applying WAAM in the connection.

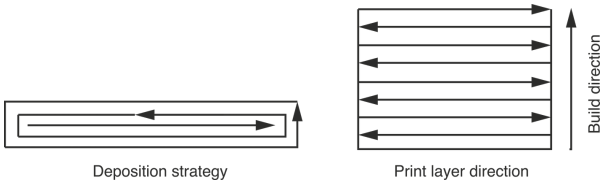

Figure 5.2: Print strategy

A proposed print strategy for the pins is shown in Figure 5.2. The average WAAM material properties from tensile coupon tests are shown in table 4.3. The print layer direction and build direction of the pins allow to use the material properties of vertical, 90° coupons. Machining the pins to smooth edges is preferably prevented since it implies an extra step in the manufacturing process and additional costs. The surface roughness of the WAAM manufactured pins is accounted for by allowing tolerances in the grip-plate's slots. So the material properties of as-built, 90° WAAM are used in the numerical model, see Table 5.1.

Table 5.1: WAAM material properties 90° [14]

Feedstock wire	Condition	Build direction	Yield stress [MPa]	Ultimate stress [MPa]	Ultimate strain [-]	Young's modulus [MPa]
ER70S-6	As-built	Vertical 90 °	335.8	462.6	0.171	214000

The Von Mises analysis showed that initial yielding occurs in the pins' shanks. The grey area in Figure 5.3 shows that yielding initiates at the top of the pin shank and stretches down until the half of the pin shank. Initially, the pins' faces yield where they correspond with the pin shank area. After the load is increased, the yielding of the pins' faces stretches to their width, as shown in Figure 5.4.

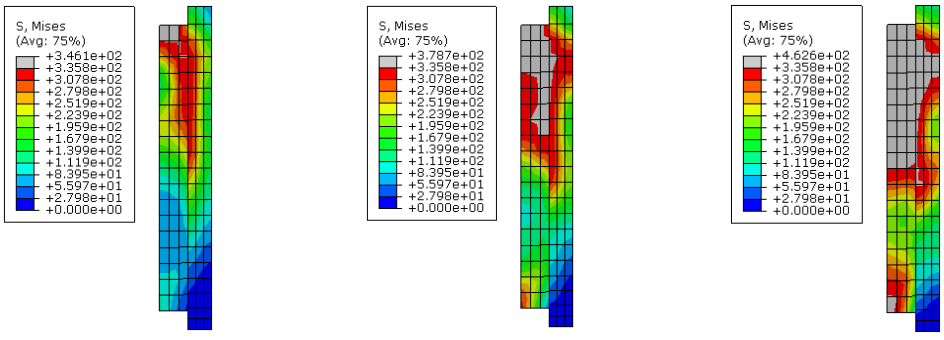

Figure 5.3: Yielding of pin shank

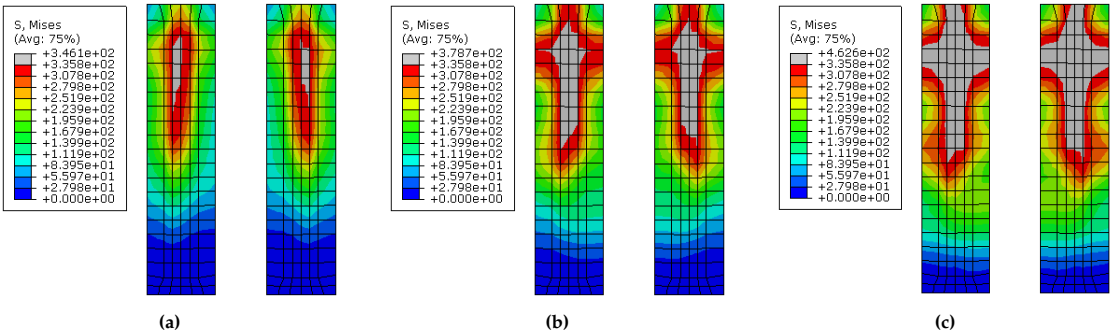

Figure 5.4: Yielding of pin face

The modification to WAAM material properties resulted in a slight reduction in the elastic and plastic moment resistances. This is assigned to the lower material properties of WAAM, relative to the end-plate material properties which were used in the previous iteration. The stiffness remained unaffected by this modification.

3. **Shortened pins (-35 mm)**
   The Von Mises stress analysis, see Figure 5.5, shows that the bottom 35 mm of the pins were very low stressed. According to the described approach, the pins were shortened with 35 mm from the bottom. This modification had minimal effect on the moment resistance but caused a slight reduction in the joint stiffness. This indicates that the removed low stressed material indeed can effectively be removed without affecting the moment resistance, and that the pin height has direct influence on the joint stiffness.

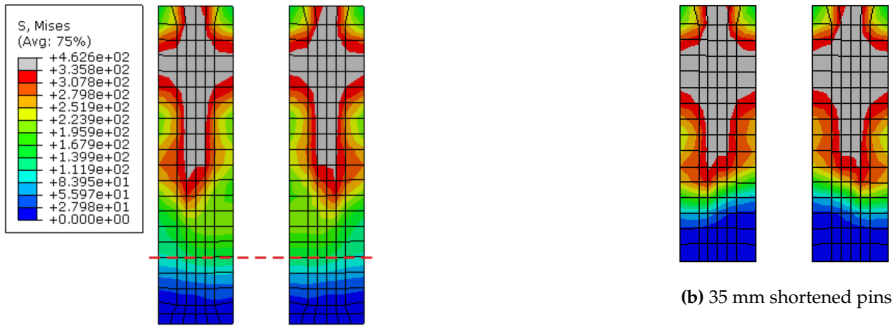

(a) Original pins' length

(b) 35 mm shortened pins

Figure 5.5: Shortening of pins (-35 mm)

4. **Oval pins and adjusted grip-plate**
   The geometry of the pins was modified to mitigate high local stresses at the corners of the pins' shank, where initial yielding occurred. The rectangular pins were modified to oval pins, see Figure 5.6. Consequently the grip-plate's geometry was adjusted to fit the oval pins.

   The oval pins also introduce self-alignment of the pins and grip-plate to ease the installation.

   The oval pins imply material reduction in the top of the pin shank. Due to this geometrical modification the stress was more evenly distributed over the width of the pin face but initial yielding remains to occur in the top of the pin shank, see Figure 5.6. Due to the reduction of material in this critical area, the elastic moment resistance of the joint decreased with 1.9%. However, self-alignment in plug-and-play joints is noticed as a required characteristic feature [17, 53]. Thus, despite the decrease in elastic moment resistance, this modification is favourable. The initial stiffness and plastic moment resistance of the joint remain essentially unaffected.

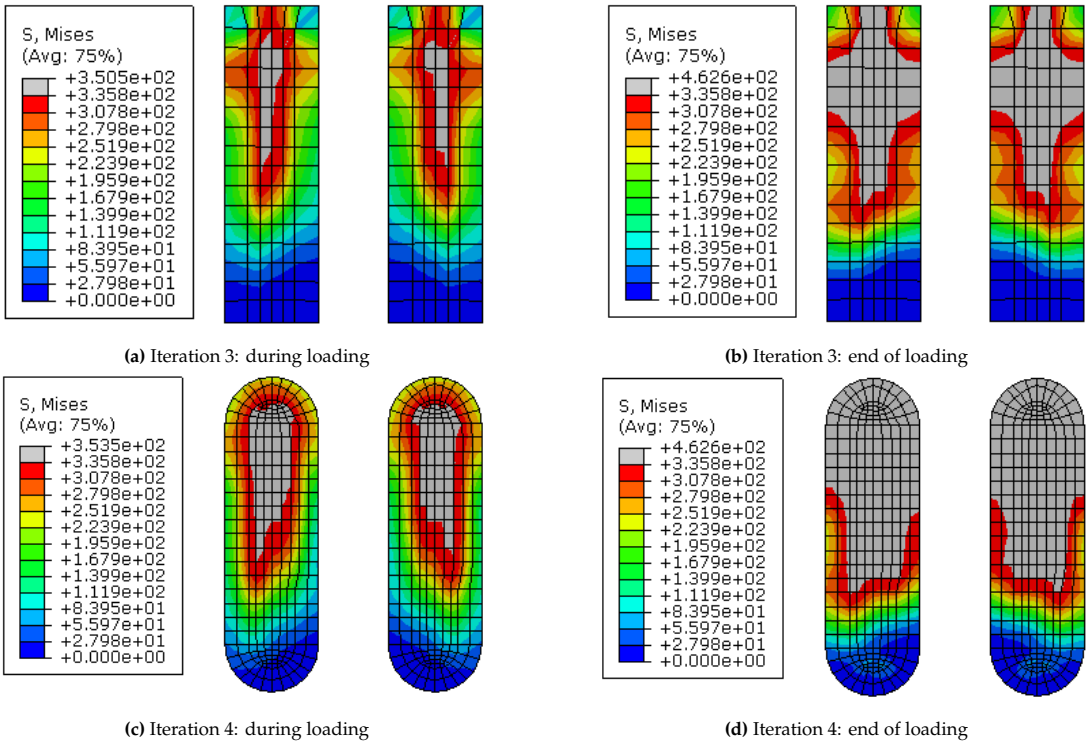

(a) Iteration 3: during loading

(b) Iteration 3: end of loading

(c) Iteration 4: during loading

(d) Iteration 4: end of loading

Figure 5.6: Stress distribution rectangular vs oval pins

5. **Further shortened pins (-18 mm)**
   The Von Mises stress analysis of the pins in iteration 4, see Figures 5.6c and 5.6d, showed that the stresses were more evenly distributed over height. Here it also showed that the stress distribution over the width of the pin face, especially in the lower section, remained uneven. At middle height of the pin, the stress was more concentrated at the middle of the pin face. At the lower end of the pin face, the stresses were low. Hence the pins were further shortened with 18 mm, as indicated by the red line in Figure 5.7a.

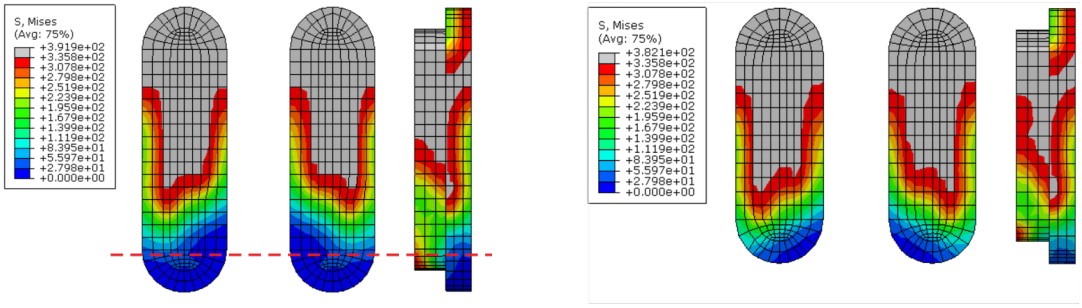

(a) Stresses in pins from iteration 4 at M_{Ed}=329 kNm

(b) Stresses in 18 mm shortened pins at M_{Ed}=324 kNm

Figure 5.7: Further shortening of pins (-18 mm)

Due to this modification almost all material in the pin was significantly stressed, and most inactive material has been removed. However, the shortening of the pins led to 0.4% decrease of the initial stiffness. This decrease was expected because the previous shortening of the pins, in iteration 3, indicated that the height of the pins influences the stiffness of the joint.

This geometrical modification had no effect on the elastic moment resistance but increased the plastic moment resistance of the joint. This is expected to be due to a slight change in stress distribution in the joint.

6. **Additional 2 mm tolerance for WAAM pins**
The WAAM manufactured pins will have a surface roughness, as this is inherent to WAAM. This surface roughness will be accounted for by reducing the pin size to create additional tolerances. The tested WAAM wall, which was used to determine the material properties, showed no more than 1.5 mm difference in wall thickness [14]. The tolerances between the pins and grip-plate initially were 2 mm. According to the analysed WAAM wall thickness, this 2 mm tolerance should be sufficient. However, in order to allow for possible greater distortions and maintain sufficient tolerances for installation, the pins were made 2 mm smaller, as shown in figure 5.8.

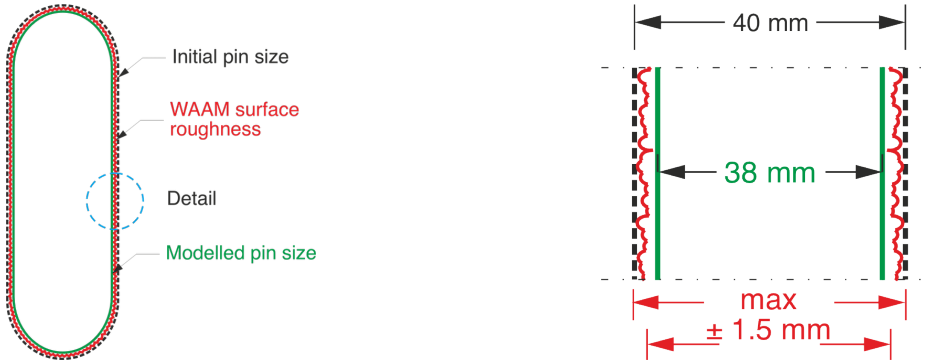

(a) WAAM surface roughness **(b)** WAAM surface roughness detail

Figure 5.8: Pin tolerances

This modification reduced the stiffness and the plastic moment resistance of the joint. It is noted that the elastic moment resistance remained unaffected due to this modification. So the application of WAAM has a twofold negative impact of the joint behaviour, due to the lesser material properties and the required tolerances. Figure 5.9 shows that due to the smaller pins, higher stresses are present in the pins, which led to the decrease in stiffness and moment resistance.

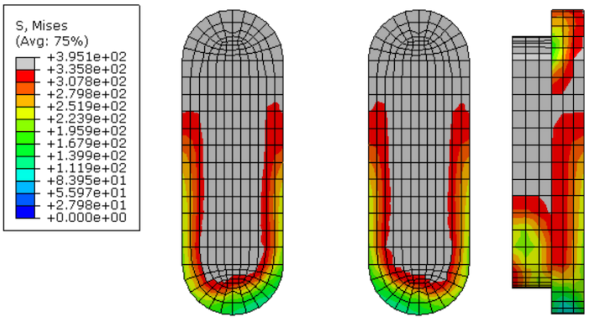

Figure 5.9: Stresses in pins with additional tolerances at M_{Ed}=320 kNm

7. **Lowered compression foot**
Initially, the compression foot was positioned 15 mm above the bottom of the grip-plate to allow sufficient space for the fillet weld, to weld the compression foot to the grip-plate. However, the Von Mises stress analysis showed that the back-plate of the grip-plate was very low stressed. It was anticipated that this back-plate would be removed because it was low stressed, and the compression foot would be welded directly to the beam-end. Because the compression foot will be welded directly to the beam-end, it is possible to lower its position and increase the lever arm. In this iteration the position of the compression foot was lowered 15 mm, as shown in Figure 5.10.

(a) Initial compression foot position **(b)** Lowered compression foot

Figure 5.10: Lowering of compression foot

This modification led to a substantial improvement of the initial stiffness (+4.8%) and plastic moment resistance (+3.2%) of the joint. Figure 5.11 shows the Von Mises stress before and after lowering the compression foot. As mentioned, initial yielding occurs in the pins and is closely followed by the column web panel in shear. Due to lowering of the compression foot the pins and the column web panel in shear are less stressed, as shown in Figures 5.11c to 5.11f. Thus the increase of the initial stiffness and plastic moment resistance of the joint due to lowering of the compression foot is due to lower stresses in these two critical components.

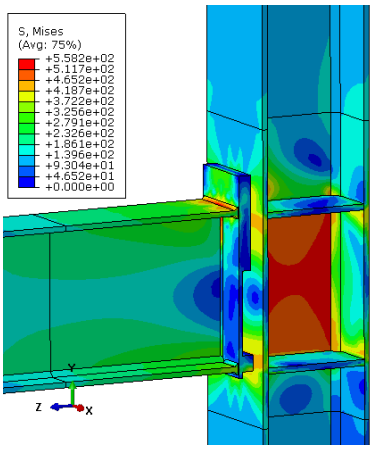

(a) Iteration 6 global stresses

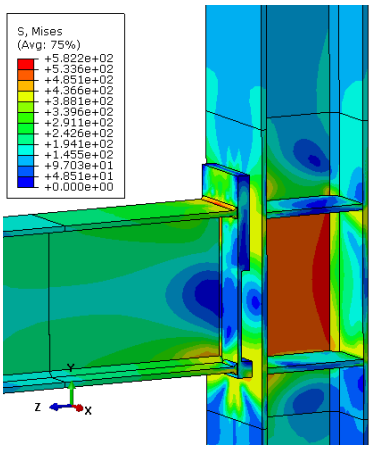

(b) Iteration 7 global stresses

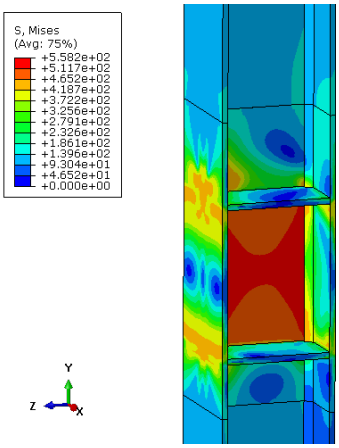

(c) Iteration 6 column stresses

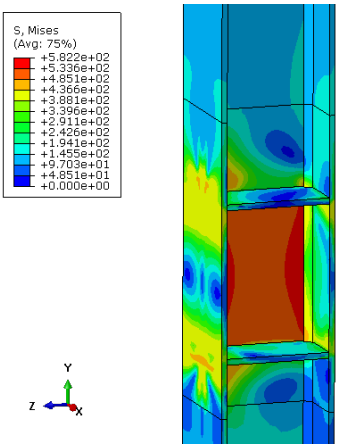

(d) Iteration 7 column stresses

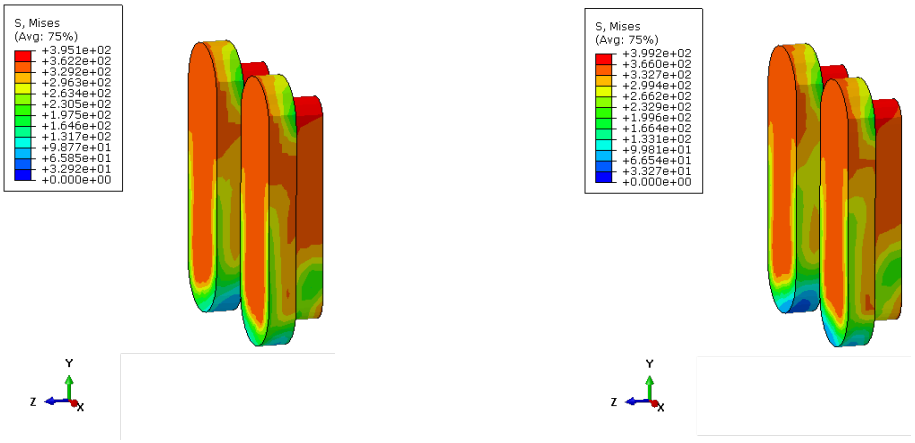

(e) Iteration 6 stresses in pins

(f) Iteration 7 stresses in pins

Figure 5.11: Change of stresses due to lowering of compression foot, at M_{Ed}=330 kNm

8. **Shortened grip-plate (-55 mm)**
   As shown in Figure 3.2, the grip-plate is divided in three parts: the back-, middle- and front-plates. The middle- and front-plates form the slots for the pins. The Von Mises stress analysis showed that the front- and middle-plate were very low stressed at the bottom, due to the shortening of the pins in iterations 3 and 5. The stresses in stressed regions of the grip-plate were non-uniformly distributed, with stress peaks over its width. The lower 55 mm of the front- and middle-plates, indicated by the red line in Figure 5.12a, were removed. This maintained sufficient height for the pins to fit in the slots, but removed low stressed material, and redistributed stresses more uniform over its width.

   This modification led to a decrease in the initial stiffness of the joint. The reduction of stiffness is expected, because the shortening of the front- and middle-plates leads to a reduction of the grip-plate's stiffness.

   The shortening of the front- and middle-plates also led to a slight reduction of the plastic moment resistance (-0.8%), which indicates that the removed material was not very actively contributing. The shortening led to a higher stress concentration in the grip-plate, see Figures 5.12a and 5.12b, and a slight increase in the stresses in the pins, see Figures 5.12e and 5.12f.

   The elastic moment resistance increased with 2.0%. The reduction of the grip-plate led to a redistribution of stresses in the joint components. The slight increase of stresses in the pins was indicated. Since the pins are critical for yielding, the increase of stresses negatively influences the elastic moment resistance of the joint. However, the increase is very small thus the influence on the elastic moment resistance is expected to be small.

   The column web is yielding almost simultaneously with the pins. Figures 5.12c and 5.12d show that stresses in the column web are decreased significantly due to the shortening of the front- and middle-plates. The increase of the elastic moment resistance is expected to be due to the decrease of stresses in the column web.

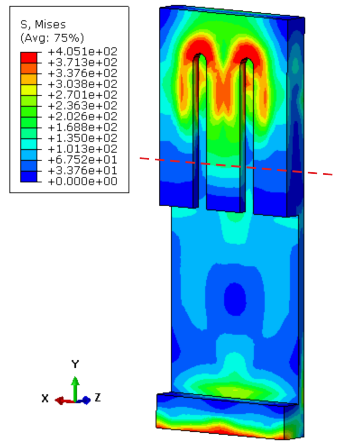

(a) Iteration 7 grip-plate stresses

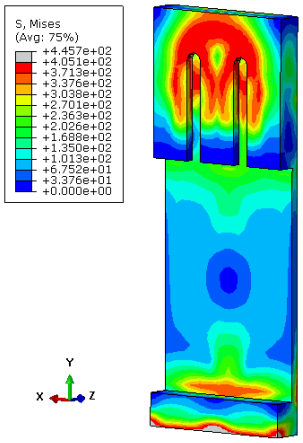

(b) Iteration 8 grip-plate stresses

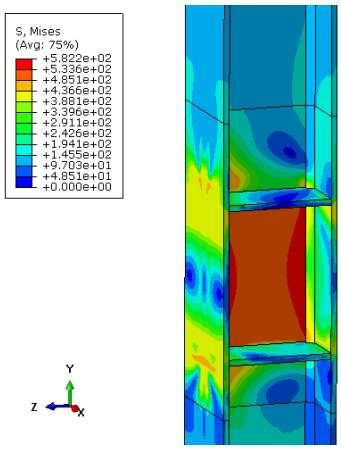

(c) Iteration 7 column stresses

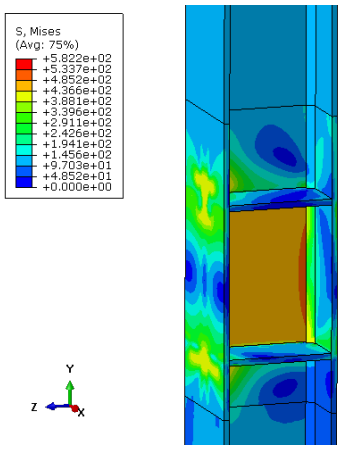

(d) Iteration 8 column stresses

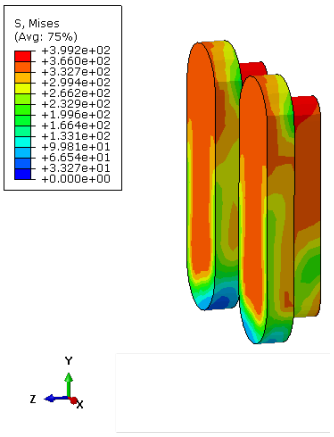

(e) Iteration 7 stresses in pins

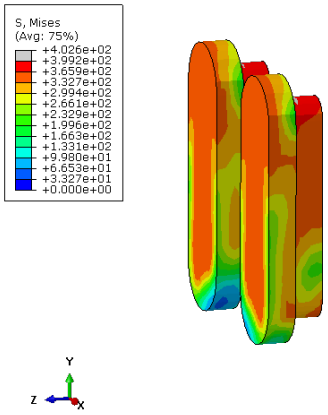

(f) Iteration 8 stresses in pins

Figure 5.12: Change of stresses due to shortening of grip-plate, at M_{Ed}=330 kNm

9. **Removal of back-plate**
   It was already indicated that the back-plate was very low stressed. During this iteration the back-plate was removed in the regions where the compression foot or the middle-plate were not present. This separated the compression foot from the grip-plate.

   The removed back-plate was very low stressed and contained much material.

This geometrical modification led to a slight reduction of the initial stiffness (-0.4%) and plastic moment resistance (-0.7%) relative to the previous iteration, as expected because the material was very low stressed. The elastic moment resistance remained unaffected.

The removal of the back-plate resulted in a more local transfer of tensile stresses through the grip-plate to the pins and column web, and compressive stresses through the compression foot to the column web. Though, the distribution of stresses was minimally affected, see Figure 5.13.

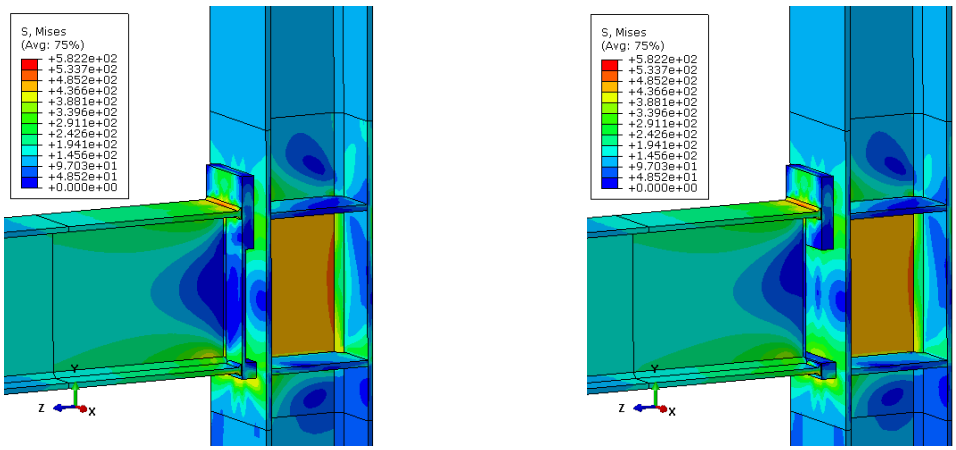

(a) Iteration 8 global stresses **(b)** Iteration 9 global stresses

Figure 5.13: (no) Change of stresses due to removal of back-plate, at M_{Ed}=328 kNm

The goal of these modifications is to minimise material usage in the connection. The removal of the back-plate is the largest material reduction during this process.

The removal of the back-plate was also motivated by the separation of the compression foot and the grip-plate. Initially, the approach was to weld the three separate plates and the compression foot to manufacture the grip-plate from rolled steel, see Figure 5.14a. Due to the removal of the back-plate, the compression foot and grip-plate can be manufactured separately. The compression foot is a rectangular steel part which can easily be manufactured. The grip-plate no longer needs to be manufactured from three separate plates which are welded to each other, but can be manufactured as a single steel part, see Figure 5.14b. The pin slots can be milled. It is expected that this modification will enhance the ability to mass-produce and make the connection more cost-competitive [8, 17, 53].

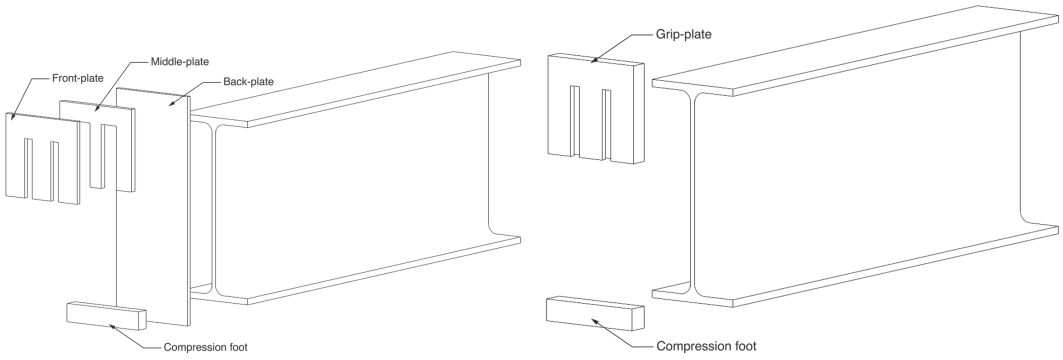

(a) With back-plate **(b)** Without back-plate

Figure 5.14: Removal of back-plate

10. **Smaller compression foot**
    The Von Mises stress analysis of the compression foot show that the stress was mostly concentrated at the middle of the compression foot, see Figure 5.15a. Therefore the compression foot was reduced to a total width of 90 mm, as indicated by the red lines in Figure 5.15a. This modification had no effect on the plastic moment resistance of the joint. However, it led to a significant decrease (-2.1%) of the initial stiffness of the joint, and of the elastic moment resistance (-1.9%).

    The smaller compression foot led to a higher stresses in the compression foot, see Figure 5.15b, the column flange and web, see Figure 5.15d, and in the pins, see Figure 5.15f. The increase of stresses in the critical column web and pins led to the decrease of the initial stiffness and elastic moment resistance.

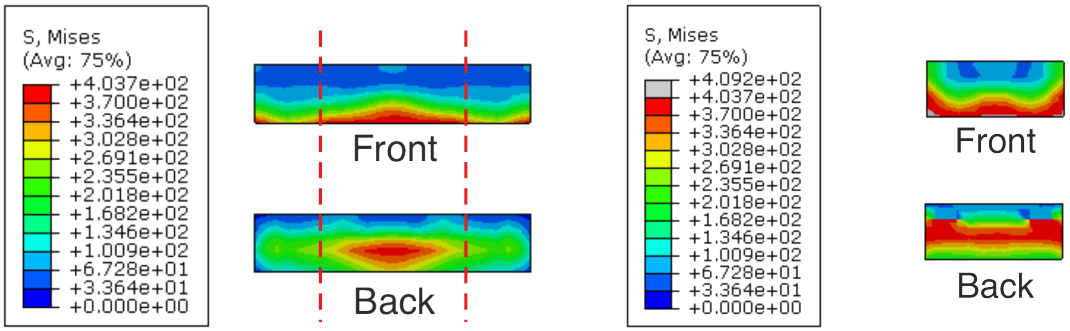

(a) Iteration 9 compression foot stresses

(b) Iteration 10 compression foot stresses

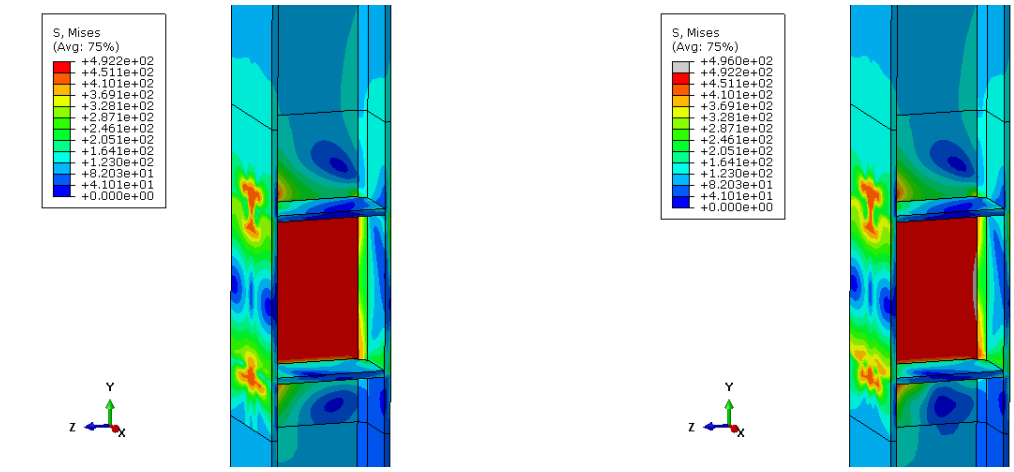

(c) Iteration 9 column stresses

(d) Iteration 10 column stresses

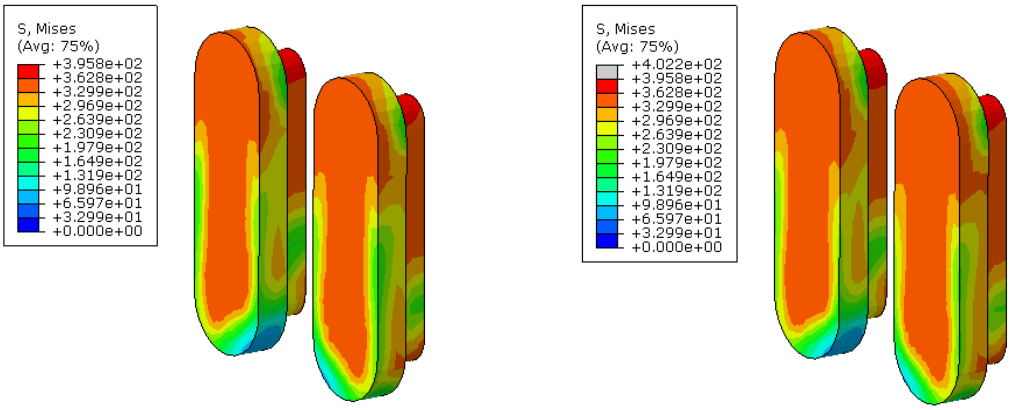

(e) Iteration 9 stresses in pins

(f) Iteration 10 stresses in pins

Figure 5.15: Change of stresses due to smaller compression foot, at M_{Ed}=328 kNm

11. **Higher compression foot**
    As mentioned, the stresses were concentrated at the middle of the compression foot. The removed material from the compression foot in the previous iteration was added on top of the remaining compression foot, see Figure 5.16. This modification led to an increase in the joint's initial stiffness (+2.7%). The repositioning of the removed material led to an effective increase of 0.6% of the joint stiffness relative to iteration 9.

    Furthermore, repositioning increased the plastic moment resistance significantly (+1.3%). The elastic moment resistance remains unaffected. Figures 5.17a and 5.17b show that the compression foot has higher stresses than in the previous iteration, and more material is stressed than previously. Figures 5.17c and 5.17d show that there is a redistribution of stresses in the compressive zone of the column. The increase in moment resistance is expected to be due to this redistribution of stresses in the column. The stresses in the pins remain almost unaffected, see Figures 5.17e and 5.17f.

    This iteration demonstrates that the approach to reposition low stressed material to high stressed regions, improved the material effectiveness.

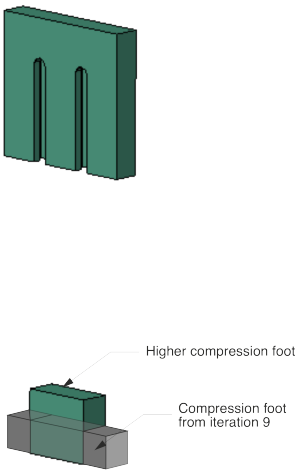

Figure 5.16: Repositioning material on top

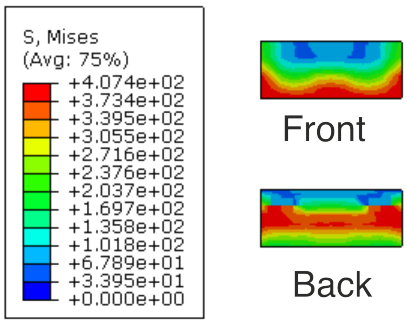

(a) Iteration 10 compression foot stresses

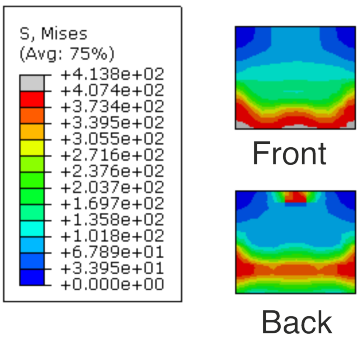

(b) Iteration 11 compression foot stresses

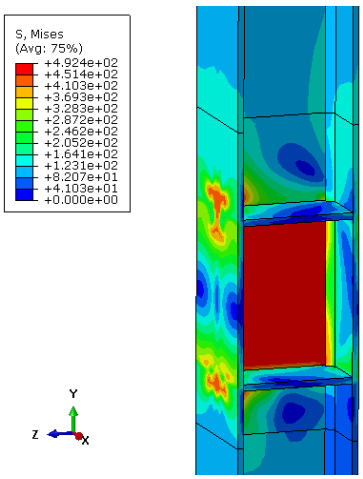

(c) Iteration 10 column stresses

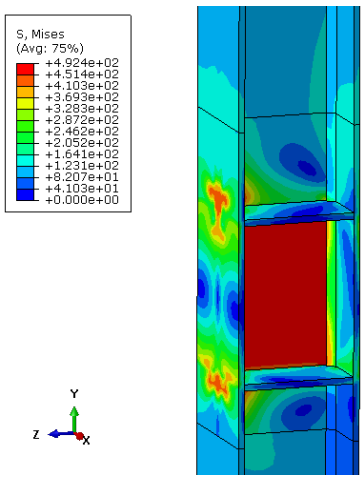

(d) Iteration 11 column stresses

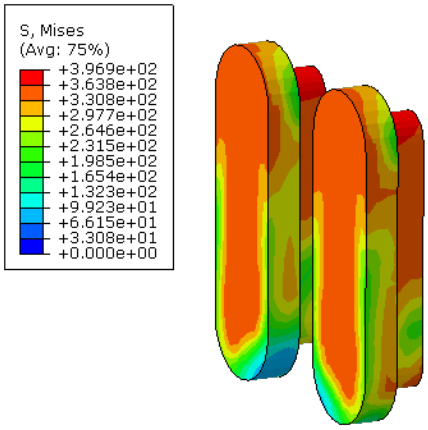

(e) Iteration 10 stresses in pins

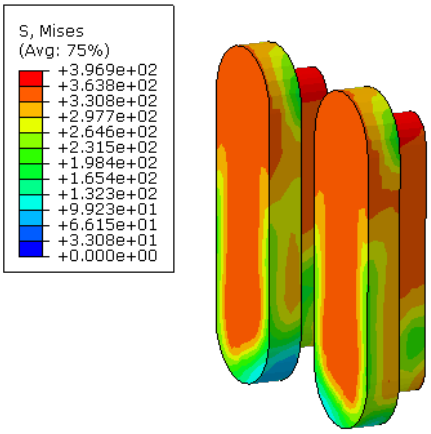

(f) Iteration 11 stresses in pins

Figure 5.17: Change of stresses due to higher compression foot, at M_{Ed}=325 kNm

12. **Further lowered compression foot**
    Since the lowering of the compression foot in iteration 7 yielded a higher initial stiffness and plastic moment resistance, during this iteration the compression foot was 40 mm further lowered, see Figure 5.18.

    The lowering of the compression foot yielded similar results as in the preceding iteration. The configuration of iteration 11 is preferred because the connection is more compact.

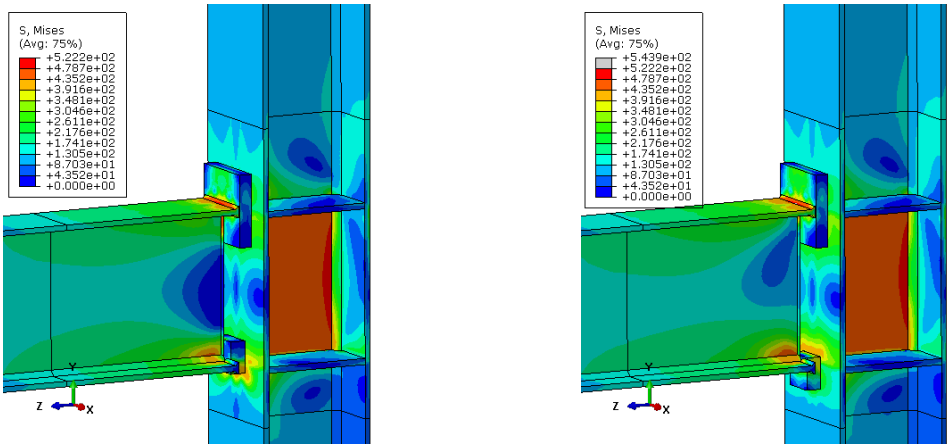

(a) Iteration 11 global stresses **(b)** Iteration 12 global stresses

Figure 5.18: Change of stresses due to lowering compression foot, at M_{Ed}=329 kNm

13. **Adjusted column section with finer mesh**
    Sections 4.5 described that the column was divided in three sections, and that the column part in the joint region has a finer mesh. The stresses in the column beyond the determined joint region remained significantly high. Therefore, the height of the column part in the joint region with a finer mesh is increased during this iteration.

    This modification improved the accuracy of the stress distribution, and resulted in slight adjustments of the initial stiffness and plastic moment resistance of the joint.

Table 5.2 shows the values of the initial stiffness, elastic and plastic moment resistances of the conceptual plug-and-play joint as the initial values of the iterative analysis. It shows the impact of each modification on these joint characteristics, relative to its preceding iteration. Lastly, the table shows the total impact of all modifications on the joint characteristics, relative to the conceptual design of the plug-and-play joint.

Table 5.2: Iteration impacts on joint characteristics

Iteration	**Description**	**Initial stiffness [kNm/rad]**	**Elastic moment resistance [kNm]**	**Plastic moment resistance** [kNm]
	Conceptual design	**72044**	**265**	**321**
1	Conventional pins	-0.1%	0.0%	-0.5%
2	WAAM pins	0.0%	-1.9%	-1.0%
3	Shortened pins (-35 mm)	-1.4%	0.0%	+0.3%
4	Rounded pins	+0.2%	-1.9%	-0.1%
5	Shortened pins (-18 mm)	-0.4%	0.0%	+1.2%
6	Pins 2 mm tolerance	-1.4%	0.0%	-2.2%
7	Compr. foot 15 mm lower	+4.8%	0.0%	+3.2%
8	Shorter grip-plate	-2.3%	+2.0%	-0.8%
9	Removal back-plate	-0.4%	0.0%	-0.7%
10	Smaller compr. foot	-2.1%	-1.9%	+0.1%
11	Higher compr. foot (on top)	+2.7%	0.0%	+1.3%
12	Compr. foot 40 mm lower	-0.1%	0.0%	0.0%
13	Adjust. middle column part with finer mesh	-0.3%	0.0%	+0.5%
All	**Total change from conceptual to final design**	**-1.1%**	**-3.8%**	**+1.2%**
		71478	**255**	**325**

5.1.2. Final design plug-and-play connection

The conceptual design, as shown in Figure 5.19a is through these iterations developed to the final design, as shown in Figure 5.19b. The configuration of the final plug-and-play connection is presented in Figure 5.20.

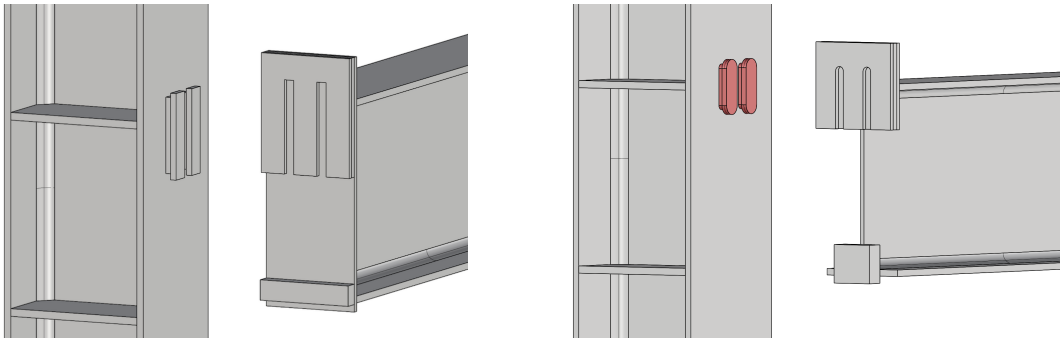

(a) Conceptual design **(b)** Final design

Figure 5.19: Plug-and-play connection designs

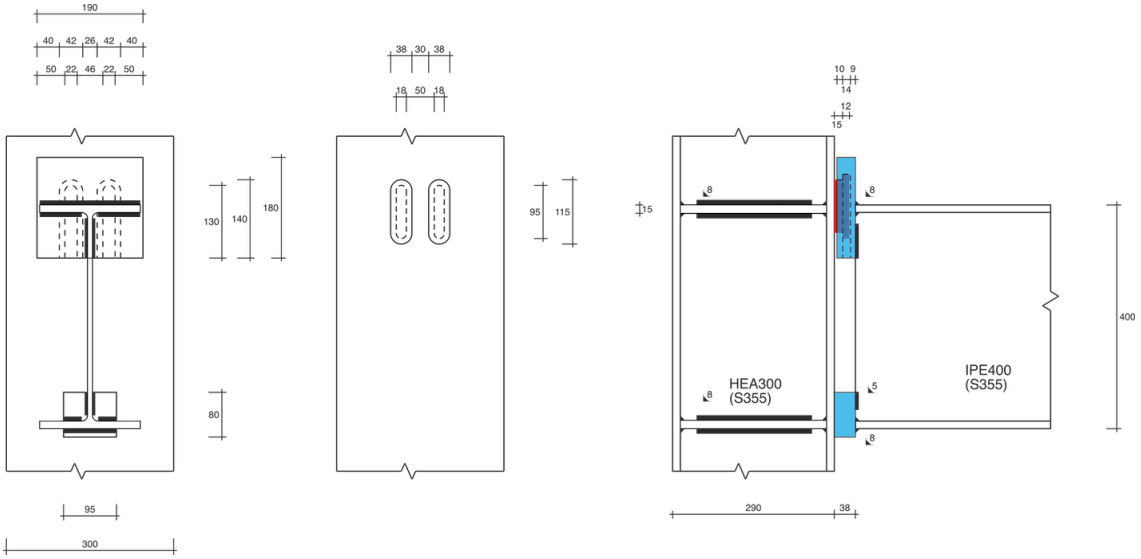

Figure 5.20: Details of the final plug-and-play joint

Table 5.2 indicates that the final plug-and-play joint has almost an identical initial stiffness and plastic moment resistance as the conceptual design. The elastic moment resistance of the final design is slightly lower (-3.8%) than the conceptual design, which is caused due to the introduction of WAAM material, the oval shape of the pins, and removing material from the grip-plate. This decrease of elastic moment resistance relative to the conceptual design is acceptable, because the requirement for the plug-and-play connection was to have equal joint characteristics as the single extended end-plate bolted connection. This requirement is fulfilled with the final design, as will be demonstrated in the comparative analysis.

The material reduction due to the modifications is high, -38.3%. Table 5.3 lists the change of material usage in different parts of the connection for the conceptual and final plug-and-play design. The major reduction in absolute material usage is due to reducing the grip-plate.

Table 5.3: Comparison of material usage conceptual and final plug-and-play connection

Connection	**End-plate/Grip-plate** [mm^3]	**Pins** [mm^3]	**Compression foot** [mm^3]	**Total volume** [mm^3]
Initial P&P conn.	1.700.150	236.040	288.800	**2.224.990**
Rel. change ↓	-44.9%	-37.9%	± 0.0 %	**-38.3%**
Final P&P conn.	936.322	146.658	288.800	**1.371.780**

Figure 5.21 and table 5.4 present the test setup of the final plug-and-play joint.

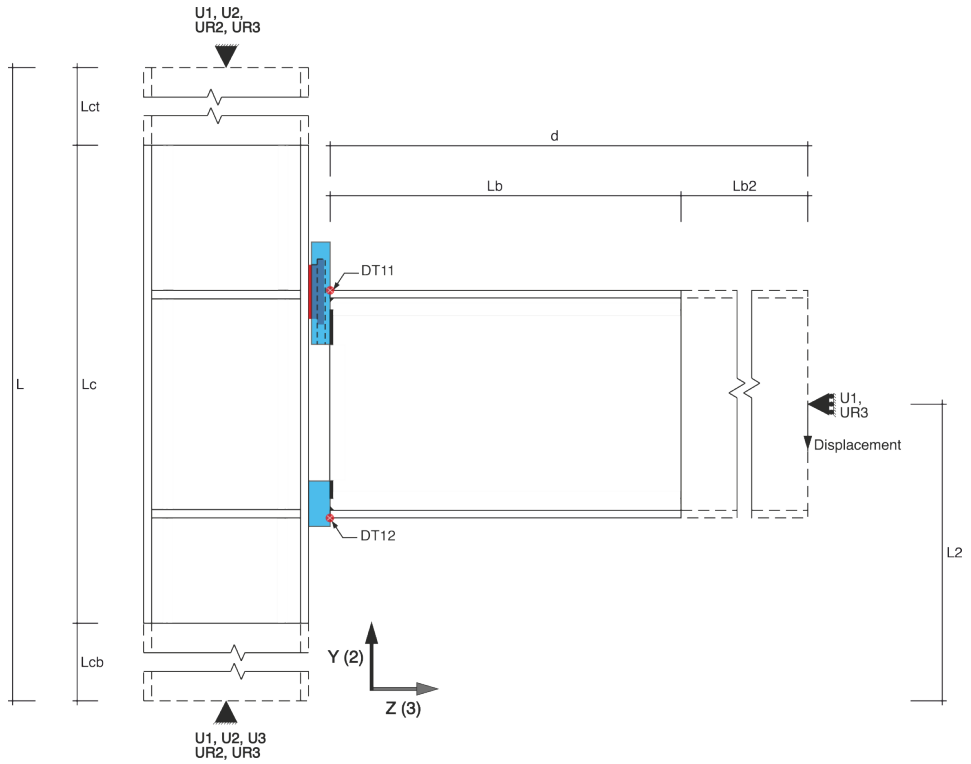

Figure 5.21: Test setup final plug-and-play design numerical model

Table 5.4: Geometrical properties of final plug-and-play model

L (mm)	3000
Lc (mm)	840
Lct (mm)	1375
Lcb (mm)	785
L2 (mm)	1220
Lb (mm)	468
Lb2 (mm)	660
d (mm)	1128

5.1.3. Joint classification

The classification of the plug-and-play joint is according to the strength and stiffness criteria defined in Eurocode 3, part 1-8. The stiffness limits for joint classification are outlined in equations 5.1 and 5.2.

$$\begin{aligned} S_{j,ini,pinned} &\leq 0.5 \cdot \frac{EI_b}{L_b} \\ &\leq 1.98 \cdot 10^{10} Nmm/rad \end{aligned} \tag{5.1}$$

$$\begin{aligned} S_{j,ini,rigid} &\geq 25 \cdot \frac{EI_b}{L_b} \\ &\geq 7.90 \cdot 10^{10} Nmm/rad \end{aligned} \tag{5.2}$$

The initial stiffness of the plug-and-play joint, $S_{j,ini} = 7.15 \cdot 10^{10} Nmm/rad$, is between the boundaries for pinned and rigid classifications, thus classifies as a semi-rigid joint.

The strength classification is similarly determined according to the moment resistance criteria outlined in equations 5.3 and 5.4. The plastic moment resistance of the plug-and-play joint, $M_{pl,Rd} = 325kNm$, is between the limits for pinned and full-strength classifications. Therefore the joint is classified as partial strength.

$$\begin{aligned} M_{full-strength} &= min(M_{b,pl,Rd}, 2 \cdot M_{c,pl,Rd}) \\ &= min(562.44, 1244.49) \\ &= 562.44kNm \end{aligned} \tag{5.3}$$

$$M_{pinned} = 0.25 \cdot M_{full-strength} = 140.61kNm \tag{5.4}$$

5.2. Comparative analysis

The final design of the plug-and-play connection is compared to the single extended end-plate bolted connection which was used as the case study in this thesis, shown in Figure 3.1. The comparison is done in terms of structural behaviour and material usage.

5.2.1. Structural behaviour

The structural behaviour is compared in terms of stiffness, elastic and plastic moment resistance of the joint. Figure 5.22 compares the global behaviour of the single extended end-plate bolted joint and the plug-and-play joint, at their respective plastic moment resistance.

In the bolted joint initial yielding occurs in the end-plate due to bending in the end-plate. It is noted that due to bending in the end-plate, there are low stresses present in the column web above the upper transverse stiffener, see Figure 5.22a.

In the plug-and-play joint initial yielding occurs in the pins in tension and the column web panel. Figure 5.22b shows that higher stresses are present in the column web panel, and in the column web above the upper transverse stiffener, than is the case with the bolted joint.

Thus, the stress distribution in the joints differ in the tension zone of the joints because different joint components are failing. In the compressive zone of the joints, the behaviour of both joints is similar.

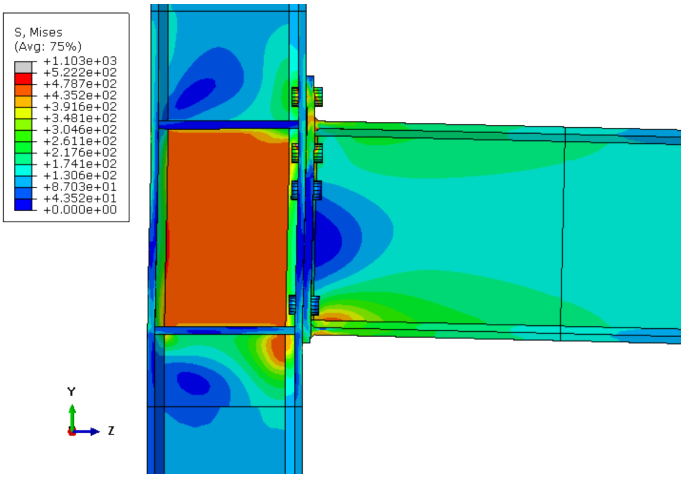

(a) Single extended end-plate joint global behaviour at M_{Pl} = 309 kNm

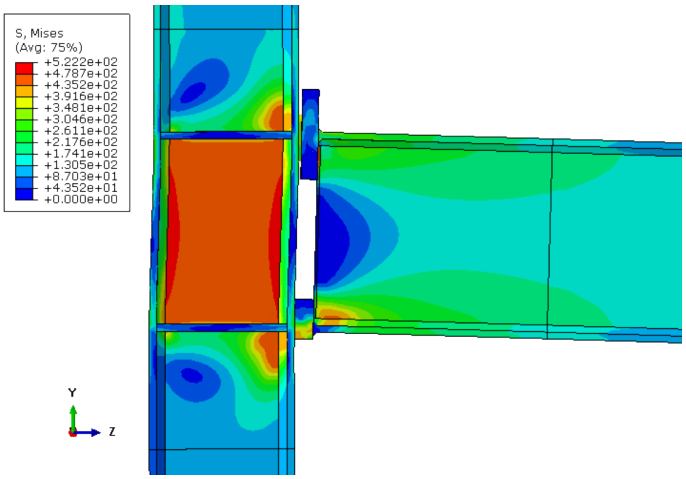

(b) Plug-and-play joint global behaviour at M_{Pl} = 325 kNm

Figure 5.22: Comparison structural behaviour at respective M_{Pl}

The joint characteristics for both joint are shown in Table 5.5. Table 5.5 shows that the plug-and-play joint has higher values for each characteristic compared to the bolted connection. This demonstrates that the plug-and-play connection provides an improved joint with regard to its structural behaviour compared to the single extended end-plate bolted connection in this particular configuration.

Table 5.5: Comparison between bolted and final plug-and-play connection results

	$S_{j,ini}$ [kNm/rad]	$M_{el,Rd}$ [kNm]	$M_{Pl,Rd}$ [kNm]
Bolted connection	57494	205	309
Plug-and-play connection	71478	250	325
Difference	+24.3%	+22.0%	+5.2%

5.2.2. Material usage

The material usage of the final plug-and-play connection is compared to the single extended end-plate bolted connection. In the comparison, the following parts are related to each other: end-plate and grip-plate, bolts in tension and pins, bolts in compression zone and compression foot. Table 5.6 lists the change in material use of the final plug-and-play connection relative to the bolted connection. The total material usage of the plug-and-play connection is much lower than for the bolted variant, 26.1% less. The difference is mainly due to the grip-plate using less steel than the end-plate.

It is noted the plug-and-play connection uses less material (-60.4%) in the tensile zone and more material (+133.9%) in the compressive zone, than the bolted connection. However, the pins and compression foot combined use less material than all the bolts in the bolted connection (-11.8%).

Table 5.6: Comparison of material usage bolted connection and final plug-and-play connection

Connection	**End-plate/ Grip-plate** $[mm^3]$	**Bolts in tension/ Pins** $[mm^3]$	**Bolts in compr./ Compr. foot** $[mm^3]$	**All bolts/ Pins & compr. foot** $[mm^3]$	**Total volume** $[mm^3]$
Single extended end-plate connection	1.361.289	370.420	123.470	493.880	**1.855.169**
Rel. change ↓	**-31.2%**	**-60.4%**	**+133.9%**	**-11.8%**	**-26.1%**
Plug-and-play connection	936.322	146.658	288.800	435.458	**1.371.780**

5.3. Summary

The iterative analysis developed the plug-and-play connection to its final design. Through iterations significant material reduction is acquired in the final design, while maintaining the joint's stiffness and moment resistance. The plug-and-play connection uses less material than the equivalent single extended end-plate bolted connection. The reduction in material use leads to less use of resources during manufacturing. Considering that the plug-and-play joint has higher stiffness and moment resistance than its equivalent bolted joint, it shows that less material is used in a more effective manner in the plug-and-play joint. Thus the optimisation process was effective but further optimisation of the connection, through advanced techniques such as topology optimisation, is possible to further reduce the material use.

The higher stiffness and moment resistance of the plug-and-play joint, relative to its equivalent single extended end-plate bolted joint, implies that plastic deformations occur at a higher load in the plug-and-play joint than in the bolted joint. The reusability of steelwork is limited due to plastic deformations in connecting elements [21]. Thus the plug-and-play connection is expected to remain reusable up to a certain higher load, when the bolted connection already has plastic deformations.

The plug-and-play joint is semi-rigid and partial strength. This allows to design structures as moment resisting frames [8]. Designing with semi-rigid joints can lead to savings in steel weight and more economical designs [54]. The plug-and-play connection is not designed for seismic loading, like ConXtech and SidePlate connections are, but semi-rigid frames can have sufficient flexibility and good hysteretic behaviour and semi-rigid moment resisting buildings can be economical and safe for seismic application [55]. This study was limited to monotonic loading and the behaviour of the plug-and-play connection to cyclic and seismic loading, remains a subject to explore in further studies.

6

Component analysis

In the component analysis the plug-and-play joint is divided into separate joint components, which act together to establish the stiffness and moment resistance of the joint. The approach is based on the component method, as described in Eurocode 3, part 1-8, and is an adaptation of an extraction procedure to characterise joint components in numerical models [18]. The global analysis indicated that initial yielding occurs in the pins, followed closely by yielding of the column web. This analysis aims to further understand the stress development in the components and how the stress in the joint is distributed among its components, to conclude what the contribution of each component is to the joint's stiffness and moment resistance.

First, the active joint components are identified. These components are subsequently analysed in terms of stiffness and strength. Finally, the resulting structural behaviour of the joint from the component analysis is compared to its behaviour resulting from the global analysis, to assess the accuracy of the component analysis.

6.1. Active joint components

The active joint components of the plug-and-play joint are based on the joint components of the single extended end-plate bolted connection. The joint components for the bolted connection are identified in Eurocode 3, part 1-8, and listed in table 6.1.

The components regarding the column and beam remain the same for the plug-and-play joint, as for the bolted connection because there is no difference of the column and beam between both configurations.

As mentioned, the grip-plate resembles the end-plate. Therefore, the grip-plate in bending is identified as an active component, similar to the end-plate in bending.

The pins in tension are identified as an active component, similar to the bolts in tension for the bolted connection.

The compression foot in compression is identified as an active component, based on the understanding that the compression foot is a separate part of the connection and transfers compressive stresses to the column. The component method in Eurocode 3, part 1-8 does not identify bolts in compression, hence there is no equivalent component of the compression foot in compression in the bolted joint.

The vertical shear resistance of the bolted joint is established by the bolts in shear, bearing of the bolts, and the welds. The vertical shear resistance of the plug-and-play joint is expected to be established by the metallurgical bond between the WAAM pins and the column flange, the shear resistance of the pins, the pins in bearing on the grip-plate, and the welds of the beam to the grip-plate. It is noted that the welds of the beam to the compression foot do not contribute to the vertical shear resistance. The components vertical shear resistance, beam flange and web in compression, and beam web in tension are not considered within this study and need to be designed with sufficient overstrength. Since the metallurgical bond between the WAAM pins and the column flange, and the pins' shanks, have a greater

area than the welds it is expected that the welds will be determining for the vertical shear resistance of the plug-and-play joint. The vertical shear resistance needs to be analysed to confirm this.

Table 6.1: List of active joint components

	Plug-and-play connection	**Single extended end-plate connection**
1	Column web panel in shear	Column web panel in shear
2	Column web in transverse compression	Column web in transverse compression
3	Column web in transverse tension	Column web in transverse tension
4	Column flange in bending	Column flange in bending
5	**Grip-plate in bending**	**End-plate in bending**
6	**Compression foot in compression**	
7	Beam flange and web in compression	Beam flange and web in compression
8	Beam web in tension	Beam web in tension
10	**Pins in tension**	**Bolts in tension**
11	Vertical shear resistance a) Welds to grip-plate b) Pins in shear c) Pins in bearing d) WAAM bond to column in shear	Vertical shear resistance a) Welds to end-plate b) Bolts in shear c) Bolts in bearing

The identified active joint components from table 6.1 are illustrated in Figure 6.1. The mechanical model, as shown in Figure 6.2, is used as an idealisation of the joint to assess the forces and deformations which follow from the analysis of independent components.

Eurocode 3, part 1-8 characterises the column web panel in shear to be in the compression zone of the joint, which is a simplification of the distortion of the column web. The distortion of the column web panel is associated with shear and the effect of load introduction due to beam forces. The distortion of the column web is occurring in the tensile and compressive zone. The adopted mechanical model characterises the distortion of the column web panel in shear as a horizontal deformation in the tensile zone [18, 56].

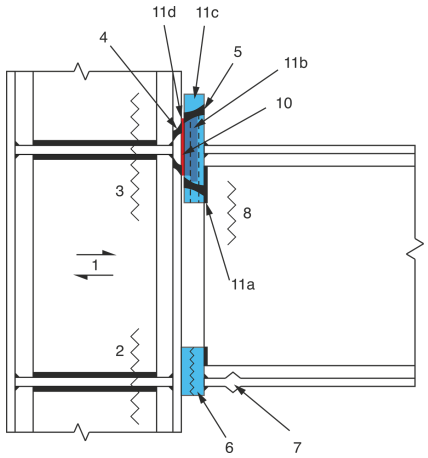

Figure 6.1: Identification of active joint components

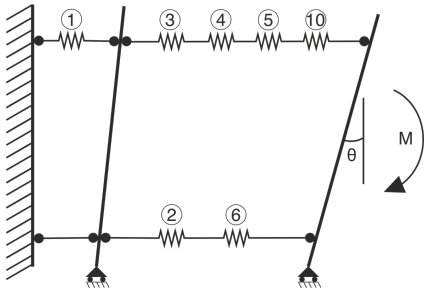

Figure 6.2: Mechanical model plug-and-play connection

The accuracy of the mechanical model will be evaluated by forming the moment-rotation curve from the forces and deformations of the separate components, using the mechanical model and comparing it to the moment-rotation curve formed in the global analysis of the joint.

6.2. Strength analysis of components

The strength analysis of the components is aimed to provide insight into the stress development in the separate joint components and stress distribution among the components in the joint. The strength analysis of the identified active components is accomplished according to the following process. Firstly, the nodes in the numerical model that correspond to the particular joint component are identified. The relevant stress component in these nodes is extracted and processed for each increment of the simulation. This data analysis results in a graphical representation of the stress distribution in the component. The graph of the stress distribution shows areas of high stress concentration, and the stress development in the joint component over time. Henceforth, the resulting force of the joint component is determined from the extracted data.

Eventually, the resulting forces of all joint components are applied to the presented mechanical model in Figure 6.2, to determine the bending moment resistance of the joint. The line of action of the tensile forces is assumed to be at the top of the upper beam flange, and for the compressive forces at the bottom of the bottom beam flange.

Lastly, the contribution of individual joint components to the bending moment resistance is determined. The results of the strength analysis of the components are compiled in Table 6.2. At the end of this section the contribution of the joint components, and the distribution of stresses in the joint are evaluated.

6.2.1. Column web panel in shear

The column web panel in shear (CWS) includes the column web and the fillet root up to the midpoint of the column flanges, as depicted in Figure 6.3. The relevant stress component for this analysis is the shear stress τ_{23}. The shear stress τ_{23} for each node in the column web panel in shear region, as shown in Figure 6.3, is extracted and processed.

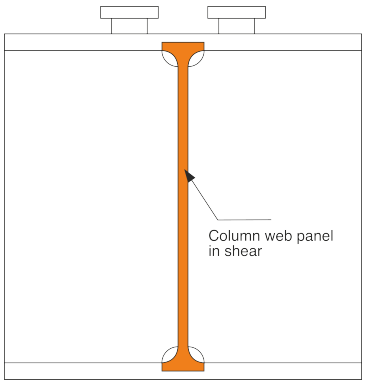

Figure 6.3: Column web panel in shear region - top view

During the processing of the stress data, the shear stress for each node at a horizontal plane over the height of the column web panel, is summed up. This leads to a shear force that acts at the height of every horizontal plane over the height of the column web panel. This force distribution over the height of the column web panel is shown in Figure 6.4. Figure 6.4 shows several lines which represent the force distributions for every increment during the simulation, and therefore the stress development in the column web panel during load application.

Figure 6.4 clearly shows that the stress is concentrated between the stiffeners. It also shows that during load application the stress distribution in the column web panel remains similar.

The resulting shear force is determined by accumulating the stress data of all the nodes in the column web panel in shear region. The resulting shear force is applied in the mechanical model to determine the bending moment resistance of the column web panel in shear, by multiplying it by its distance to the neutral axis. The resulting contribution of the column web panel in shear to the elastic and plastic moment resistance is listed in Table 6.2.

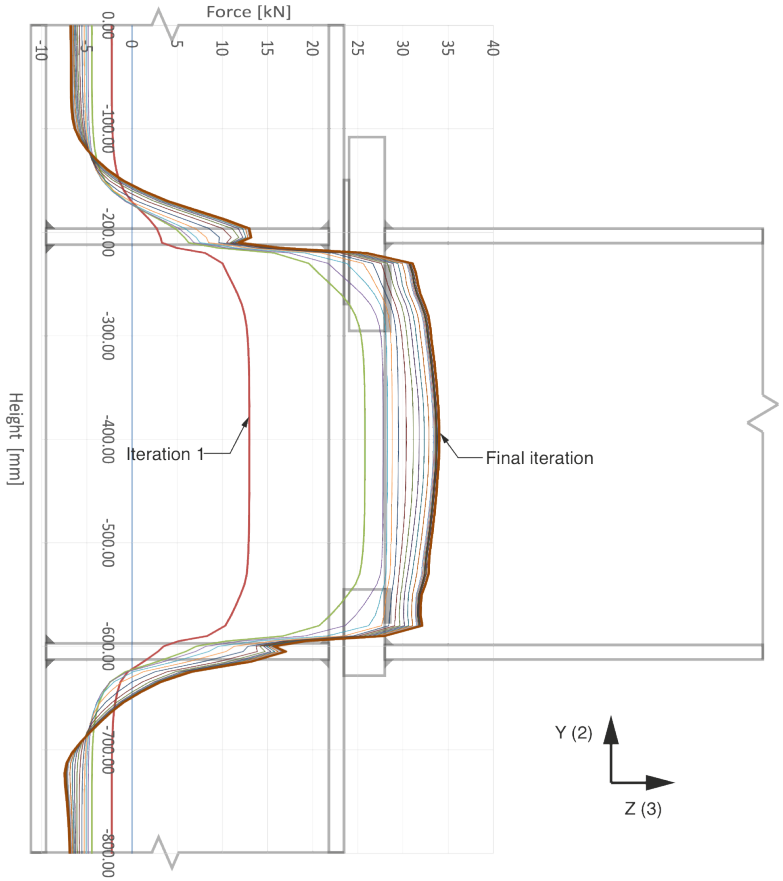

Figure 6.4: CWS shear force distribution over height

6.2.2. Column web in transverse compression and tension

The region of the column web in transverse compression (CWC) and tension (CWT) is the column web, excluding the fillet root, as shown in Figure 6.5. The relevant stress component for this analysis is the normal stress σ_{33}. The normal stress σ_{33} for each node in the CWC and CWT region, as shown in Figure 6.5, is extracted and processed.

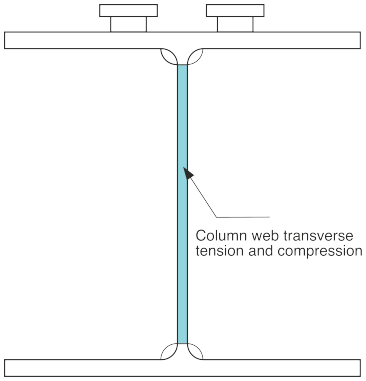

Figure 6.5: Column web in transverse tension and compression - top view

The stresses for each node in a horizontal plane over height of the column are accumulated to form the force distribution over height, for each increment during the simulation, as shown in Figure 6.6.

The force distribution of the first increment clearly shows that the neutral axis is located at the middle height of the beam. The force distribution in the column web between the transverse stiffeners changes during the load application. Initially, the forces are distributed somewhat linear, with a tensile zone above the neutral axis and a compressive zone under the neutral axis. But it is observed that with increasing load, the entire column web between the stiffeners is loaded in tension. This means that the neutral axis is shifting down during load application. This shifting has not been taken into account in this analysis.

The net force in each horizontal plane determines whether that plane is in tension or compression. The resulting compression force for the CWC is the cumulative force of all compressive planes. Similarly, the resulting tensile force for the CWT is the cumulative force of all tensile planes. The resulting forces are applied in the mechanical model. The contribution of each component to the bending moment resistance of the joint is calculated by multiplying the resulting force with its distance to the neutral axis. The resulting contribution of the CWC and CWT to the elastic and plastic moment resistance is listed in Table 6.2.

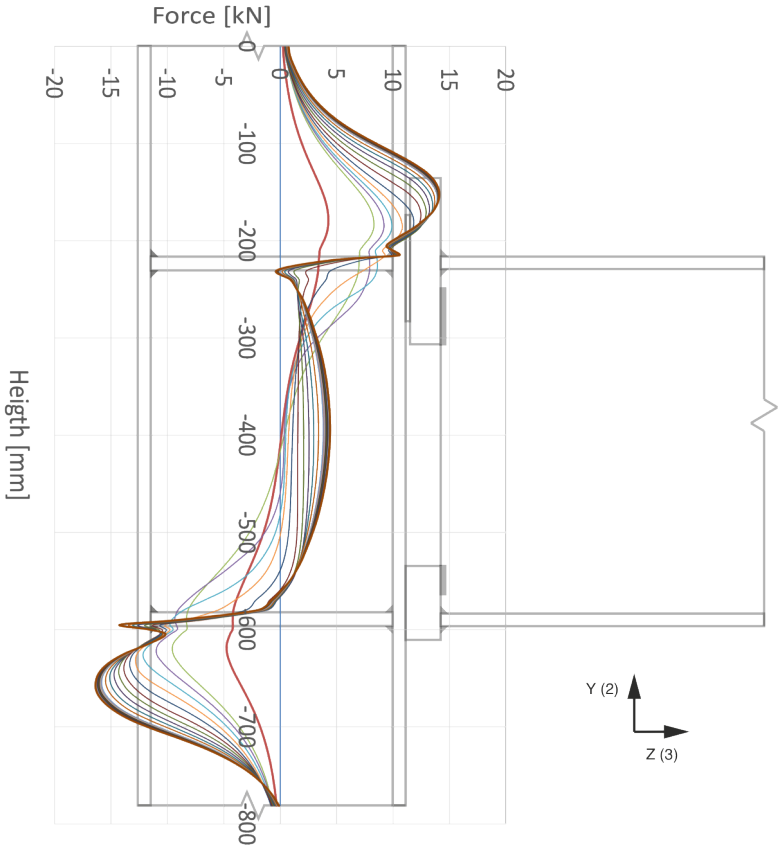

Figure 6.6: CWC & CWT force distribution over height

6.2.3. Column flange in bending

The region defining the column flange in bending is the column flange excluding the portion which contributes to the column web panel in shear, as shown in Figure 6.7. The normal stress σ_{33} is the relevant stress component. The normal stress σ_{33} for each node in the column flange in bending region is extracted and processed. It is noted that this is a simplification, and the influence of stress σ_{22} is neglected.

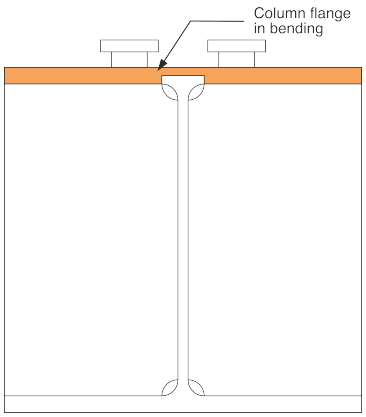

Figure 6.7: Column flange in bending - top view

The stresses for each node in a horizontal plane over height of the column flange are cumulated to form the force distribution over height, for each increment during the simulation, as shown in Figure 6.8.

The column flange in bending is only active in the tensile zone of the joint, which means that the force distribution is only assessed above the neutral axis.

Figure 6.8 shows that the stresses are concentrated at the height of the top of the pins. It also shows that the force distribution remains similar during the load application. This force distribution supports the assumption that the line of action for the tensile forces is at the top of the upper beam flange.

The resulting tension force of the column flange in bending is the accumulation of the stresses of all the nodes in the defined region. The resulting force is applied in the mechanical model, to determine the bending moment resistance of the column flange in bending. The contribution of the column flange in bending to the bending moment resistance of the joint is determined by multiplying the resulting force with its distance to the neutral axis, and is listed in Table 6.2.

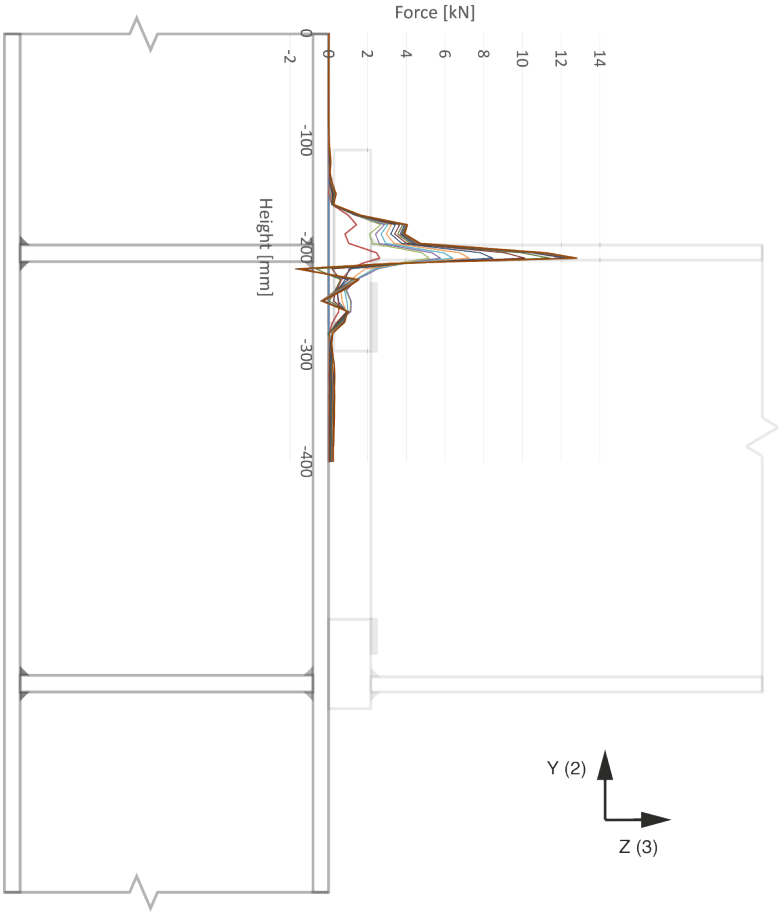

Figure 6.8: Column flange in bending force distribution over height

Pins in tension

The pins, with the pin shank and face, are analysed as one component, as shown in Figure 6.9. The relevant stress component the pins in tension is the normal stress σ_{33}. The normal stress σ_{33} for each node in the pins' region is extracted and processed. It is noted that this is a simplification, and the influence of stress σ_{22} is neglected.

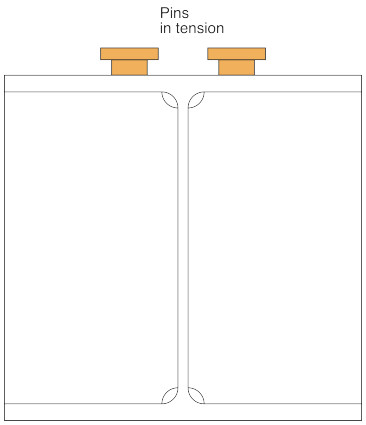

Figure 6.9: Pins in tension - top view

The stresses for each node in a horizontal plane of the height of the pins are accumulated to form the force distribution over height, for each increment during the simulation, see Figure 6.10.

The force distribution clearly shows a high stress concentration at the top of the pin shank. This is the failing component as initial yielding occurs at the top of the pin shank. Yielding in the top of the pin shank is determined by analysing the Von Mises stress to the yield stress of the pins' material. The force distribution develops during the load application. The stress remains concentrated at the top of the pin, but as the load increases the force in the upper half of the pin increases. The bottom half of the pin remains relatively low stressed, and does not increase much during increase of the load.

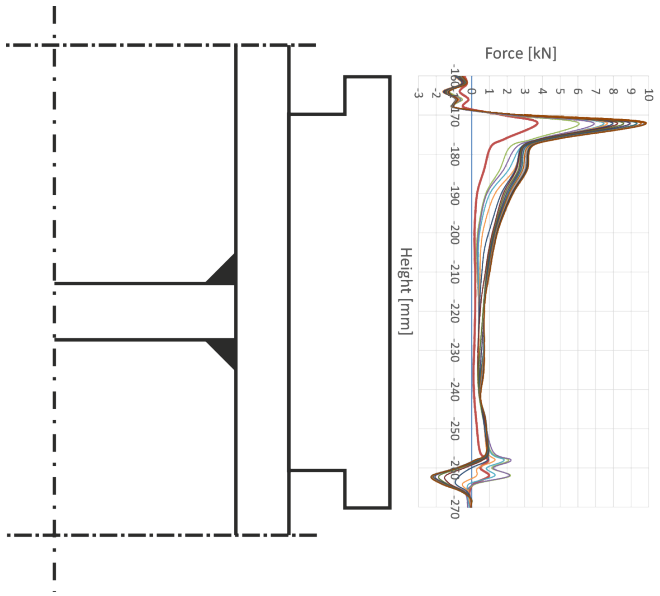

Figure 6.10: Pin force distribution over height

The resulting tension force of the pins is the accumulation of the stresses of all the nodes in both pins. The contribution of the pins in tension to the bending moment resistance of the joint is determined by applying the resulting force of both pins to the mechanical model and multiplying it with its distance to the neutral axis. The result is listed in Table 6.2.

6.2.4. Grip-plate in bending

The grip-plate is analysed as a whole. The relevant stress for the grip-plate in bending is the normal stress σ_{33}. The σ_{33} stress of all nodes in the grip-plate are accumulated to determine the resulting

tensile force of the grip-plate in bending. This resulting force is applied to the mechanical model and its contribution to the bending moment resistance is determined. It is noted that only considering σ_{33} is a simplification, and the influence of σ_{22} is neglected. The result is listed in Table 6.2.

6.2.5. Compression foot in compression

The compression foot is analysed as a whole. The relevant stress for the compression foot in compression is the normal stress σ_{33}. The stresses of all nodes in the compression foot are accumulated to determine the resulting compressive force of the compression foot. This resulting force is applied to the mechanical model and its contribution to the bending moment resistance is determined. The result is listed in Table 6.2.

6.2.6. Assembling of components

The resulting forces of the strength analysis of the individual joint components are assembled in the mechanical model, as shown in Figure 6.11. The contribution of each individual component to the bending moment resistance is determined by multiplying the resulting force of that component to its distance to the neutral axis. As mentioned, the neutral axis is located at the middle height of the beam. The total resulting tensile force is the accumulation of the forces of all components in the tension zone. Similarly, the total compressive force is the accumulation of the forces of all components in the compression zone. The total bending moment resistance is determined with equations 6.1 to 6.3.

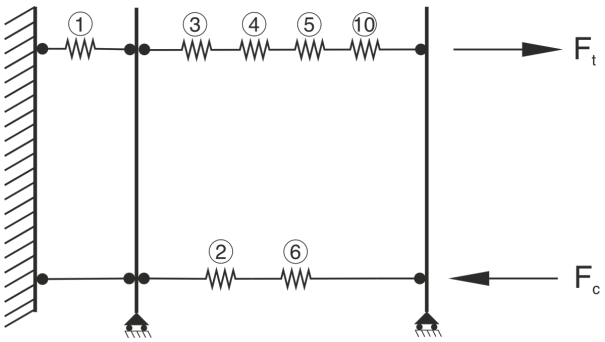

Figure 6.11: Forces acting in mechanical model

$$F_t = F_{webshear} + F_{webtension} + F_{flangebending} + F_{GPbending} + F_{Pinstension} \tag{6.1}$$

$$F_c = F_{webcompression} + F_{compr.foot} \tag{6.2}$$

$$M_{Rd} = F_t \cdot \frac{1}{2} h_b + F_c \cdot \frac{1}{2} h_b \tag{6.3}$$

To further understand the stress distribution in the joint, the contribution of each component to the bending moment resistance is analysed as a percentage of the total bending moment resistance. The percentage contribution of each component at M_{el} and M_{pl} is listed in Table 6.2. The results show that the column web panel in shear is dominating the behaviour of the joint. Due to plastic deformation redistribution of stresses occur. Table 6.2 shows that the redistribution of stresses occurs in the column web panel in shear and the pins in tension. These two components are the critical yielding components. The stresses are redistributed to the column web in transverse tension and compression.

Table 6.2: Component's contribution to joint strength

	Elastic moment resistance [kNm]	Contr. [%]	Plastic moment resistance [kNm]	Contr. [%]
Total	250.00	100.00	325.12	100.00
Column web panel in shear	136.90	**54.76**	173.04	**53.22**
Column web transverse compression	24.93	**9.97**	34.25	**10.53**
Column web in transverse tension	25.46	**10.18**	40.04	**12.32**
Column flange in bending	5.65	2.26	7.53	2.32
Grip-plate in bending	15.89	6.36	20.47	6.30
Compression foot in compression	16.89	6.76	22.16	6.82
Pins in tension	24.29	**9.72**	27.63	**8.50**

6.3. Stiffness analysis of components

The stiffness analysis of the components is aimed to provide insight into the deformation of individual joint components, and what the contribution of each component's deformation is to the joint stiffness. The stiffness analysis is accomplished according to the following process. Firstly, strategic nodes are selected in the component. The relative displacement between these strategic nodes was used to assess the deformation of the component. The deformation of the component is then used in the mechanical model to determine a corresponding rotation. The contribution of the component to the stiffness of the joint is evaluated as the contribution of its rotation to the total rotation of the joint. The results of the stiffness analysis of the components are compiled in Table 6.3.

All the strategic nodes are aligned with the height where their respective component is acting in the mechanical model, which is to say at height of the top or bottom of the beam flanges.

6.3.1. Column web panel in shear

The deformation of the column web panel in shear is characterised as a horizontal deformation in the tension zone. The distortion of the column web panel in shear can be divided in two components, a horizontal and vertical. The horizontal distortion is represented by the relative horizontal displacement of nodes DT1 and DT2, and the vertical distortion by the relative vertical displacement of nodes DT3 and DT4, see Figure 6.12.

Nodes DT1 and DT2 are located in the back-flange of the column and not in the middle of the column web to avoid the influence of elongation and shortening of the column web which occur due to transverse tension and compression. The middle plane's rotation is measured by the relative vertical displacement of nodes DT3 and DT4 and is translated to the horizontal displacement it causes at the height corresponding with the top of the beam flange.

The total horizontal deformation due to the column web panel in shear is calculated according to equation 6.4.

$$\delta_{shearweb} = (DT1_{U3} - DT2_{U3}) + \frac{DT3_{U2} - DT4_{U2}}{h_c} \cdot \frac{1}{2} h_b \tag{6.4}$$

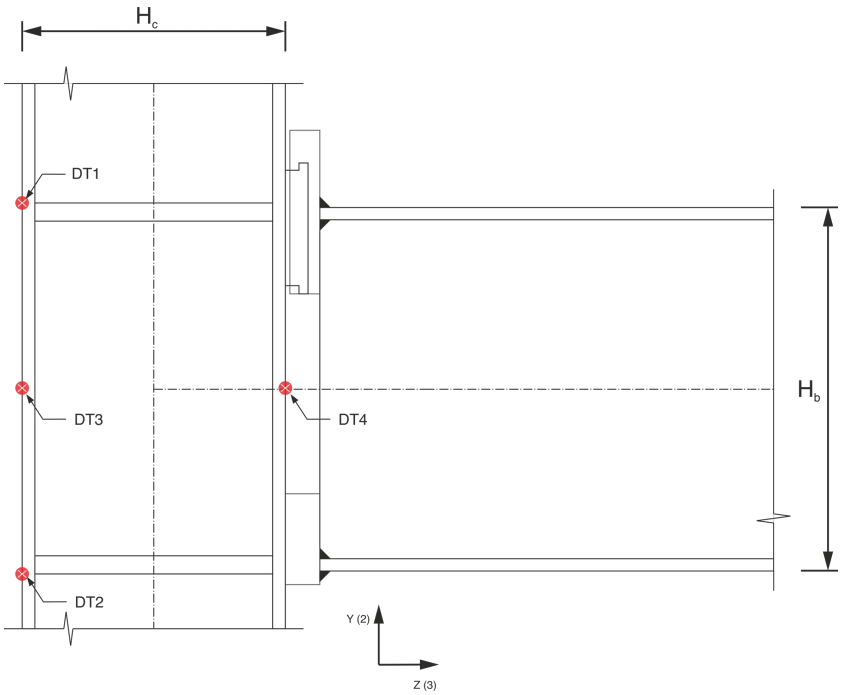

Figure 6.12: Nodes column web panel in shear

6.3.2. Column web in transverse compression and tension

The deformation of the column web due to transverse compression and tension is respectively characterised as shortening and elongation of the column web. The shortening of the column web in transverse compression is characterised by the horizontal displacements of nodes DT5 and DT6. The relative horizontal displacement of these nodes, according to equation 6.5, determines the shortening.

The elongation of the column web in transverse tension is characterised with the horizontal displacements of nodes DT7 and DT8. The relative horizontal displacement of these nodes, according to equation 6.6, determines the elongation.

$$\delta_{comp.web} = DT5_{U3} - DT6_{U3} \tag{6.5}$$

$$\delta_{tens.web} = DT7_{U3} - DT8_{U3} \tag{6.6}$$

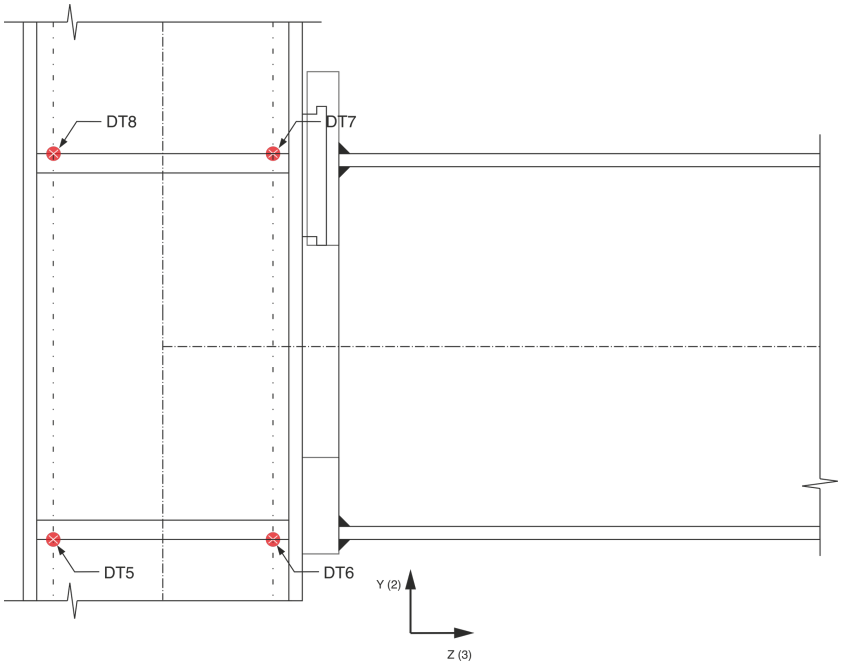

Figure 6.13: Nodes column web in transverse tension and compression

6.3.3. Column flange in bending

The deformation of the column flange due to bending is characterised by a gap which is formed between the middle of the column flange and the outer edges of the pins, see Figure 6.14. The formed gap is determined using the horizontal displacements of nodes DT13, DT14 and DT15. Node DT15 is located at the centre of the column flange, where minimal deformation occurs, while nodes DT13 and DT14 are positioned at the outer edges of the pins where the maximum deformation is expected to occur.

The average of the horizontal displacements of nodes DT13 and DT14 is used, to exclude any local effects. The deformation of the column flange is calculated according to equation 6.7.

$$\delta_{col.flange} = \frac{DT13_{U3} + DT14_{U3}}{2} - DT15_{U3} \tag{6.7}$$

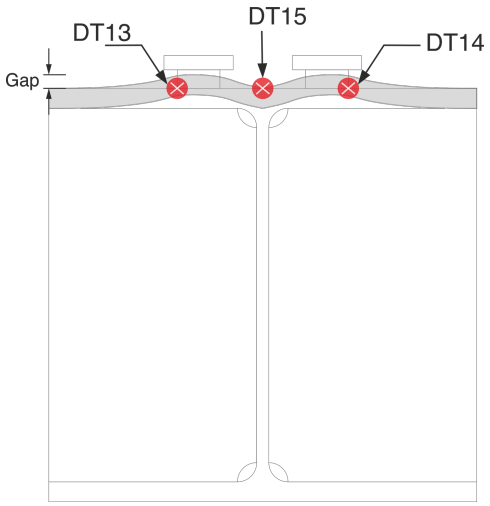

Figure 6.14: Nodes column flange in bending

6.3.4. Pins in tension

The deformation of the pins in tension is characterised as the elongation of the pins. The pins' elongations are determined using nodes DT16 and DT17, and nodes DT18 and DT19, see Figure 6.15.

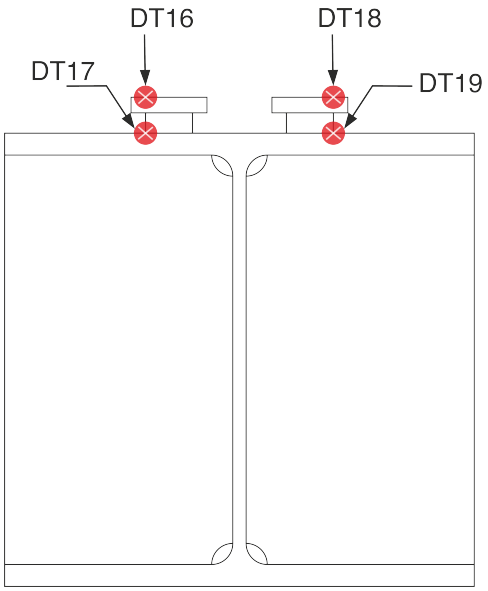

Figure 6.15: Nodes pins in tension

The average elongation of both pins is used to exclude any local effects. The deformation of the pins is calculated according to equation 6.8.

$$\delta_{pinelon.} = \frac{(DT16_{U3} - DT17_{U3}) + (DT18_{U3} - DT19_{U3})}{2} \tag{6.8}$$

6.3.5. Grip-plate in bending

The deformation of the grip-plate in bending is, similarly to the column flange in bending, characterised by a formed gap between the middle of the grip-plate and the outer edges of the pin slots. The formed gap is determined using the horizontal displacements of nodes DT9, DT10 and DT11, see Figure 6.16. Node DT11 is located at the centre of the grip-plate where minimal deformation occurs, while nodes DT9 and DT10 are positioned at the outer edges of the pins' slots where the maximum deformation is occurring.

The average of the horizontal displacements of nodes DT9 and DT10 is used, to exclude any local effects. The deformation of the grip-plate is calculated according to equation 6.9.

$$\delta_{GP} = \frac{DT9_{U3} + DT10_{U3}}{2} - DT11 \tag{6.9}$$

It is noted that node DT11 was also used in the global analysis to determine the global rotation of the joint. This was intended because the horizontal displacement of DT11, which was used to calculate the global rotation, is split into smaller portions which eventually trace back to node DT11.

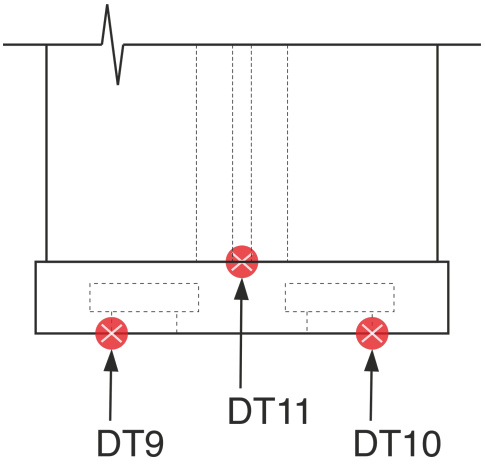

Figure 6.16: Nodes grip-plate in bending

6.3.6. Compression foot in compression

The deformation of the compression foot in compression is characterised as shortening of the compression foot. The shortening of the compression foot is determined using nodes DT19 and DT12, see Figure 6.17.

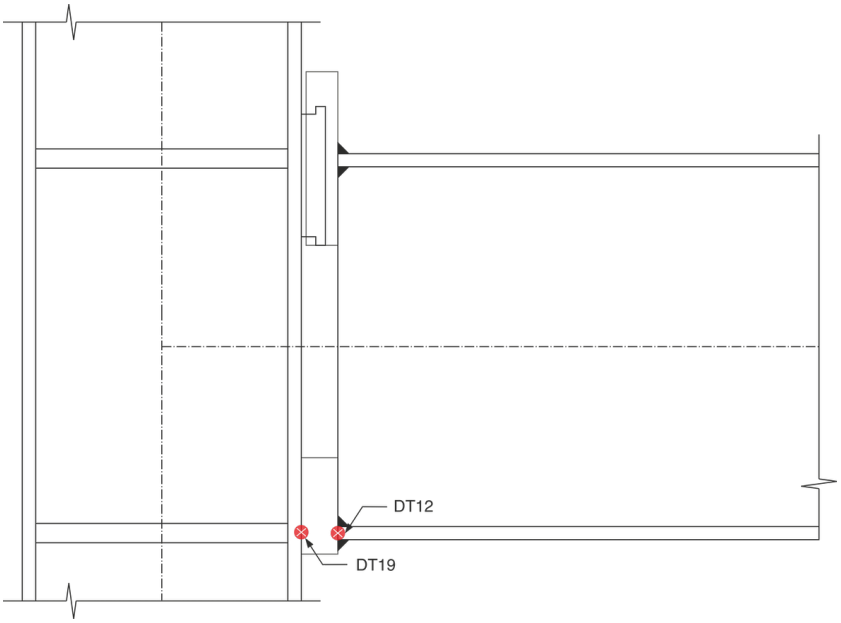

Figure 6.17: Nodes compression foot in compression

The deformation of the compression foot is calculated according to equation 6.10.

$$\delta_{comp.foot} = DT12_{U3} - DT19_{U3} \tag{6.10}$$

It is noted that node DT12 was also used in the global analysis to determine the global rotation of the joint. This was intended because the horizontal displacement of node DT12, which was used to calculate the global rotation, is split into smaller portions which eventually trace back to node DT12.

6.3.7. Assembling of components

The results of the stiffness analysis of the components are assembled in the mechanical model. The contribution of each individual component to the stiffness of the joint is determined by calculating the rotation that is induced due to the horizontal deformation of each component, according to equation 6.11. The contribution of the component is the ratio of its individual rotation to the total rotation of the joint.

$$\phi_i = arctan\left(\frac{\delta_i}{h_b}\right) \tag{6.11}$$

The total deformation in the tension and compression zone are calculated using equations 6.12 and 6.13 respectively. The total rotation of the joint is determined with the deformations of all components, using equation 6.14.

$$\delta_{tension} = \delta_{shearweb} + \delta_{tens.web} + \delta_{col.flange} + \delta_{pinelon.} + \delta_{GP} \tag{6.12}$$

$$\delta_{compression} = \delta_{comp.web} + \delta_{comp.foot} \tag{6.13}$$

$$\phi_{totalcomp.} = arctan\left(\frac{\delta_{tension} - \delta_{compression}}{h_b}\right) \tag{6.14}$$

The initial stiffness is used to classify the joint's rigidity. The stiffness of the joint deviates from the initial stiffness after the joint yields. Therefore, the contribution of the components to the joint stiffness is evaluated at a bending moment of $M_{Ed} = 130kNm$, which is smaller than the elastic moment resistance of the joint and is corresponding to the initial stiffness. Table 6.3 lists the contribution of each component to the joint stiffness at $M_{Ed} = 130kNm$. It shows that the deformation of the column web panel in shear dominates the behaviour of the joint. The deformation of the column web due transverse compression and tension contribute with 13.0%. Thus, the column web deformation is dominating the joint's deformation, and therefore its stiffness, with 88.9%.

Table 6.3: Component's contribution to joint stiffness

at $M_{Ed} = 130kNm$	Contribution [%]
Column web panel in shear	75.90
Column web transverse compression	7.34
Column web in transverse tension	5.66
Column flange in bending	1.72
Grip-plate in bending	5.70
Compression foot in compression	1.74
Pins in tension	1.95

6.4. Comparison to global analysis

The joint behaviour in the global analysis was determined by analysing the moment-rotation curve of the joint. The moment-rotation curve was obtained by analysing the bending moment from the reaction force at the open beam-end where the load is applied. The global rotation was determined by analysing the rotation of the column-side beam-end.

The component analysis assessed the strength and stiffness of each component separately. The bending moment resistance of each component was determined by evaluating the resulting force in each component. The rotation of each component was determined by evaluating the deformation of each component. The forces and deformation were evaluated, using a mechanical model, as an idealisation of the joint. In order to assess the accuracy of this idealisation, the moment-rotation curve which follows from the application of the forces and deformation to the mechanical model, is compared to the moment-rotation curve which followed from the global analysis, shown in Figure 6.18.

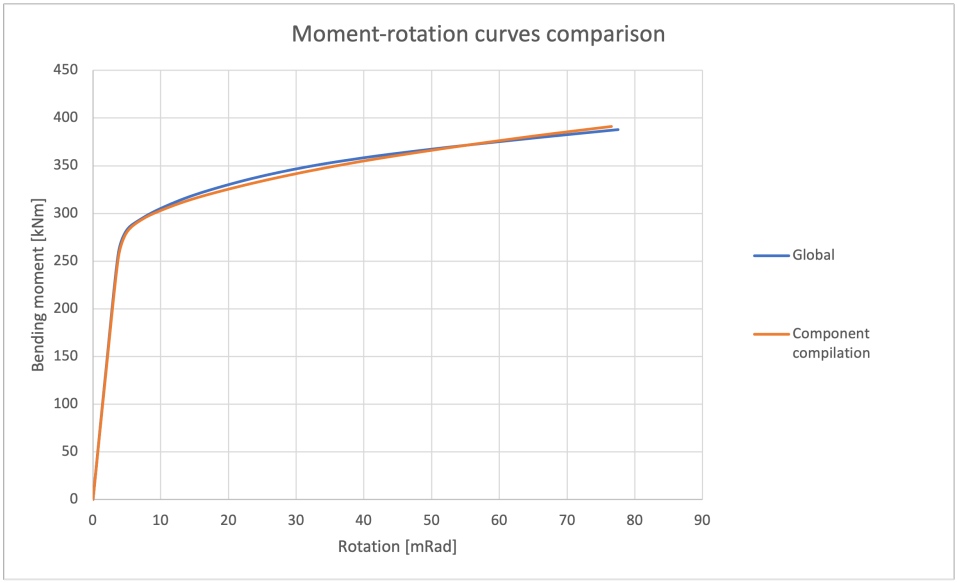

Figure 6.18: Comparison of $M - \theta$ curves

The graph illustrates that the moment-rotation curve from the component analysis nearly matches the moment-rotation curve from the global analysis. The maximum deviation between both curves is ± 2%. The matching of these curves allows to conclude that the right components were identified, the components were correctly defined for strength analysis, and that the strategic nodes were accurately representing the deformation of the components. The mechanical model, which is a simplification of the joint, accurately represents the joint's behaviour.

6.5. Summary

The component analysis identified the active joint components, which act together to determine the joint behaviour. The identified joint components' strength was assessed by the analysis of stress data in defined nodes of the numerical model. The analysis concluded that the highest stress concentration occurs in the top of the pins and that initial yielding occurs there, and that the bending moment resistance of the joint is dominated by the column web panel in shear. To avoid failing in the column, reinforcing of the column web through diagonal web stiffeners or supplementary web plates is suggested. The force distribution and development in the pins suggest that the upper transverse column stiffeners can be more effective if located higher, in line with the peak force in the pins, which can also influence the behaviour of the column web panel in shear.

In many situations the column web panel controls the behaviour of the joint [18], but a more balanced stress distribution in the joint makes more efficient use of each component's capacity. It is expected that a more balanced stress distribution can be achieved through modifications of the geometry and material of the pins, grip-plate and compression foot.

The stiffness of the joint components were assessed by analysing the deformation of the components. The deformation of the components were determined by analysing the displacement data in selected nodes. The determined deformations of joint components were translated to rotations, which indicate the contribution of each component to the joint stiffness. The analysis concluded that the stiffness of the joint is dominated by the column web panel in shear.

The comparison of the moment-rotation curves from the global and component analysis showed near matching, which concludes that the correct active joint components have been identified, and an accurate method has been applied to determine the strength and stiffness of each component, and of the joint.

The global analysis measured the negative effect of WAAM material properties and the necessary tolerances due to the surface roughness of the pins, to the joint stiffness and moment resistance. The negative influence of the lower material mechanical properties, and additional tolerances, is small, because of the low contribution of the pins and grip-plate to the joint's global behaviour. Minimal application of WAAM is therefore deemed correct. In case of open section columns, application of WAAM can be completely prevented, because the shape of the pins is simple enough to be manufactured with rolled steel and off-site welded to the column flange. In that case additional tolerances due to the surface roughness of WAAM are also prevented.

The insights into the stress distribution and deformation of individual joint components, and the contribution of components to the bending moment resistance and stiffness of the joint are utilised to adapt the plug-and-play connection to be applicable with a CHS column.

7

Adaptation to CHS column

Circular hollow sections provide several advantages relative to open sections, such as excellent torsion resistance, close equivalent stiffness in the two main directions, lack of sharp corners which makes them more efficient for corrosion protection, a lesser volume of fire protection material is required, concrete filling can improve load bearing and fire resistance, and their aesthetical appearance [9, 57, 58, 59]. Using CHS can obtain lighter structures when compared to similar structures with open sections and be economically competitive [57]. The primary disadvantage of structures with hollow sections is the complexity and expense of beam-to-column joints [58, 60]. Currently an open-to-hollow section connection is generally constructed by directly welding the open section surface to the CHS column surface [57]. Connections can also be designed using diaphragm plates, collar plates, or passing-through solutions [58, 60].

Conventional, directly welded I-beam-to-CHS-column connections are prone to local distortion of the tube-wall in presence of a bending moment which reduce the resistance and rigidity [60]. In these connections, the failure was dominated by local yielding of the CHS column, which disturbs the stability of the whole structure and limits the use of these connections [57, 60].

The application of the plug-and-play connection to CHS columns can provide a off-site manufacturable and easy to install connection for structures with hollow sections, eliminating the primary challenge for the use of hollow sections. An adaptation of the plug-and-play connection can even prevent local yielding in the CHS column to maintain stability of the whole structure, and herewith stimulate the use of hollow sections. However, the adaptation of the plug-and-play connection is not straight forward, because of the curved surface of the CHS column. Furthermore, it is assumed that bending is mainly resisted in the side chords of the column [9], and therefore the pins' shape will have to be adapted to effectively direct stresses to the side chords, to limit failing of the column. The adaptation of the pins' shape further complicates the application of the plug-and-play connection to CHS columns, and to conventionally manufacture and weld the pins to the curved surface of the columns.

To overcome the complication to manufacture and weld complex shaped pins, the innovative technology of WAAM can be employed. WAAM has the advantage that it only requires access to the surface it has to print on. This makes WAAM very suitable to manufacture the pins directly on the CHS column face, and to avoid welding of the pins to the column face. Thereby, WAAM has the ability to manufacture complex shapes on curved surfaces, making it very suitable to apply for the manufacturing of the pins.

This section proposes an adaptation of the plug-and-play connection to a CHS column, using insights from the global and component analysis. Firstly, the adapted plug-and-play connection is applied to a CHS column with a similar moment of inertia as the HEA300 column from the preceding configuration. The joint characteristics of the adapted plug-and-play joint with CHS column are compared with the single extended end-plate bolted joint and plug-and-play joint with the open section column, to assess the global structural effects of the adaptation and change to CHS column. Then the Von Mises stresses are analysed to determine the failure mode.

Finally, the adapted plug-and-play connection with CHS column is compared to an equivalent welded

I-beam-to-CHS-column joint, in terms of stiffness and bending moment resistance. In this comparative analysis the CHS column has a thinner wall thickness than in the previous analysis.

7.1. Proposed adaptation

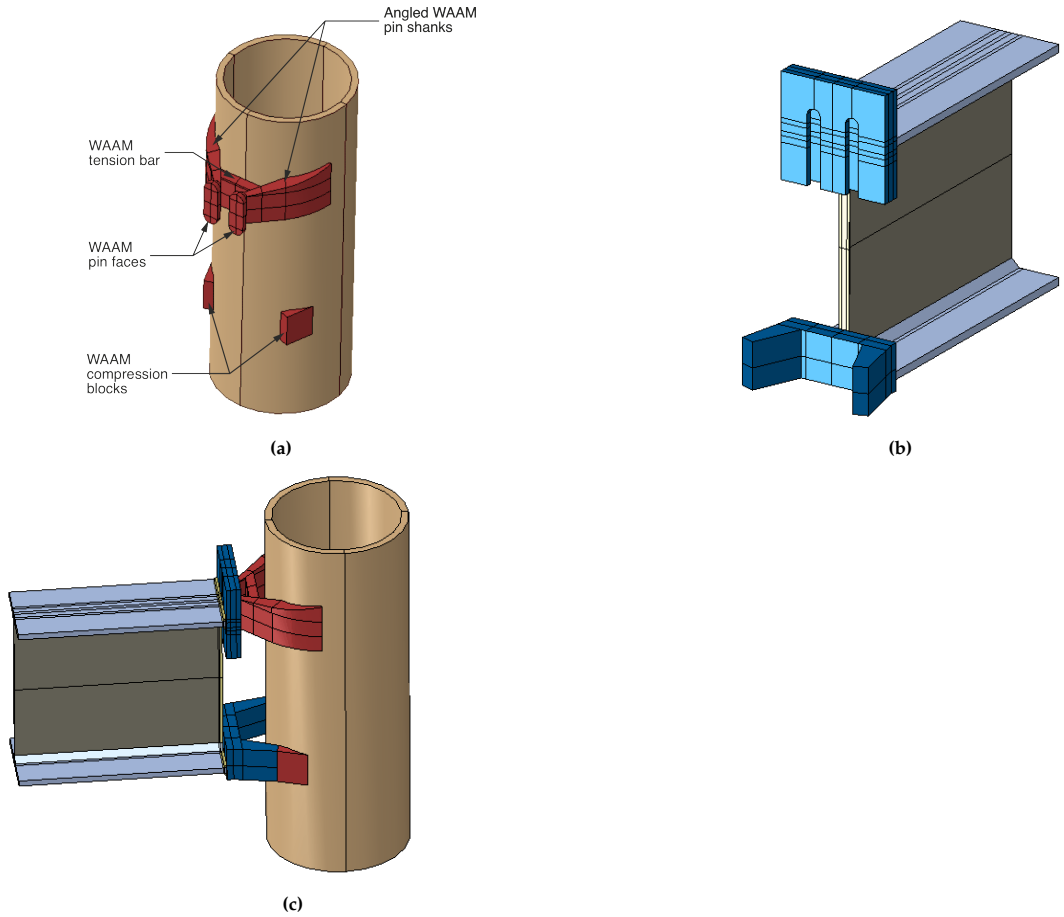

Figure 7.1: Plug-and-play joint with CHS column

An advantage of CHS columns is that they provide similar stiffness for different directions. Therefore, it is proposed to substitute the employed HEA300 profile in the test setup, with a CHS column with a diameter of 323.9 mm and a wall thickness of 16 mm. This is motivated by a similar moment of inertia for both section, $18264 \cdot 10^4 mm^4$ compared to $18390 \cdot 10^4 mm^4$ respectively. It is noted that the CHS 323.9 16 has a larger cross-sectional area than the HEA300, 154.77 mm^2 compared to 112.53 mm^2 respectively.

In order to direct the tensile stresses from the pins to the side chords of the column, the pins' shanks are angled to the side chords, see Figure 7.1a. The pins' shanks are angled to maintain the pins' faces at the same location. Translating the complete pins to the side chords would imply a wider grip-plate, which is not preferred due to the additional required material. As mentioned, local yielding of the column is dominating the failure for direct welded I-beam-to-CHS-column connections [57]. Due the inclination of the pins' shanks the tensile stresses on the column face have a smaller normal stress component, which reduces the risk of local yielding of the column.

The space between the column face and beam is increased, so that the inclined pins have enough space to reach the side chords in an angle of approximately 40°. This means that the pin shank is longer. The force distribution over the height of the pins, which followed from the component analysis of the pins in tension in section 6.2.3, shows that the stresses are concentrated at the top of the pin shank, see Figure 7.2. It is expected that the pin shank will rotate due to the excentric tensile forces. To mitigate the rotation of the pin shank, the shank's height is increased and tapered. Since yielding initiates at the top

of the pin shank, the width of the pin shank is increased at the column face and tapered to the pin face, to mitigate stress concentrations.

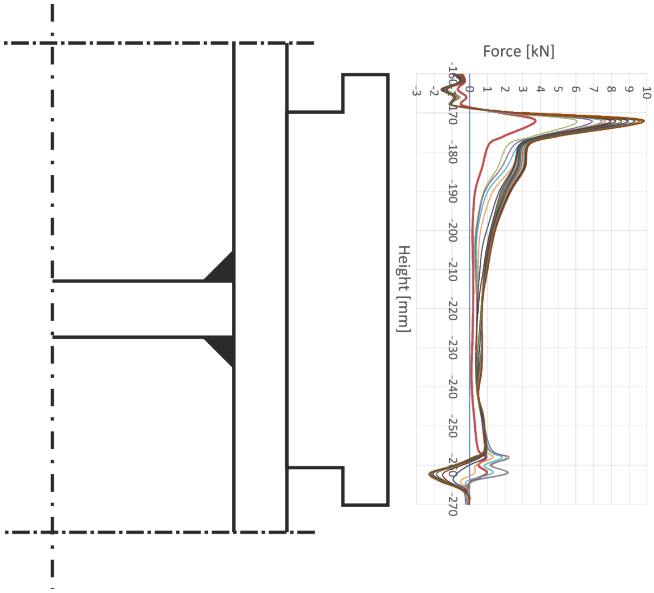

Figure 7.2: Pin force distribution over height - final design plug-and-play

Due to the angled pins' shanks it is expected that under tensile loading the shanks will deform and straighten. The component analysis showed that initial yielding occurs in the pin shank, thus it is expected that this deformation will be negatively impacting the stiffness of the joint. Therefore, the pin shanks are connected with a 'tension bar', see Figure 7.1a. This tension bar is mitigating the straightening of the pins' shanks.

The pins in tension are expected to be the failing component of the joint. To strengthen the pins a different feedstock wire for WAAM is suggested, which yields higher mechanical material properties, as shown in table 7.1.

Table 7.1: ER110S-G WAAM material properties [13]

Feedstock wire	**Condition**	**Build direction**	**Yield stress [MPa]**	**Ultimate stress [MPa]**	**Ultimate strain [-]**	**Young's modulus [MPa]**
ER110S-G	As-built	Vertical 90°	623	693	0.06	211800

The compressive stresses also need to be directed from the compression foot to the side chords of the column. To direct the stresses to the side chords, the compression foot is split in two smaller foots, which have a connected base, see Figure 7.1b. The foots are inclined, to reduce the normal stress component on the column face.

Because of the round perimeter of the column, it is expected that the compression foot will deform and slip, which will lead to a lower stiffness of the joint. In order to prevent slipping, compression block are WAAM manufactured on the side chords of the column, see Figure 7.1b. These compression blocks function as the recipient of the compression foot. The flat surface of the compression block is angled, to prevent horizontal slip of the compression foot.

These modifications incorporate some of the findings of the component analysis and leverage the advantage of WAAM to directly manufacture complex shapes on the column face.

7.2. Global analysis

The numerical model of the plug-and-play connection is modified, to assess the structural behaviour of this modified configuration. It is acknowledged that the numerical model is validated against an experiment and the component method, and it is demonstrated that geometrical modifications do not compromise the accuracy of the model. However, the column is expected to have a large influence in the accuracy of the numerical model. Therefore, it is acknowledged that such a great modification of the numerical model can negatively impact the accuracy of the model.

The modification of the numerical model of the plug-and-play connection are the geometrical modification of the column, pins, compression blocks, and compression foot; assigning the HEA300 column web material properties to the CHS column; assigning the WAAM material properties to the pins and compression blocks. Remaining aspects of the numerical model are identical.

The moment-rotation curves of the single extended end-plate bolted connection (SEEP bolted), plug-and-play I-beam-to-HEA300-column connection and the plug-and-play I-beam-to-CHS-column connection are shown in Figure 7.3. The joint characteristics are listed in table 7.2.

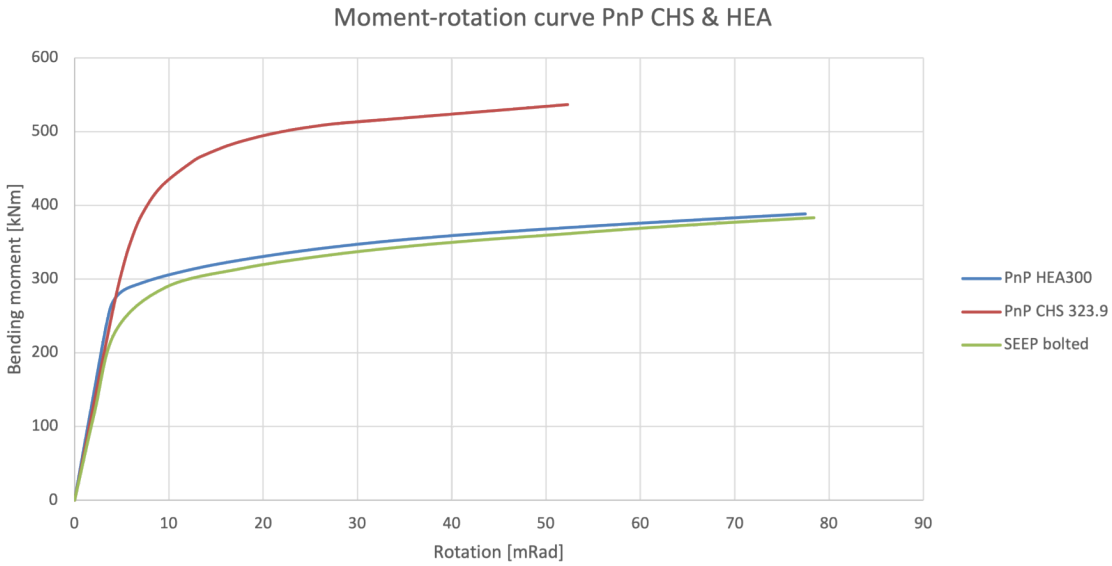

Figure 7.3: Comparison of moment-rotation curves

Table 7.2: Comparison of joint characteristics

	$S_{j,ini}$ [kNm/rad]	$M_{el,Rd}$ [kNm]	$M_{pl,Rd}$ [kNm]
Bolted connection with HEA300 column	57494	205	309
Plug-and-play connection with HEA300 column	71478	250	325
Plug-and-play connection with CHS 323.9/16 column	63903	300	490

The plug-and-play joint with the CHS column is stiffer (+11.1%) than the bolted connection with the open section column, although the columns have similar moments of inertia. The plug-and-play joint with the CHS column has a much higher elastic (+46.3%) and plastic (+58.5%) moment resistance. The Von Mises stress analysis shows that initial yielding occurs in the pin shanks and compression blocks and the column face is not yielding.

The plug-and-play joint with the CHS column compared to the plug-and-play connection with the open section column, has a lower stiffness (-10.3%). It is expected that this decrease is due to pin deformation and column shear deformation. However, the configuration with the CHS column exhibits a higher elastic (+20.0%) and plastic (+50.7%) moment resistance. It is expected that this increase is due to the prevention of column face plastification.

7.3. Comparative analysis

The conventional method to connect open section beams to CHS column is by direct welding of the beam surface to the CHS column face, see Figure 7.4 [57, 60]. Eurocode 3, part 1-8 provides very limited rules regarding the resistance of welded tubular joints and the stiffness of joints is entirely not considered.

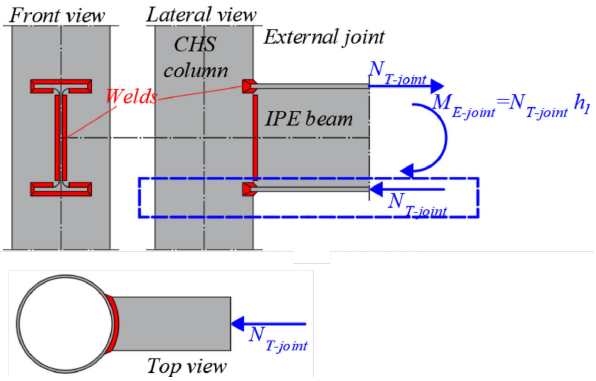

Figure 7.4: Welded I-beam-to-CHS-column joint [58]

Since Eurocode 3, part 1-8 provides very limited rules, a research was conducted wherein a parametric analysis of I-beam-to-CHS-column joints was done [58]. Validated numerical models were used to assess the stiffness and yield strength of such joints. The research explored a range of configurations with different IPE profile beams and CHS columns. Similar to the employed numerical models in this study, S355 material properties were adopted for the steel members, and all simulations underwent monotonic loading through a displacement. That research also analysed the stiffness and yield strength of the joint with an IPE400 beam to a CHS 323.9 column, with 6.3 mm wall thickness.

The results of the welded joint were compared to an equivalent plug-and-play joint. The adapted plug-and-play numerical model with CHS 323.9/16 column was modified by adjusting the column wall thickness from 16 mm to 6.3 mm, to match the welded joint's configuration. Simulation of the adapted plug-and-play numerical model with CHS 323.9/6.3 column resulted in the moment-rotation curve, as shown in Figure 7.5. The joint characteristics are determined from the moment-rotation curve, and compared to the equivalent welded joint in Table 7.3.

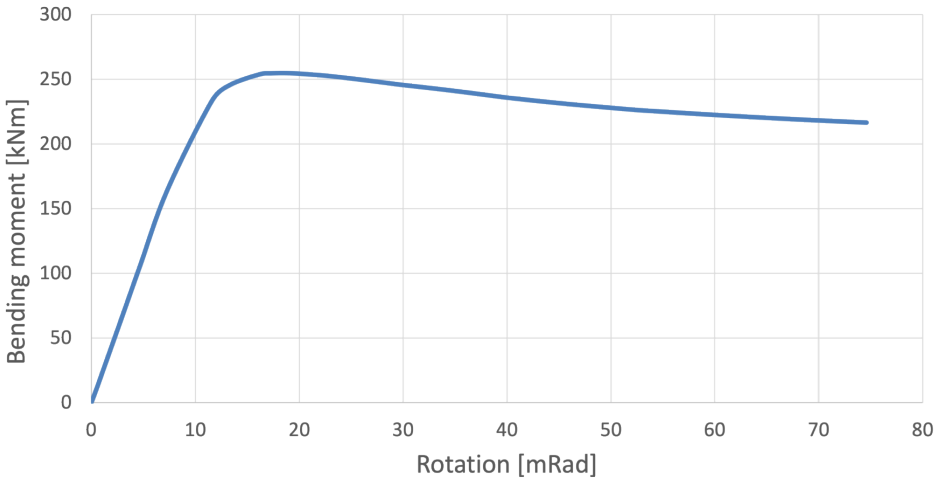

Figure 7.5: Moment-rotation curve of adapted plug-and-play joint with CHS 323.9/6.3 column

Table 7.3: Comparison of welded and plug-and-play joint characteristics [58]

	$S_{j,ini}$ [kNm/mrad]	$M_{el,Rd}$ [kNm]
Welded connection with CHS 323.9/6.3 column	18.74	92.8
Adapted plug-and-play connection with CHS 323.9/6.3 column	22.59	170.0
Difference	+20.5 %	+83.2%

The results show that the adapted plug-and-play joint has a significant higher initial stiffness than the conventional welded joint. Additionally, the plug-and-play joint has a much higher elastic moment resistance. This shows that this adapted plug-and-play connection establishes a stiffer and more resistant joint, compared to its equivalent welded joint. Additionally the plug-and-play joint provides the benefits to manufacture the connection off-site and simply install it on-site, and the possibility to reuse the connection.

Surely, the adapted plug-and-play connection uses more material than the welded connection, but the benefits of a plug-and-play connection as described throughout this study have been enabled for CHS columns with this connection. Particularly, the discarding of on-site welding avoids the need for skilled welders and extensive quality control of the welds. The construction process will be more efficient, since it is expected that welding requires more time than installation of the plug-and-play connection. These benefits and the reusability of the plug-and-play connection indicate that the plug-and-play connection can serve as a viable solution to the challenges to use CHS columns in structures.

7.4. Summary

The geometrical adaptation of the plug-and-play connection due to the CHS column led to complex shaped pins, and the need for compression blocks. The employment of WAAM to manufacture the pins and compression blocks directly on the column is a feasible solution, because of the complex shaped pins and the curved surface of the column. Utilising WAAM led to a plug-and-play connection which is applicable to CHS columns. The adapted plug-and-play connection offers an off-site manufacturable connection which eases on-site installation by preventing on-site welding and subsequent quality control of the welds.

The adapted plug-and-play connection establishes a relative stiffer and more resistant joint, than the generally applied welded joint. In this configuration failing occurs in the pins of the plug-and-play joint, and the column face of the CHS does not yield, whereas the column face fails in case of the welded joint, leading to disturbance of the whole structure.

In comparison to the considered single extended end-plate bolted connection with HEA300 column, the adapted plug-and-play joint with a CHS column with comparable moment of inertia, exhibits a higher initial stiffness and bending moment resistance. This demonstrates that the plug-and-play connection can lead to more and easier application of CHS columns, which can improve the overall structure due to stiffer and more resistant joints.

The plug-and-play connection to CHS columns is a novelty in the field, because it provides a plug-and-play beam-column connection for open section beams to hollow section columns, and in particular CHS columns. The plug-and-play joint yields a higher stiffness and moment resistance, than the equivalent direct welded connection. Hence, the plug-and-play connection, due to the integration of WAAM, provides a new solution to connect open section beams to CHS columns. Furthermore, it enables reusability, which is not possible with direct welded connections.

8

Conclusion and recommendations

8.1. Research question

The research question of this thesis is :

What novel plug-and-play beam-column joint can be designed to address the challenges of conventional connections, and what is its structural behaviour in terms of stiffness and moment resistance?

Design
The design of the plug-and-play connection arose as the result of a design scope, which addresses limitations of existing conventional and plug-and-play connections. It resulted in a connection of three parts, the pins, grip-plate and compression foot. The pins and grip-plate function as a 'key and lock,' and transfers tensile stresses. The compression foot leans onto the column surface, and transfers compressive stresses.

The plug-and-play connection has the following features, which address challenges of conventional connections:

- Completely off-site manufacturable
- No on-site welding required
- Simple connection
- Easy installation with a single downward movement
- Provides immediate support after emplacement
- Independently applicable to any column side
- Adaptable to CHS columns, through employment of WAAM
- Demountable and reusable connection

The structural behaviour of the plug-and-play joint in terms of stiffness and moment resistance was comprehensively evaluated through the global and component analyses.

Global analysis
The global analysis assessed the global joint behaviour using the moment-rotation curve. The plug-and-play joint was determined to have:

- **Stiffness:** An initial stiffness of $7.15 \cdot 10^{10} Nmm/rad$, classifying it as a semi-rigid joint, according to Eurocode 3, part 1-8.
- **Moment resistance:** An elastic moment resistance of $250 kNm$ and plastic moment resistance of $325 kNm$, classifying it as partial strength, according to Eurocode 3, part 1-8.

The global analysis confirms the suitability to design the plug-and-play joint as semi-rigid and partial strength.

Component analysis
The component analysis provided detailed insights into how individual joint components contribute to the global stiffness and moment resistance. Each component's strength and deformation was evaluated, and their contribution to the global joint's behaviour were quantified.

- **Column web panel in shear:** The joint's stiffness (76.3%) and moment resistance (elastic 54.8%; plastic 53.2%) are dominated by the column web panel in shear. The column web panel controls the behaviour of the joint. It yields almost immediately after initial yielding occurs in the pins.
- **Pins in tension:** The pins in tension contribute for 9.7% to the elastic moment resistance, and 8.5% to the plastic moment resistance. Initial yielding occurs in the pin shank, as stresses are highly concentrated at the top of the pin shank.
- **Column web in transverse tension and compression:** Both contribute approximately 10% to the elastic moment resistance. After yielding, the stresses are redistributed to the column web in transverse tension and less to the column web in transverse compression.
- **Remaining components:** The remaining components contributed less than 10% to the global stiffness or moment resistance of the joint. No stresses were redistributed to these components after yielding.

The component analysis demonstrated that the pins in tension and the column web panel in shear are the critical components.

The structural behaviour of the plug-and-play joint is an improvement compared to the equivalent single extended end-plate bolted joint in terms of stiffness (+24.3%) and moment resistance (+22.0% elastic; +5.2% plastic).

Adaptation to CHS column
The employment of WAAM resulted in an adapted plug-and-play connection which is applicable to CHS columns. The adapted connection provides a plug-and-play I-beam-to-CHS-column connection, which avoids on-site welding and simplifies and fastens on-site construction with CHS columns. Due to the higher stiffness and moment resistance of the adapted plug-and-play joint, relative to the considered equivalent conventional joints, the overall structure is improved. Further, the plug-and-play joint enables reusability and circularity, which is very challenging with conventional welded connections.

Assessment of the structural behaviour of the adapted plug-and-play joint led to the following conclusions:

- Analysis of the adapted plug-and-play joint with a CHS 323.9/16 column, with similar moment of inertia as HEA300, showed a higher stiffness (+11.1%), elastic moment resistance (+46.3%) and plastic moment resistance (+58.5%), than the single extended end-plate bolted joint with a HEA300 column.
- Analysis of the adapted plug-and-play joint with a CHS 323.9/6.3 column, showed a higher stiffness (+20.5%) and elastic moment resistance (+83.2%), than its equivalent direct welded joint. Failing occurs in the pins with the adapted plug-and-play joint but in case of a welded joint, the column face yields, and disturbs the whole structure.

8.2. Limitations of study

This study was limited to numerical simulations. The numerical model of the single extended end-plate bolted connection was validated against an experiment and the component method. The plug-and-play numerical model was developed through geometrical modifications of the validated single extended end-plate model. During iterations and the adaptation to the CHS column, the numerical model is further modified. It was shown and reasoned that sole geometrical modifications do not result in inaccuracy of the model. However, the numerical model of the plug-and-play connection is not calibrated against an experiment of the plug-and-play connection. This limits the validation of the plug-and-play numerical model.

The analyses were limited to monotonic loading. Further research should explore the joint's behaviour under cyclic loading, to assess aspects such as fatigue resistance, seismic performance and ductility.

The WAAM mechanical material properties have been adopted from tensile coupon tests but, especially the complex shaped pins on the CHS column, can have local distortions which are not taken into account in simulations.

Tolerances with regard to the surface roughness of WAAM were taken into account based on the difference of the tested WAAM wall [14]. Even though the tested wall showed no more than 1.5 mm difference, and the additional tolerance was 2 mm, bigger distortions can be possible. The tested WAAM wall had a simple print layer direction and build direction, but the pins have a more complex deposition path. This complexity can result in greater distortions than the expected 2 mm, and require additional tolerances.

The inaccuracies, cost of manufacturing, energy consumption, manufacturing and transportation processes, and scalability due to integration of WAAM are not considered. These aspects remain challenges of WAAM and require further investigation.

The design did not take tolerances into account for possible out of plumbness of columns. The plug-and-play connection requires the pins to be at the right position to install. Additional tolerances in the grip-plate are required to ensure easy installation. Out of plumbness of the column and insufficient tolerances in the grip-plate, can also lead to additional tensile stresses in the pin shank, and lead to premature yielding.

The plug-and-play connection has a straightforward installation and demounting process. Because the connection can be off-site pre-fabricated and inspected, it is expected that installation will be simple and fast. However, aspects such as out of plumbness of columns can be challenging. The study did not conduct experiments with regard to installation efficiency.

Likewise, the design appeals to modularity and reusability, but experiments have to confirm the reusability of the connection after loading to the serviceability limit state. Furthermore, a detailed life cycle assessment, which takes the high energy consumption of WAAM relative to conventional steel manufacturing in consideration, is required to quantify the environmental impact of the plug-and-play connection.

8.3. Future research recommendations

Several subject are mentioned that should be evaluated in future research to further improve the design and assess the structural behaviour of the plug-and-play joint. It is recommended to:

- Evaluate the required tolerances in the design, taking into account the possible out of plumbness of columns.
- Evaluate the adaptation to the CHS column and further optimise the design.
- Investigate the inaccuracy and distortions of WAAM produced pins and compression blocks.
- Conduct experimental testing to calibrate the numerical model and verify the results.
- Research the practical applicability of the plug-and-play connection, by investigating the manufacturing and transportation costs and time, assessing installation challenges, simplicity and time.

- Study the joint's behaviour under cyclic loading.
- Investigate the reusability of the plug-and-play connection through experimental testing.
- Perform a life cycle assessment of the plug-and-play connection, to assess whether it contributes to sustainability. The contribution of WAAM should be separately considered, to assess the applicability of WAAM from the perspective of sustainability.
- Evaluate the costs to manufacture the plug-and-play connection, and in particular the WAAM pins on the CHS column. The evaluation should consider the possibility to mass manufacture rolled pins and weld them to the column flange.
- Determine the vertical shear resistance of the plug-and-play joint, and in particular determine the shear resistance of the metallurgical bond of WAAM and the column surface, and bearing of the WAAM pins.

8.4. Contribution to the field

This research fills a critical gap in the field due to the development of a novel plug-and-play beam-to-column connection, as an alternative to conventional bolted and welded connections. Therewith, it applies research results regarding WAAM's mechanical material properties, to assess the behaviour and implications of the application of WAAM in this plug-and-play connection, and to adapt it to a novel plug-and-play I-beam-to-CHS-column connection.

Finally, this study contributes by presenting design requirements which avoid limitations and utilise advantages of current connections, which can be applied for new plug-and-play connection designs.

8.5. Concluding remarks

This study presents a promising step towards sustainable and circular structural design, through the development of a novel plug-and-play beam-column connection. By addressing challenges in conventional bolted and welded connections, and leveraging WAAM technology, the research contributes valuable insights to the field of structural engineering. However, further research and development are essential to realise the full potential of this plug-and-play connection in practice.

References

[1] *Paris Agreement*. URL: https://treaties.un.org/pages/ViewDetails.aspx?src=TREATY&mtdsg_no=XXVII-7-d&chapter=27&clang=_en (visited on 11/25/2024).

[2] M.J. Costello, M.M. Vale, W. Kiessling, S. Maharaj, J. Price, and G.H. Talukdar. "Cross-Chapter Paper 1: Biodiversity Hotspots". In: *Climate Change 2022: Impacts, Adaptation and Vulnerability. Contribution of Working Group II to the Sixth Assessment Report of the Intergovernmental Panel on Climate Change*. Ed. by H. O. Pörtner, D. C. Roberts, M. Tignor, E. S. Poloczanska, K. Mintenbeck, A. Alegría, M. Craig, S. Langsdorf, S. Löschke, V. Möller, A. Okem, and B. Rama. Cambridge, UK and New York, USA: Cambridge University Press, 2022, pp. 2123–2161. ISBN: 9781009325844. DOI: 10.1017/9781009325844.018.2123.

[3] B.C. Glavovic, R. Dawson, W. Chow, M. Garschagen, M. Haasnoot, C. Singh, and A. Thomas. "Cross-Chapter Paper 2: Cities and Settlements by the Sea". In: *Climate Change 2022: Impacts, Adaptation and Vulnerability. Contribution of Working Group II to the Sixth Assessment Report of the Intergovernmental Panel on Climate Change*. Ed. by H. O. Pörtner, D. C. Roberts, M. Tignor, E. S. Poloczanska, K. Mintenbeck, A. Alegría, M. Craig, S. Langsdorf, S. Löschke, V. Möller, A. Okem, and B. Rama. Cambridge, UK and New York, USA: Cambridge University Press, 2022, pp. 2163–2194. ISBN: 9781009325844. DOI: 10.1017/9781009325844.019.2163.

[4] Joint Research Centre. *EU climate targets: how to decarbonise the steel industry*. June 2022. URL: https://joint-research-centre.ec.europa.eu/jrc-news/eu-climate-targets-how-decarbonise-steel-industry-2022-06-15_en.

[5] IEA. *Iron and Steel Technology Roadmap*. https://www.iea.org/reports/iron-and-steel-technology-roadmap. License: CC BY 4.0. Paris, 2020.

[6] EN CEN. *Eurocode 3: Design of steel structures*. 2005.

[7] Frans Bijlaard. "Eurocode 3, a basis for further development in joint design". In: *Journal of Constructional Steel Research* 62.11 (2006). In Honour of Professor Patrick Dowling. Proceedings of a Symposium on Innovative and Sustainable Steel Construction held at the University of Surrey, pp. 1060–1067. ISSN: 0143-974X. DOI: https://doi.org/10.1016/j.jcsr.2006.06.012.

[8] Trayana Tankova, Hélder Craveiro, Luís Carlos Silva, Fernando F. Ribeiro, Rui Simões, Claúdio Martins, Ricardo Costa, and Luís Simões da Silva. "Behaviour of plug-and-play joints between RHS columns and CFS trusses". In: *Structures* 41 (2022), pp. 1719–1745. ISSN: 2352-0124. DOI: https://doi.org/10.1016/j.istruc.2022.05.099.

[9] J Wardenier, J Packer, Xiao-Ling Zhao, and G Vegte. *Hollow sections in structural applications*. Bouwen met staal, 2010.

[10] Sian I. Evans, Jie Wang, Jian Qin, Yongpeng He, Paul Shepherd, and Jialuo Ding. "A review of WAAM for steel construction – Manufacturing, material and geometric properties, design, and future directions". In: *Structures* 44 (2022), pp. 1506–1522. ISSN: 2352-0124. DOI: https://doi.org/10.1016/j.istruc.2022.08.084.

[11] Donghong Ding, Zengxi Pan, Dominic Cuiuri, and Huijun Li. "Wire-feed additive manufacturing of metal components: technologies, developments and future interests". In: *The International Journal of Advanced Manufacturing Technology* 81 (2015), pp. 465–481.

[12] Dong-Gyu Ahn. "Directed energy deposition (DED) process: state of the art". In: *International Journal of Precision Engineering and Manufacturing-Green Technology* 8 (2021), pp. 703–742.

[13] Cheng Huang, Pinelopi Kyvelou, Ruizhi Zhang, T. Ben Britton, and Leroy Gardner. "Mechanical testing and microstructural analysis of wire arc additively manufactured steels". In: *Materials & Design* 216 (2022), p. 110544. ISSN: 0264-1275. DOI: https://doi.org/10.1016/j.matdes.2022.110544.

[14] Trayana Tankova, David Andrade, Ricardo Branco, Carlos Zhu, Dulce Rodrigues, and Luís Simões da Silva. "Characterization of robotized CMT-WAAM carbon steel". In: *Journal of Constructional Steel Research* 199 (2022), p. 107624. ISSN: 0143-974X. DOI: https://doi.org/10.1016/j.jcsr.2022.107624. URL: https://www.sciencedirect.com/science/article/pii/S0143974X22004941.

[15] Mariela Mendez-Morales, Ricardo Branco, Trayana Tankova, and Carlos Rebelo. "Assessment of cyclic deformation behaviour of wire arc additively manufactured carbon steel". In: *International Journal of Fatigue* 184 (2024), p. 108307. ISSN: 0142-1123. DOI: https://doi.org/10.1016/j.ijfatigue.2024.108307.

[16] Lele Sun, Mei Liu, Yuanjian Liu, Peijun Wang, Hui Zhao, Jian Sun, and Yanwei Shang. "Studies on T-shaped one-side bolted connection to hollow section column under bending". In: *Journal of Constructional Steel Research* 175 (2020), p. 106359. ISSN: 0143-974X. DOI: https://doi.org/10.1016/j.jcsr.2020.106359.

[17] Cristian Vasile Miculas. *Innovative plug and play joints for hybrid tubular constructions*. July 2023. URL: https://hdl.handle.net/10316/110990.

[18] Hugo Renato Gonçalves da Silva Augusto. "Characterization of the behaviour of partial-strength joints under cyclic and seismic loading conditions". PhD thesis. University of Coimbra, Apr. 2017.

[19] Luís Simões da Silva, Luís Carlos Silva, Trayana Tankova, Hélder David Craveiro, Rui Simões, Ricardo Costa, Mario D'Aniello, and Raffaele Landolfo. "Performance of modular hybrid cold-formed/tubular structural system". In: *Structures* 30 (2021), pp. 1006–1019. ISSN: 2352-0124. DOI: https://doi.org/10.1016/j.istruc.2021.01.066.

[20] Nizar Bel Hadj Ali, Mohamed Sellami, Anne-Françoise Cutting-Decelle, and Jean-Claude Mangin. "Multi-stage production cost optimization of semi-rigid steel frames using genetic algorithms". In: *Engineering Structures* 31.11 (Nov. 2009), pp. 2766–2778. DOI: 10.1016/j.engstruct.2009.07.004.

[21] Ana Coelho, Ricardo Pimentel, Viorel Ungureanu, Petr Hradil, and Jyrki Kesti. *European Recommendations for Reuse of Steel Products in Single-Storey Buildings*. ECCS – European Convention for Constructional Steelwork, Jan. 2020. ISBN: 978-92-9147-170-6.

[22] ConXtech. *White paper: How prefabrication and assembly can dramatically accelerate projects in the first phase of construction*. Tech. rep. 01. ConXtech, Aug. 2022.

[23] Bree Renz. "Innovative Connections". In: *Modern steel construction* (Aug. 2005).

[24] M. Bosch-Willet. *Engineering Standard, Design of Connections CX-ENG-STD-000001*. 2nd ed. ConXtech, June 2019.

[25] *ConX systems*. Mar. 2022. URL: https://www.conxtech.com/conx-systems/.

[26] AISC Connection Prequalification Review Panel. *Prequalified Connections for Special and Intermediate Steel Moment Frames for Seismic Applications*. American Institute of Steel Construction, 2022.

[27] Iman Faridmehr, Mohd Hanim Osman, Mahmood Bin Tahir, Ali Farokhi Nejad, and Reza Hodjati. "Seismic and progressive collapse assessment of SIDEPLATE moment connection system". In: *Structural Engineering and Mechanics* 54.1 (Apr. 2015), pp. 35–54. DOI: 10.12989/sem.2015.54.1.035.

[28] MiTek. *SidePlate Brochure*. https://www.sideplate.com/2022/03/09/sideplate-brochure-spring-2022/. Mar. 2022.

[29] International Association of Plumbing and Mechanical Officials. *Uniform Evaluation Service Report*. Tech. rep. 525. 24. International Association of Plumbing and Mechanical Officials, Sept. 2019.

[30] MiTek. *SidePlate Bolted Field Work*. Youtube. Jan. 17, 2015. URL: https://www.youtube.com/watch?v=mpbWQbkl8_g#t=20m15s.

[31] International Organization for Standardization. *ISO/ASTM 52900 Additive manufacturing — General principles — Fundamentals and vocabulary*. 2021.

[32] Simon Ford and Mélanie Despeisse. "Additive manufacturing and sustainability: an exploratory study of the advantages and challenges". In: *Journal of Cleaner Production* 137 (2016), pp. 1573–1587. ISSN: 0959-6526. DOI: https://doi.org/10.1016/j.jclepro.2016.04.150. URL: https://www.sciencedirect.com/science/article/pii/S0959652616304395.

[33] S. El-Sayegh, L. Romdhane, and S. Manjikian. "A critical review of 3D printing in construction: Benefits, challenges, and risks". In: *Archives of Civil and Mechanical Engineering* 20.2 (Mar. 2020). DOI: 10.1007/s43452-020-00038-w.

[34] Mohammad Hassan Baqershahi, Can Ayas, and Elyas Ghafoori. "Design optimisation for hybrid metal additive manufacturing for Sustainable Construction". In: *Engineering Structures* 301 (Feb. 2024), p. 117355. DOI: 10.1016/j.engstruct.2023.117355.

[35] Mark Armstrong, Hamid Mehrabi, and Nida Naveed. "An overview of modern metal additive manufacturing technology". In: *Journal of Manufacturing Processes* 84 (2022), pp. 1001–1029. ISSN: 1526-6125. DOI: https://doi.org/10.1016/j.jmapro.2022.10.060.

[36] C. Buchanan and L. Gardner. "Metal 3D printing in construction: A review of methods, research, applications, opportunities and challenges". In: *Engineering Structures* 180 (2019), pp. 332–348. ISSN: 0141-0296. DOI: https://doi.org/10.1016/j.engstruct.2018.11.045.

[37] Xinchang Zhang and Frank Liou. "Chapter 1 - Introduction to additive manufacturing". In: *Additive Manufacturing*. Ed. by Juan Pou, Antonio Riveiro, and J. Paulo Davim. Handbooks in Advanced Manufacturing. Elsevier, 2021, pp. 1–31. ISBN: 978-0-12-818411-0. DOI: https://doi.org/10.1016/B978-0-12-818411-0.00009-4.

[38] S. W. Williams, F. Martina, A. C. Addison, J. Ding, G. Pardal, and P. Colegrove. "Wire + Arc Additive Manufacturing". In: *Materials Science and Technology* 32.7 (2016), pp. 641–647. DOI: 10.1179/1743284715Y.0000000073.

[39] Bellamkonda Prasanna Nagasai, Sudersanan Malarvizhi, and Visvalingam Balasubramanian. "Effect of welding processes on mechanical and metallurgical characteristics of carbon steel cylindrical components made by wire arc additive manufacturing (WAAM) technique". In: *CIRP Journal of Manufacturing Science and Technology* 36 (2022), pp. 100–116. ISSN: 1755-5817. DOI: https://doi.org/10.1016/j.cirpj.2021.11.005. URL: https://www.sciencedirect.com/science/article/pii/S1755581721001887.

[40] Jörg Lange, Thilo Feucht, and Maren Erven. "3D printing with Steel". In: *Steel Construction* 13.3 (Aug. 2020), pp. 144–153. DOI: 10.1002/stco.202000031.

[41] Jerzy K. Szlendak and Adrian Szpyrka. In: *Open Engineering* 10.1 (2020), pp. 563–570. DOI: doi:10.1515/eng-2020-0056. URL: https://doi.org/10.1515/eng-2020-0056.

[42] Jerzy Szlendak and Adrian Szpyrka. "Research on AM non welded N RHS truss joints – resistance criteria". In: June 2021, pp. 356–362. ISBN: 9781003132134. DOI: 10.1201/9781003132134-45.

[43] Salomé Galjaard, Sander Hofman, Neil Perry, and Shibo Ren. "Optimizing Structural Building Elements in Metal by using Additive Manufacturing". In: Aug. 2015.

[44] A. H. Snijder, L. P. van der Linden, C. Goulas, C. Louter, and R. Nijsse. "The glass swing: A vector active structure made of glass struts and 3D-printed steel nodes". In: *Glass Structures & Engineering* 5.1 (2019), pp. 99–116. DOI: 10.1007/s40940-019-00110-9.

[45] ARUP. "Printing the build environment". In: *The Arup Journal* 01 ().

[46] MX3D. *Connector for takenaka*. Mar. 2023. URL: https://mx3d.com/industries/construction/connector-for-takenaka/.

[47] Yiqi Zhang, Fangjie Cheng, and Shaojie Wu. "The microstructure and mechanical properties of duplex stainless steel components fabricated via flux-cored wire arc-additive manufacturing". In: *Journal of Manufacturing Processes* 69 (2021), pp. 204–214. ISSN: 1526-6125. DOI: https://doi.org/10.1016/j.jmapro.2021.07.045. URL: https://www.sciencedirect.com/science/article/pii/S1526612521005429.

[48] J.M. Cabrero and E. Bayo. "Development of practical design methods for steel structures with semi-rigid connections". In: *Engineering Structures* 27.8 (2005), pp. 1125–1137. ISSN: 0141-0296. DOI: https://doi.org/10.1016/j.engstruct.2005.02.017.

[49] Pedro Nuno Gonçalves Nogueiro. *Comportamento cíclico de ligações metálicas*. Nov. 2009. URL: https://bibliotecadigital.ipb.pt/bitstream/10198/4334/1/Tese%20Doutoramento%20PN.pdf.

[50] Dassault Systèmes. *Abaqus Analysis User's Guide*. Abaqus Inc. 2016. URL: http://130.149.89.49:2080/v2016/books/usi/default.htm.

[51] Structural Safety European Convention for Constructional Steelwork. Technical Committee 1 and Seismic Design Loadings. Technical Working Group 1.3. *Recommended Testing Procedure for Assessing the Behaviour of Structural Steel Elements Under Cyclic Loads*. European Convention for Constructional Steelwork nrs. 45-49. ECCS, 1986. URL: https://books.google.nl/books?id=qeBRAAAAMAAJ.

[52] Tongxi Yu and Pu Xue. "Chapter 4 - Yield criteria". In: *Introduction to Engineering Plasticity*. Ed. by Tongxi Yu and Pu Xue. Elsevier, 2022, pp. 67–87. ISBN: 978-0-323-98981-7. DOI: https://doi.org/10.1016/B978-0-323-98981-7.00004-X.

[53] A. Lytle, K. Saidi, W. Stone, and J. Gross. "Report of the NIST Workshop on Automated Steel Construction". In: *Proceedings of the 19th International Symposium on Automation and Robotics in Construction (ISARC)*. Ed. by William C. Stone. Washington, DC, USA: International Association for Automation and Robotics in Construction (IAARC), Sept. 2002, pp. 247–253. DOI: 10.22260/ISARC2002/0039.

[54] E. Bayo, J.M. Cabrero, and B. Gil. "An effective component-based method to model semi-rigid connections for the global analysis of steel and composite structures". In: *Engineering Structures* 28.1 (2006), pp. 97–108. ISSN: 0141-0296. DOI: https://doi.org/10.1016/j.engstruct.2005.08.001. URL: https://www.sciencedirect.com/science/article/pii/S0141029605002804.

[55] Abed Rigi, Behtash JavidSharifi, Mohammad Ali Hadianfard, and T.Y. Yang. "Study of the seismic behavior of rigid and semi-rigid steel moment-resisting frames". In: *Journal of Constructional Steel Research* 186 (2021), p. 106910. ISSN: 0143-974X. DOI: https://doi.org/10.1016/j.jcsr.2021.106910.

[56] Sandra Jordão, L. Simões da Silva, and Rui Simões. "Behaviour of welded beam-to-column joints with beams of unequal depth". In: *Journal of Constructional Steel Research* 91 (2013), pp. 42–59. ISSN: 0143-974X. DOI: https://doi.org/10.1016/j.jcsr.2013.07.023.

[57] Rajarshi Das, Alper Kanyilmaz, Mael Couchaux, Benno Hoffmeister, and Herve Degee. "Characterization of moment resisting I-beam to circular hollow section column connections resorting to passing-through plates". In: *Engineering Structures* 210 (2020), p. 110356. ISSN: 0141-0296. DOI: https://doi.org/10.1016/j.engstruct.2020.110356. URL: https://www.sciencedirect.com/science/article/pii/S0141029619317389.

[58] Ali Ajwad, Sabatino Di Benedetto, Massimo Latour, and Gianvittorio Rizzano. "A component method approach for single-sided beam-to-column joints with CHS column and welded double-tee beam". In: *Thin-Walled Structures* 202 (2024), p. 112055. ISSN: 0263-8231. DOI: https://doi.org/10.1016/j.tws.2024.112055. URL: https://www.sciencedirect.com/science/article/pii/S0263823124004981.

[59] Rui Yan and Milan Veljkovic. "Component method for bolted SHS end plate splice joints loaded in tension". In: *Structures* 59 (2024), p. 105704. ISSN: 2352-0124. DOI: https://doi.org/10.1016/j.istruc.2023.105704. URL: https://www.sciencedirect.com/science/article/pii/S2352012423017927.

[60] Maël Couchaux, Carlo Castiglioni, Mohammed Hjiaj, and Frantisek Wald. "I-beam-to-CHS-column moment resisting joints using passing-through plates". In: *Journal of Constructional Steel Research* 184 (2021), p. 106703. ISSN: 0143-974X. DOI: https://doi.org/10.1016/j.jcsr.2021.106703. URL: https://www.sciencedirect.com/science/article/pii/S0143974X21001851.

A

Validation numerical model

A.1. Experimental Setup

The considered experiment which served as a validation for the FE model is conducted in 2009 at the University of Coimbra [49]. The setup of the experiment consisted of a 3.0 meter high column, an 1.15 meter long beam, an 18 mm thick double extended end-plate and eight 10.9 bolts and nuts.

The column was a HEA320 profile supported by a concrete block with a pinned joint at the bottom. The top of the column was supported horizontally but allowed vertical displacement and rotations. The transverse stiffeners were aligned with the beam flanges and welded to the column flanges and web.

The end-plate was welded with 45° fillet welds to the beam-end. The drilled holes in the end-plate and column flange were 26 mm. The beam is connected to the column by eight M24 10.9, full-threaded, hand-tightened bolts.

The open beam-end was loaded through an hydraulic actuator. The load was applied as a displacement in a constant rate, creating a bending moment in the joint. No axial force was present in the column. Figure A.1 shows the experimental setup and the joint details are illustrated in figure A.2.

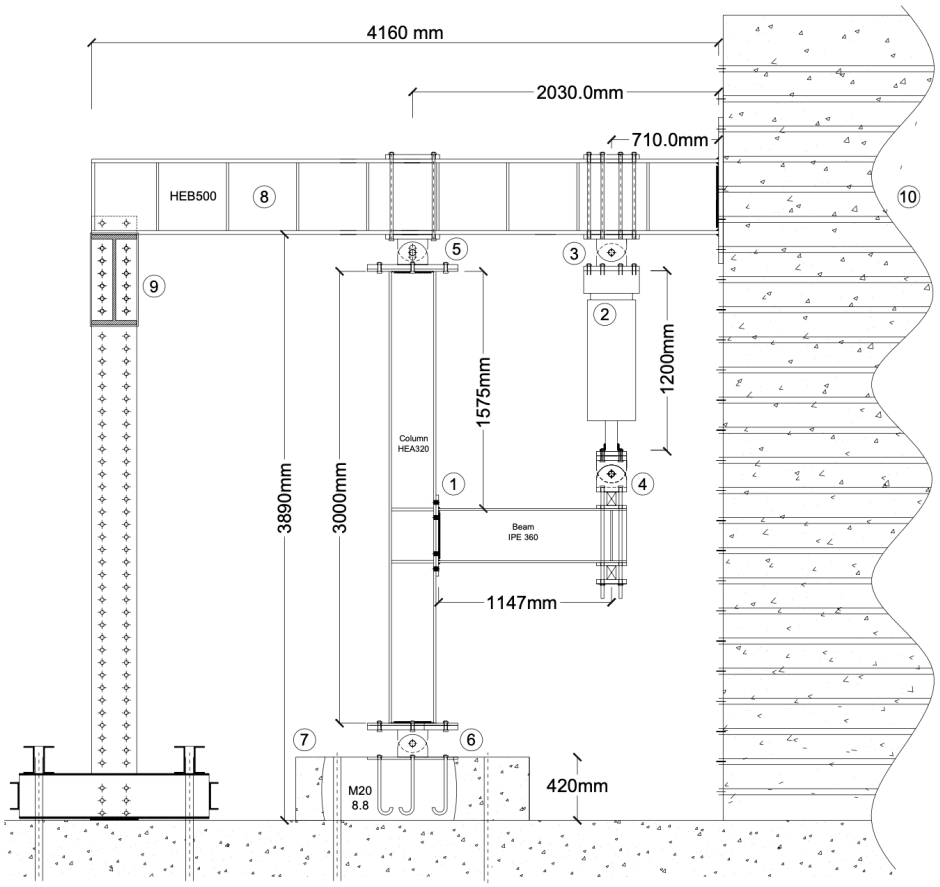

Figure A.1: Experimental setup [49]

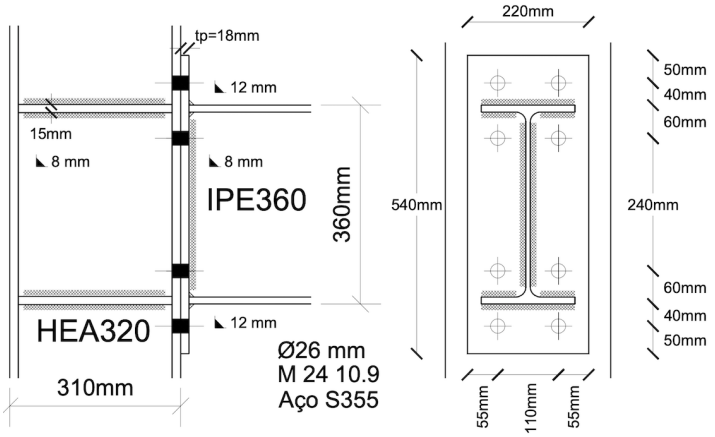

Figure A.2: Joint details of experiment [49]

The test setup was equipped with strain gauges to measure the surface deformations, as shown in figure A.3.

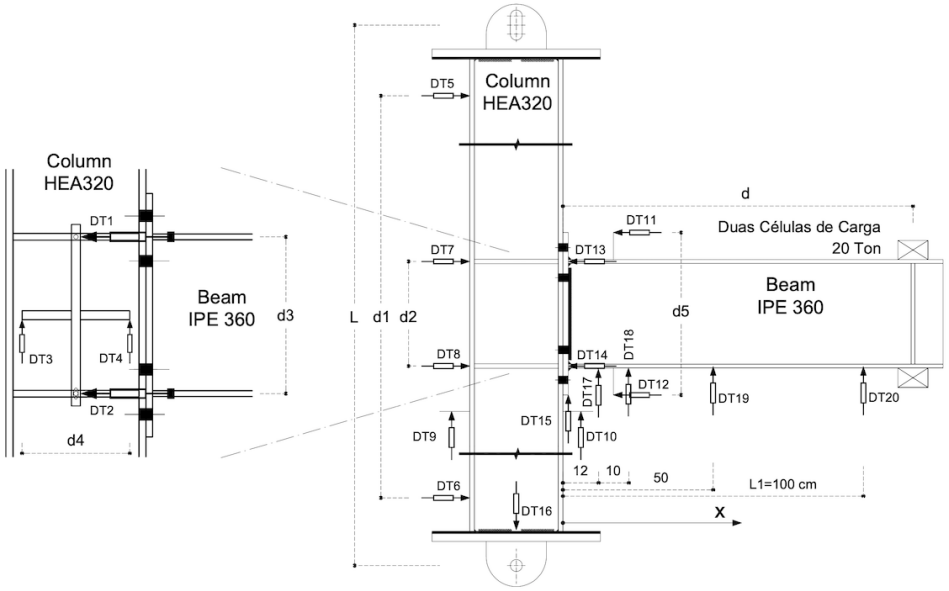

Figure A.3: Strain gauges' arrangement [49]

A.2. Numerical model

The detailed setup of the double extended end-plate bolted connection numerical model is presented in this section. Key aspects such as element type, material properties, constraints and interaction between parts are described. It also covers the partitioning and meshing strategies used to optimise computational efficiency and accuracy. Additionally, the loading steps are explained. The double extended end-plate bolted connection numerical model's characteristics are identical to the single extended end-plate bolted connection numerical model, as described in the report. Each aspect of the numerical model is summarised here, and a more elaborate description is to found in chapter 4 of the report.

A.2.1. Element type

The numerical model employs solid C3D8R finite elements. The elements used enhanced hourglass control to mitigate hourglassing. Three layers of elements are maintained across the thicknesses of the parts.

A.2.2. Parts

The individual parts of the joint region in the model are illustrated in figure A.4. The column is divided in three parts, and the beam in two parts. A finer mesh is applied to the column in the joint region, to reduce computation time.

For simplicity, the bolt and nut are modelled as a single part. The end-plate and stiffeners, are modelled as individual parts with the shown dimensions.

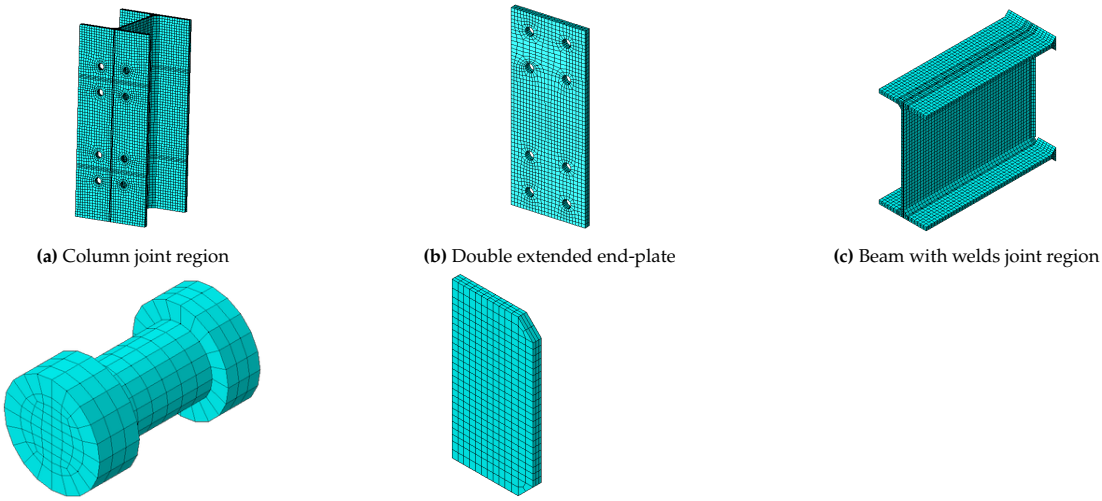

(a) Column joint region

(b) Double extended end-plate

(c) Beam with welds joint region

(d) Bolt

(e) Stiffener

Figure A.4: Parts in joint region

As a simplification of the fillet root of the column and beam profiles, the fillet is modelled as a triangle with an equivalent area.

The different parts are then positioned and connected according to the experimental setup, as shown in figure A.1, for simulation. In the assembly the orientations, interactions, constraints and boundary conditions are defined in accordance to the experiment [49]. Figure A.5 illustrates the joint region of the assembled model.

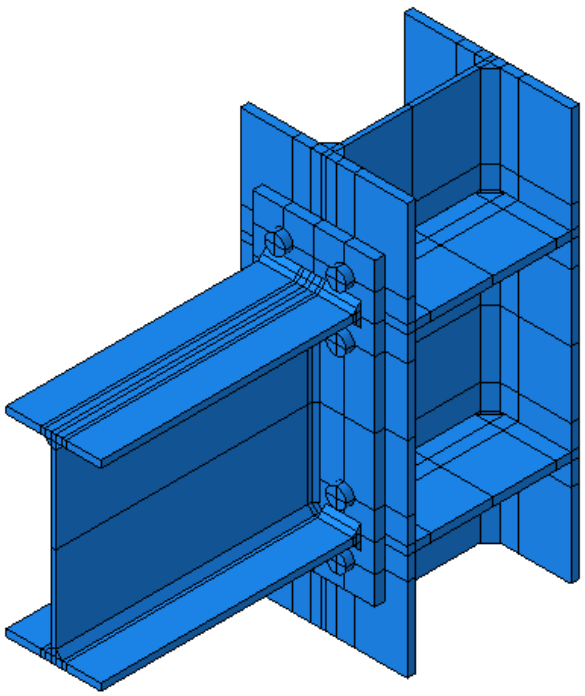

Figure A.5: Assembled numerical model

A.2.3. Material properties

The material properties in the numerical model are derived from the average mechanical properties of tensile tested steel coupons in the experiment [49]. Steel coupons were extracted from the web and flanges of the beams and column, end-plate and stiffeners. The material properties of the bolts are also derived from the average mechanical properties of tensile tested bolts in the experiment [49]. ABAQUS requires the true stress and true plastic strain data as input for the material properties. The material properties of the tensile coupon tests are converted to the tri-linear true stress and true strain data, as shown in table 4.2 [18]. These material properties are used in the numerical model.

A.2.4. Constraints and interactions

Reference points are created at the centre of the top and bottom surfaces of the column. The reference points are constrained to the column surfaces using rigid body constraints. The boundary conditions are applied to the reference points.

A reference point is created at the centre of the open beam-end. The displacement is applied to the reference point.

The fillet welds are modelled directly on the beam. The welds are constrained to the corresponding regions of the end-plate using a tie constraint. The transverse stiffeners are constrained to the column web and flanges, using a tie constraint.

Normal behaviour of contact interactions is modelled by the general contact algorithm. A friction coefficient of 0.3 is applied, and separation after contact is allowed.

A.2.5. Mesh

The parts are partitioned and meshed, in such a that a structured mesh is generated. The mesh size is determined by analysing models SENS 1 until SENS 5. Model SENS 1 has a relative coarse mesh, and the mesh size is reduced for each model, until model SENS 5 with the finest mesh in the sequence. The moment-rotation curve for each model was formed and compared, as shown in figure A.6. The graph shows that the models SENS 2 to 5 generate similar moment-rotation curves. The stiffness of the joint is determined for each model to determine the most appropriate mesh size. Table A.1 shows that model SENS 4 generates similar results as SENS 5, but the simulation of SENS 5 required significant more time and computational power. Hence, the mesh size of model SENS 4 is adopted as optimal. The global seed sizes of the generated mesh are listed in table A.2. In the perimeter of the bolts holes additional seeds are created, such that 20 elements are generated in the entire perimeter.

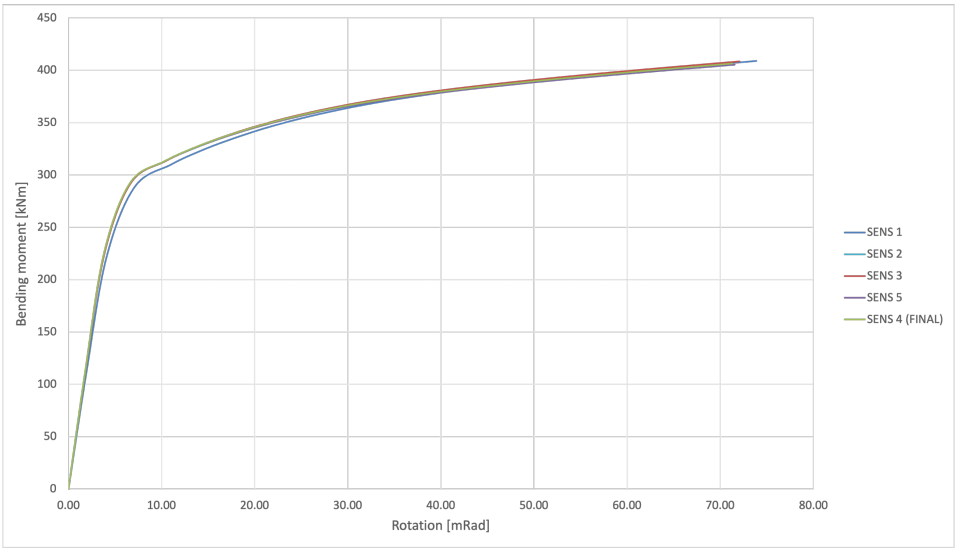

Figure A.6: Moment rotation curves - mesh sensitivity

Table A.1: Initial stiffness - mesh sensitivity

Model	Initial stiffness [kN-m/rad]
SENS 1	57.966
SENS 2	61.577
SENS 3	61.596
SENS 4	62.355
SENS 5	62.361

Table A.2: Global seed sizes SENS 4

Part	Global seed size
Column top	30
Column joint region	10
Column bottom	30
End-plate	10
Bolts	5
Beam - column side	10
Beam - open end	20

A.2.6. Steps and loading

The analysis of the model is organised into three sequential steps, which are conform to the experiment [49]. In the first step, the boundary conditions are established. In the second step, the bolts are pre-tensioned to 20% of their ultimate strength. The pre-tensioning load is applied to the shank areas of the bolts. After this pre-tensioning step, the lengths of the bolts are fixed at their current lengths and are propagated to the third step.

During the third step, a downward displacement of 100 mm is applied to the reference point at the open beam-end, resulting in a bending moment and shear force in the joint. This displacement is applied at a constant rate.

A.3. Validation

The numerical model is validated by comparing the moment-rotation curve of the experiment to the numerical model's.

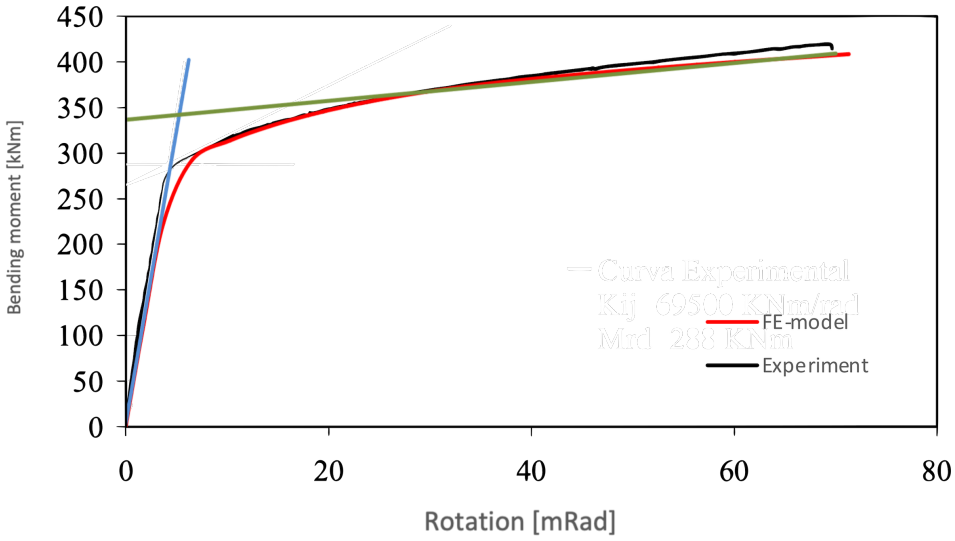

Figure A.7: Comparison moment-rotation curves experiment and numerical model

The initial stiffness and plastic moment resistance is determined from the moment-rotation curves. The joint characteristics from both results are compared in table A.3. The close alignment of the moment-rotation curves show that the numerical model is reliable to represent the experiment's physical behaviour. The numerical model shows a relative lower initial stiffness than the experiment, but the difference is acceptable. The plastic moment resistance is approximately the same. Hence the numerical model is regarded reliable and valid.

Table A.3: Comparison between experimental and numerical results

	M_{Pd} [kNm]	Error [%]	$S_{j,ini}$ [kN-m/rad]	Error [%]
Experiment	344		69500	
Numerical model	348	+1.1	62355	-10.3